sid.inpe.br/mtc-m21c/2020/11.11.23.48-TDI

PARAMETERIZATION OF ATMOSPHERIC ELECTRIC DISCHARGES AND THE EFFECTS ON RAIN AND NOX PRODUCTION

José Davi Oliveira de Moura

Doctorate Thesis of the Graduate Course in Meteorology, guided by Dra. Chou Sin Chan, approved in December 11, 2020.

URL of the original document:
<http://urlib.net/8JMKD3MGP3W34R/43JCLGB>

INPE
São José dos Campos
2020

PUBLISHED BY:

Instituto Nacional de Pesquisas Espaciais - INPE
Gabinete do Diretor (GBDIR)
Serviço de Informação e Documentação (SESID)
CEP 12.227-010
São José dos Campos - SP - Brasil
Tel.:(012) 3208-6923/7348
E-mail: pubtc@inpe.br

sid.inpe.br/mtc-m21c/2020/11.11.23.48-TDI

PARAMETERIZATION OF ATMOSPHERIC ELECTRIC DISCHARGES AND THE EFFECTS ON RAIN AND NOX PRODUCTION

José Davi Oliveira de Moura

Doctorate Thesis of the Graduate Course in Meteorology, guided by Dra. Chou Sin Chan, approved in December 11, 2020.

URL of the original document:
<http://urlib.net/8JMKD3MGP3W34R/43JCLGB>

INPE
São José dos Campos
2020

Cataloging in Publication Data

Moura, José Davi Oliveira de.

M865p Parameterization of atmospheric electric discharges and the effects on rain and NOx production / José Davi Oliveira de Moura. – São José dos Campos : INPE, 2020.

xviii + 114 p. ; (sid.inpe.br/mtc-m21c/2020/11.11.23.48-TDI)

Thesis (Doctorate in Meteorology) – Instituto Nacional de Pesquisas Espaciais, São José dos Campos, 2020.

Guiding : Dra. Chou Sin Chan.

1. Lightning. 2. Heavy rain. 3. Eta model. 4. .Autoconversion. 5. NOx. I.Title.

CDU 551.594.22

MINISTÉRIO DA CIÊNCIA, TECNOLOGIA E INOVAÇÕES

INSTITUTO NACIONAL DE PESQUISAS ESPACIAIS

[Secretaria]

[Departamento]

ATA DE REUNIÃO

DEFESA FINAL DE TESE : JOSÉ DAVI OLIVEIRA DE MOURA

No dia 11 de dezembro de 2020, às 09h, por videoconferência, o aluno mencionado acima defendeu seu trabalho final, intitulado "PARAMETERIZATION OF ATMOSPHERIC ELECTRIC DISCHARGES AND THE EFFECTS ON RAIN AND NOx PRODUCTION", (apresentação oral seguida de arguição) perante uma Banca Examinadora, cujos membros estão listados abaixo. O aluno foi **APROVADO** pela Banca Examinadora, por unanimidade, em cumprimento ao requisito exigido para obtenção do Título de Doutor em Meteorologia.

Eu, Paulo Nobre, como Presidente da Banca Examinadora, assino esta ATA em nome de todos os membros.

Membros da Banca

Dr. Paulo Nobre – Presidente - INPE

Dra. Chou Sin Chan - Orientadora - INPE

Dr. Osmar Pinto Junior - Membro da Banca - INPE

Dr. Guy Pierre F. G Brasseur - Convidado(a) - Max Plank Institut, Alemanha

Dra. Judith Johanna Hoelzemann - Convidada - Universidade Federal do Rio Grande do Norte

Atenciosamente,

Documento assinado eletronicamente por **Paulo Nobre**, **Pesquisador**, em 19/02/2021, às 10:52 (horário oficial de Brasília), com fundamento no art. 6º do Decreto nº 8.539, de 8 de outubro de 2015.

A autenticidade deste documento pode ser conferida no site http://sei.mctic.gov.br/verifica.html, informando o código verificador **6528850** e o código CRC **A39AF30A**.

ACKNOWLEDGMENT

PhD program is a demanding environment that tries to expose the maximum knowledge of each student. No doubt, no one can get through a PhD program without help. In addition to all the common difficulties of the PhD program, I experienced the situation of the COVID-19 pandemic away from friends and family in Germany. The difficulties added up, but luckily I managed to get through everything with a lot of help. I would like to thank my parents who gave me all the support I needed to get here. My parents are dedicated, loving, and made a difference in difficult times. I thank my wife who was by my side every day and believed in my potential. During the PhD program, my dear wife was my friend, my psychologist, my safe haven. Without her, the doctoral program would be chaotic. I would also like to thank my in-laws who, like a father and mother, gave me full support at crucial moments and they were always available to help. I am grateful to the friends I made during this period, the professors, CNPq, CAPES, CPTEC/INPE, and the Max Planck institute.

ABSTRACT

A parameterization of lightning with effects on the production of rain and nitrogen oxides is developed and applied to the regional Eta model. The lightning parameterization scheme is a function of variables diagnosed in the cloud microphysics and convection parameterizations. The parameterization diagnoses the total lightning (cloud-to-ground and intracloud), which affects the process of collision and coalescence of cloud droplets and acts in the chemistry of the atmosphere through the production, destruction, and transport of nitric oxide (NO), nitrogen dioxide (NO_2), nitric acid (HNO_3), nitrogen trioxide (NO_3) and dinitrogen pentoxide (N_2O_5). The scheme is calibrated using observational data of lightning. Numerical experiments are conducted to evaluate lightning simulations and the effects during three rainy months in southeastern Brazil. To assess the lightning scheme, observed electric atmospheric discharge data, estimated precipitation by satellite, and reanalysis data are used. The results showed that the lightning scheme is able to reproduce the monthly production and distribution of electrical discharges over southeastern Brazil when compared to the observed data. The lightning simulations showed a small underestimation concerning the observed data. The inclusion of the effects of lightning in the production of rain caused the intensification of electrical activity. The lightning effects on rain production also caused an increase in the mixing ratio of cloud ice at upper levels and a decrease in cloud water at the lower levels in the troposphere. In the case analyzed, the inclusion of the lightning effects in the production of precipitation caused a decrease in specific humidity in the lower levels of the troposphere and a decrease in the vertical movement. The proposed scheme increases the frequency of intense rains during the summer of 2017 and improves the performance of the rain forecast in the model. The lightning scheme showed a reasonable vertical profiles o NO and NO2 against reanalysis data. The average values of the mixing ratio of the chemical species simulated by the scheme are within the typical magnitude as those found in the literature and reanalysis data. Improvements could be applied in the lightning parameterization scheme in the future as the simulation of ozone, simulation of acid rain, better representation of the sinks of HNO3, and diagnosis cloud-to-ground and intracloud lightning separately.

Keywords: Lightning. Heavy Rain. Eta model. autoconversion. NOx. Nitrogen oxides.

PARAMETRIZAÇÃO DE DESCARGAS ELÉTRICAS ATMOSFÉRICAS E OS EFEITOS NA CHUVA E NA PRODUÇÃO DE NOx

RESUMO

Uma parametrização de descargas elétricas atmosféricas com efeitos na produção de chuva e óxidos de nitrogênio foi desenvolvida e aplicada ao modelo regional Eta. O esquema de parametrização de relâmpagos é função de variáveis diagnosticadas na parametrização de microfísica da nuvens e de convecção. A parametrização gera o diagnóstico do total de relâmpagos (nuvem-solo e intranuvem) na grade do modelo que afeta o processo de colisão e coalescência de gotículas de nuvem e atua na química da atmosfera por meio da produção, destruição e transporte de óxido nítrico (NO), dióxido de nitrogênio (NO_2), ácido nítrico (HNO_3), trióxido de nitrogênio (NO_3) e pentóxido de dinitrogênio (N_2O_5). O esquema foi calibrado usando dados observacionais de relâmpagos. Experimentos numéricos foram conduzidos para avaliar simulações do esquema de relâmpagos durante três meses chuvosos no sudeste do Brasil. Para avaliar o esquema de relâmpagos, dados observados de descargas elétricas atmosféricas, precipitação estimada por satélite e dados de reanálise foram utilizados. Os resultados mostraram que o esquema de descargas elétricas atmosféricas é capaz de reproduzir a produção e distribuição mensal de relâmpagos na região sudeste do Brasil quando comparados aos dados observados. As simulações de relâmpagos mostraram uma pequena subestimativa em relação aos dados observados. A inclusão dos efeitos dos relâmpagos na produção da chuva ocasionou na intensificação da atividade elétrica das simulações. Os efeitos dos relâmpagos na produção de chuva também causaram um aumento na razão de mistura do gelo de nuvem nos níveis superiores da troposfera e uma diminuição na água de nuvem nos níveis mais baixos da troposfera. No caso analisado, a inclusão dos efeitos de relâmpago na produção de precipitação causou uma diminuição da umidade específica nos baixos níveis da troposfera e uma diminuição do movimento vertical. O esquema proposto aumentou a frequência de chuvas intensas durante o verão de 2017 e melhorou o desempenho da previsão de chuva no modelo. O esquema de relâmpagos foi capaz de reproduzir os perfis verticais de NO e NO2 em relação aos dados de reanálise. Os valores médios da razão de mistura das espécies químicas simuladas pelo esquema estão dentro da magnitude típica encontrada na literatura e em dados de reanálise. Melhorias podem ser aplicadas no esquema de parametrização de raios no futuro como a simulação de ozônio, simulação de chuva ácida, melhor representação dos sumidouros de HNO_3 e diagnóstico descargas elétricas nuvem-solo e intranuvem separadamente.

Palavras-chave: Relâmpago. Chuva intensa. Modelo Eta. autoconversão. NOx. Óxidos de nitrogênio.

LIST OF FIGURES

Pág.

LIST OF TABLES

Pág

SUMMARY

1 INTRODUCTION

Electrical activity in the atmosphere is a meteorological phenomenon that intrigues the scientific community for its complexity. Although not fully understood, electrical discharges in the atmosphere have been slowly unraveling over the past few centuries.

It is known that the atmospheric electrical discharge (also called lightning) is produced when the separation of electrical charges is very intense within a storm, increasing the magnitude of the cloud's electric field until the dielectric strength of the air is broken (there is no concrete comprehension regarding the dielectric strength breakdown of the air at the moment of discharge).

Despite puzzles in the electrical activity of storms, many studies have advanced to detail the effects or consequences of lightning in the atmosphere. In addition to the damage caused to buildings, the electrical sector, the production of fires, the death of farm animals, and human beings, lightning also causes other types of consequences.

Studies that relate the cloud electrical field to changes in the collision and coalescence of cloud droplets are an example of how the electrical activity has consequences for rain production by modifying the size of cloud droplets (PLUMLEE; SEMONIN, 1965; SEMONIN; PLUMLEE, 1966; FLETCHER, 2013).

Goyer (1960) conducted a laboratory study about the effects of the electric field on cloud microphysics. The author concluded that the electric field is able of generating an increase in the coalescence of cloud droplets. Moore et al. (1964) carried out an observational study with radar and noted that, after an electrical discharge, the cloud droplets increase in size up to 100 times and the precipitation intensifies.

Sator (1973), in an observational study, using an aircraft equipped with equipment to photograph the microphysical activity of convective clouds, stated that the electrical conditions of storm clouds can produce a rapid increase in the

growth rate of small cloud droplets, which would grow very slowly in the absence of electrical activity.

Based on works such as Goyer (1960) and Sator (1973), Zhou et al. (2002) developed an empirical equation to estimate precipitation based on the number of electrical discharges from a storm. Their results have proved to be very useful in regions that do not have good weather radar coverage to determine precipitation.

Currently, there are few numerical models of weather and climate that predict lightning activity and the effects of this process are even rarer to be included in the model grid. The relationship between electrical activity and rain production is widely discussed in the literature, but it is not represented in the Eta mesoscale numerical model.

The challenge in the prognosis of precipitation is present in any atmospheric model. This is due to the lack of understanding and numerical representation of the physical processes of clouds, as well as the scarcity of observations.

Precipitation is a subgrid process in a model. That is, it is resolved implicitly through parameterization schemes. The cloud and convection microphysics schemes are responsible for managing the production of rain in the atmospheric models. Cloud microphysics works by removing excessive moisture from the vertical column of the model, while convection works by redistributing heat, moisture, and momentum to reduce the thermodynamic instability of the grid.

The Betts-Miller-Janjic convection parameterization (JANJIC, 1994) is used in the operation of the Eta model at the Center for Weather Forecasting and Climate Studies (CPTEC). Evaluative studies of the rain prognosis of the Eta model showed that the Betts-Miller-Janjic convection parameterization scheme (BETTS; MILLER, 1986; JANJIC, 1994), combined with Ferrier (1994) or Zhao and Carr (1997) cloud microphysics parameterization, can represent the location of the cells with maximum rainfall intensity, but there are

underestimations in the magnitude of precipitation in these cells (CATALDI ET AL., 2007; CHOU; SILVA, 1999; CALADO ET AL., 2017).

The deficiency in simulating precipitation maxima motivated the idea of developing a new tool that can generate improvements in the rain forecasts of the Eta model. Since intense precipitations can generate floods, landslides, among other social and urban problems, the correct simulation of this variable is fundamental.

Intense precipitation cells are linked to cloud storms, which can also show electrical activity. The development of a lightning parameterization with the inclusion of its effects on rain production is a viable way to correct or adjust the precipitation intensity. Besides, of course, the parameterization can prognosis a new variable: the electrical discharge.

Beyond the effects of lightning on the production of rain, lightning also plays an important role in the chemistry of the atmosphere through a process known as the Zel'dovich mechanism (ZELDOVICH ET AL., 1947), where an air pollutant is produced as a result of the high air temperatures around the electrical discharge channel that causes the diatomic division of nitrogen (N_2) and oxygen (O_2) molecules to form nitric oxide (NO) which is later converted to nitrogen dioxide (NO_2).

Nitrogen oxides ($NO_x = NO + NO_2$) are air pollutants that have an essential contribution to the production of tropospheric ozone (O_3), an important greenhouse gas that affects negatively human health. NOx also contributes to the production of nitric acid (HNO_3), which can be removed from the atmosphere by precipitation and cause nitrogen fixation in the soil, a substantial process for the growth of many plants.

Global NO_x emissions are dominated by anthropogenic sources and concentrated close to the Earth's surface in continental areas, except for ship and aircraft routes. Among natural sources, lightning is estimated to be the largest source of NOx (GALLOWAY ET AL., 2004).

Although lightning activity produces smaller amounts of NO_x than anthropogenic sources (SCHUMANN; HUNTRIESER, 2007; LAMARQUE ET AL, 2010), the NO_x produced by lightning is mainly injected into the upper troposphere (JAEGLÉ ET AL., 1998), where the lifetime of NO_x is a few days instead of a few hours near the surface, allowing NO_x to be transported over long distances. Also, the efficiency of O_3 production in the upper troposphere per unit of NO_x is about one order of magnitude bigger than close to the surface (GREWE, 2007). Therefore, lightning has fundamental implications for the chemistry of the atmosphere and the climate of planet Earth.

From such information, questions arose: how to produce a prognosis of electrical activity in a numerical model through the knowledge of cloud microphysics? How to propagate the effects of this discharge in the model grid? What are the consequences that these changes would generate for the meteorological variables? These questions motivated the present work.

1.1 Objectives

The main objective of this work is to generate a new lightning forecasting methodology in the Eta regional model and to insert the effects of electrical activity in the production of rain and the chemistry of the atmosphere.

The specific objectives are:

- Investigate the relationship between electrical activity and cloud droplet autoconversion;
- study the algorithm of the cloud microphysics scheme of the Eta model to parameterize the electrical activity of the cloud;
- implement an electrical discharge prediction system in the Eta regional model;
- understand the effects of electrical discharge in the clouds by increasing the autoconversion of cloud droplets;
- analyze the indirect effects of the lightning parameterization in humidity, temperature, and vertical motion;
- understand the impact of lightning on the chemistry of the atmosphere;

- simulate chemical and photochemical reactions;
- analyze the vertical and horizontal transport of the chemical species produced as a result of lightning.

2 THEORETICAL FOUNDATION

The subjects covered in this chapter aim to provide content for the reader to understand the physics of formation and development of hydrometeors in clouds, the basic concepts of thermodynamics of deep convection in the atmosphere, and those of thropospheric chemistry.

2.1 Cloud microphysics

Cloud microphysics deals with the processes that govern the formation, growth, and dissipation of hydrometeors that constitute the clouds. Such processes depend on the type of cloud in which they occur. In *warm clouds*, there are only processes concerning water in the liquid and gas phases. In *cold clouds*, there may be processes concerning the liquid, solid, and gas phases of water or only for the solid and gas phase of water (HOUZE, 1993).

Water phase changes are important mechanisms for the formation and growth of hydrometeors in the cloud. These water phase changes can occur:

- From steam to liquid → Condensation
- From liquid to steam → Evaporation
- From liquid to solid → Freezing or solidification
- From solid to liquid → Melting
- From steam to solid → Deposition
- From solid to steam → Sublimation

In addition to water phase changes, the important processes for the formation and growth of hydrometeors are collision and coalescence, accretion, and aggregation. According to Houze (1993):

- Collision and coalescence occur because the droplets have different falling speeds. Large particles move faster than small particles. During the fall, the larger particles collide and coalesce with smaller particles that are in the way, thus increasing their size even more. However, not every collision implies that there will be coalescence between the particles. They can collide and coalesce (generating a larger particle),

collide and shatter, collide and coalesce for a period and then separate into 2 or more particles (Figure 2.1 a).

- Accretion (rimming) is a process similar to that of collision and coalescence but occurs between super-cooled water and ice. It is a process present in cold mixed-phase clouds (Figure 2.1 b).
- Aggregation is also a process similar to that of collision and coalescence, however, it occurs only between ice particles (Figure 2.1 c).

Figure 2.1 – Hydrometeor growth processes: a) collision and coalescence (liquid + liquid); b). Accretion (liquid + ice); c) Aggregation (ice + ice).

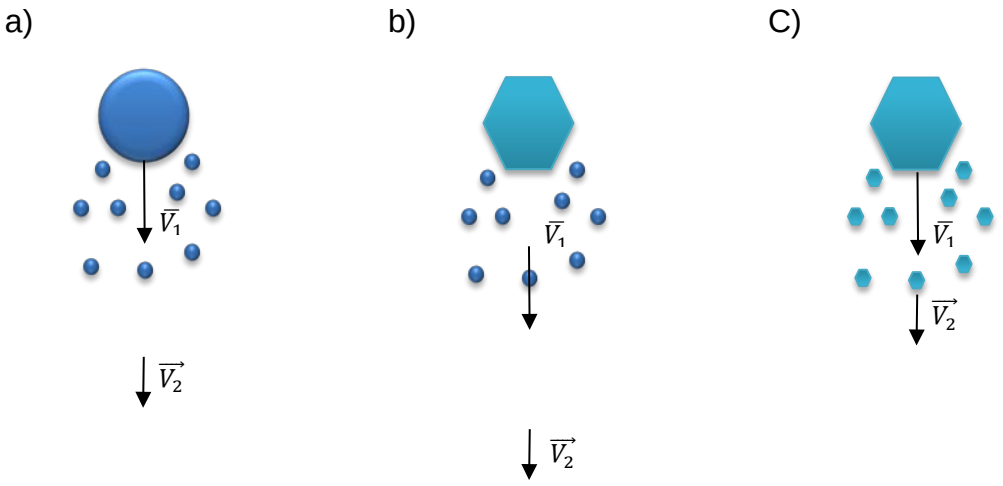

2.1.1 Warm clouds

The warm cloud microphysics deals with the physical processes of clouds that form at altitudes below the isotherm of 0ºC and, therefore, consists only of liquid particles and water vapor. The liquid particles are divided into cloud droplets and raindrops (WALLACE & HOBBS, 2006).

For the formation of the cloud, there must be initially nucleation of the water vapor, that is, that the vapor condenses and forms the cloud droplet. Once the relative humidity is above 100%, cloud droplets can be formed by condensation of water vapor on the surface of condensation nuclei (aerosols and organic material). It is not common for clouds to form in the atmosphere without the presence of condensation nuclei, since air supersaturation of around 300%

relative humidity would be necessary, which is not observed in the Earth's atmosphere (HOUZE, 1993).

Once formed, cloud droplets can grow by two processes: collision and coalescence (for larger particles) and condensation of water vapor molecules (WALLACE; HOBBS, 2006).

As the cloud droplets grow and gain mass, they become heavy enough that the upward currents cannot keep them in the air. The droplets then precipitate and are classified as raindrops. Typically, raindrops have a radius of 2mm and can develop 15 minutes after cloud formation. Like droplets, raindrops grow through the process of collision and coalescence during their fall into the cloud. As the raindrops grow, the collision and coalescence process becomes less effective due to the breaking of the larger drops into various droplets (STENSRUD, 2007).

Another important process for the formation of raindrops, present only in cold clouds, is the melting of ice particles. These particles form in cold regions of the cloud, but they melt as they pass through warmer regions during their fall, generating raindrops (PRUPPACHER; KLETT, 2010).

2.1.2 Cold clouds

According to Houze (1993), clouds that form above (or part of the cloud is above) the 0ºC isotherm level are classified as cold clouds. The cold cloud microphysics is divided into cold glaciated and cold mixed phases.

- Glaciated clouds are those that contain only ice particles.
- Mixed clouds are those formed by liquid water and ice.

Ice can form at temperatures below the freezing point of water in cold clouds. However, liquid and gas molecules do not freeze immediately in cloud regions with temperatures between 0ºC and -40ºC. In this temperature range, both ice and supercooled liquid water are observed (mixed region of the cloud). For cloud regions that have temperatures below -40ºC, only ice is present. Two

processes of cloud ice formation can be described: heterogeneous nucleation and homogeneous nucleation.

Heterogeneous nucleation occurs in the mixed region of the cloud (between 0ºC and -40ºC). Heterogeneous nucleation requires the pre-existence of a freezing core (similar to the condensation core). This process can be divided into nucleation by contact, deposition, immersion, and condensation (See Figure 2.2).

1. In contact nucleation, supercooled water instantly freezes in contact with the freezing core, forming a particle of ice.
2. In nucleation by deposition, water vapor passes directly to the solid phase in contact with freezing nuclei.
3. Nucleation by immersion occurs by freezing a drop of supercooled water in a freezing core that is immersed in a drop of water.
4. Nucleation by condensation is done by condensing water vapor in a freezing nuclei surface. Subsequently, this particle freezes to form an “ice embryo”.

Figure 2.2 – Types of heterogeneous ice nucleation processes.

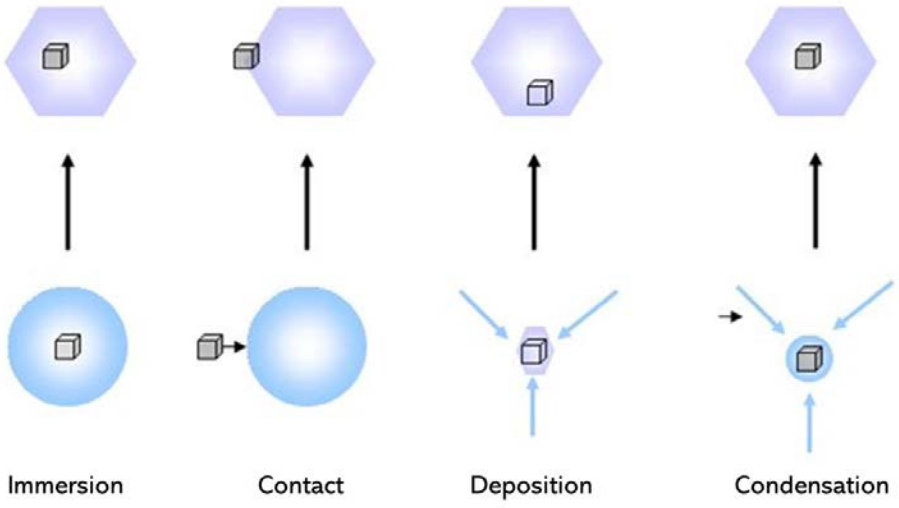

Source: Adapted from Seifert *et al.* (2009).

Homogeneous nucleation applies to regions with temperatures below -40ºC. In this case, the liquid particles freeze homogeneously and there is no need for the pre-existence of the freezing nucleus (STRAKA, 2009). However, gas-phase water still needs the presence of a freezing nucleus to freeze. It happens because it is statistically impossible that gas molecules could form the ice structure while colliding randomly.

In general, the ice particles are divided into ice crystals, snow, graupel, and hail:

a) ice Crystal: are small frozen particles that can be shaped like a column, plate, dendrite, or a combination of these shapes. They can be present in regions of the cloud with temperatures below -15ºC. The ice particles formed in the homogeneous and heterogeneous nucleation process become ice crystals when they grow through the deposition process. Deposition in mixed clouds occurs due to the Bergeron Process[1] (BERGERON, 1935), as shown in Figure 2.3;
b) graupel: It is formed when the ice particles (usually ice crystals), generated by heterogeneous and homogeneous nucleation, grow by the process of accretion and /or deposition;
c) hail: In some cases, graupel growth continues until it becomes an ice rock known as hail. The hail refers to hail that grew by the accretion process and reached the criterion of 5 mm in diameter (criterion adopted by the United States National Weather Service). When the hail grows long enough that the upward current can no longer sustain it, it precipitates and, if it does not thaw on its descent, reaches the ground;
d) snow: When particles of ice crystals grow through the aggregation process, snow is formed. Snowfall occurs in nimbostratus clouds.

[1] When cloud droplets serve as a source to increase water vapor in the environment, they cause hail and / or ice crystals to grow by deposition more quickly. This occurs when the air is supersaturated with respect to ice and saturated with respect to water. This mechanism known as the Bergeron process. More information in Bergeron (1935) and Grimm (1999).

Figure 2.3 – Exemplification of the Bergeron Process.

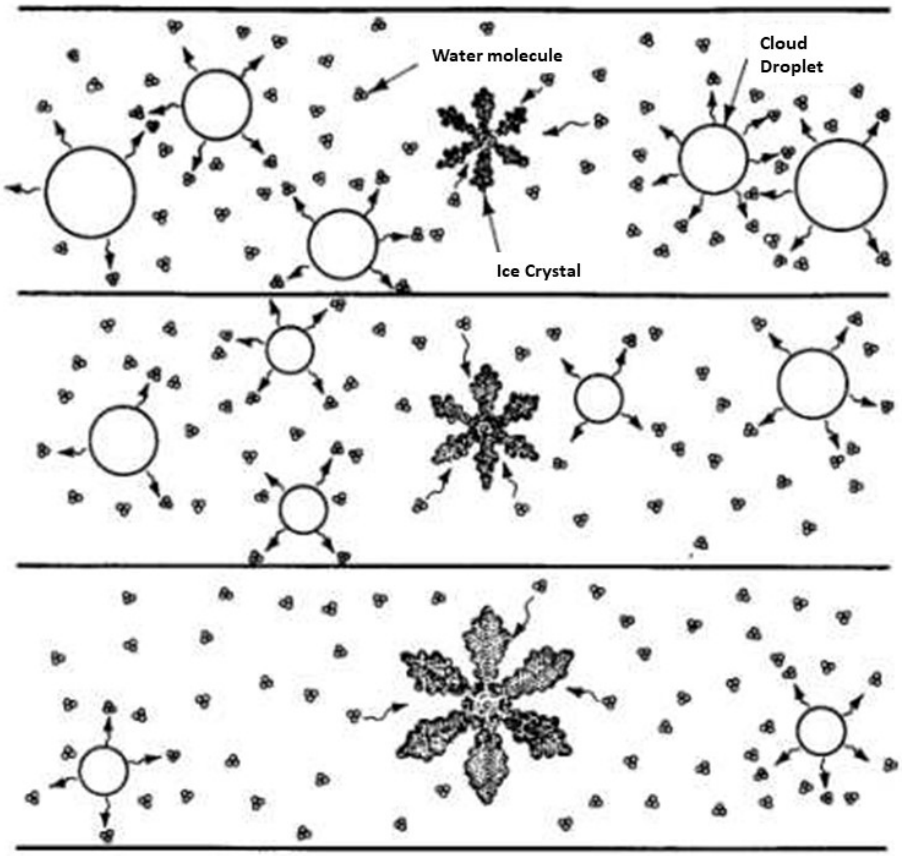

Source: Grimm (1999).

2.1.3 Cloud microphysics parameterization

Parameterizing is to represent the effects of an atmospheric process that cannot be solved directly at the grid point of the numerical model due to the low spatial resolution. Due to the computational cost, the numerical models (mainly the global ones) are executed in less refined resolutions and, sometimes, they cannot represent small-scale processes, such as convection. Processes that are not explicitly represented in the model grid are known as “subgrade processes” (STENSRUD, 2007).

Although small, subgrade processes can be very important for forecasting weather and climate, influencing the final result. Parameterization uses information from the model's resolved grid to implicitly represent the effects of subgrade processes.

Numerous parameterization schemes have been created since the development of numerical time models. Among these schemes, the parameterization of cloud microphysics aims to represent the effect of water phase changes in the model grid.

Microphysics parameterization solves intra-cloud processes using information from the model's resolved grid. It works by removing excess moisture from the model grid to produce clouds and precipitation. This procedure results in the release of latent heat from condensation, which influences the forecast of wind, temperature, and humidity (Figure 2.4).

Besides, microphysics may be producing information for other parameterization schemes, such as radiation (associated with the radiative properties of clouds) and the chemistry of the atmosphere (associated with aerosols).

Figure 2.4 – Relationship between the model grid and cloud microphysics parameterization.

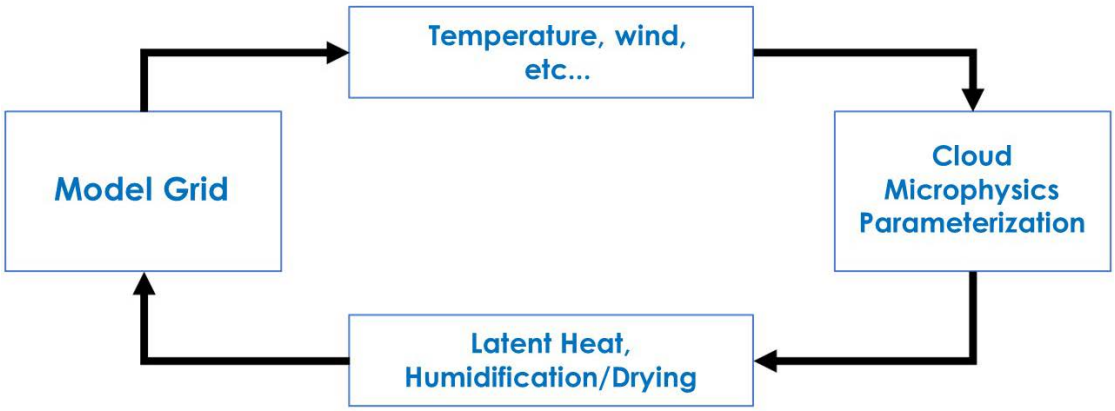

Microphysics parameterization schemes use methods with a wide range of complexity, but the complexity of the scheme is not always a function of the accuracy of the result. Two main methods of parameterizing microphysics are those of the *Bin* type and those of the *Bulk* type (STRAKA, 2009).

The Bin microphysics parameterization is considered the one that best represents the distribution of rain. The method is based on the use of small divisions that refer to a spectrum of hydrometeor sizes. Generally, the size divisions in the Bin type schemes are done exponentially, where each division

has hydrometeors that are exponentially larger (in size and mass) concerning the hydrometeors in the previous division (STENSRUD, 2007).

The Bin type schemes do not use a specific function to represent the particle distribution, instead, these schemes divide the particle distribution into a finite number of size or mass categories. This division into categories requires large use of memory and computational processing. A problem with Bin-type microphysics schemes is the excessive need for computational resources to use them (except for use in small domains or use in two-dimensional models).

Bulk schemes are more popular because they require a lower computational cost compared to Bin schemes. The parameterization of Microphysics of the Bulk type is based on functions that determine the particle size distribution and, normally, predict the mixing ratio and concentration of hydrometeors. The particle size distribution is generally approximated by the gamma function (STRAKA, 2009). The generic form for a gamma function is given by:

$$N(D) = N_0 D^{\mu} e^{-\lambda D} \qquad 2.1$$

Where N (D) is the total concentration per unit volume, D is the particle diameter, No is the total concentration, μ is the parameter that defines the shape of the hydrometeor, λ is the slope parameter.

The shape of the hydrometeors (μ) is determined by reflectivity (Z), the slope parameter (λ) is defined by the mixing ratio (q). Therefore, Bulk type schemes have 3 free parameters: λ (q), No, μ (Z). Thus, Bulk parameterization can be single-moment, double-moment, or triple-moment.

- Single Moment - Calculate the total concentration (No).
- Double Moment - Calculate the Total concentration (No) and Mixing Ratio (q).
- Triple Moment - Calculate Total Concentration (No), Mixing Ratio (q), and Reflectivity (Z).

Bulk schemes are generally double-moment. Parameters not predicted by the schemes (eg, single moment does not predict q and Z) are considered constant or empirically determined.

2.2 Thermodynamic fundamentals of deep convection

By the Bjerknes parcel method (1938, apud ZEPKA, 2011, p. 11), it is possible to analyze the behavior of a parcel of air concerning the surrounding environment. For this, the central point of the air parcel is considered as its reference. When moving vertically (eg, air movement over a mountainous region), the air portion changes its temperature due to its expansion or compression (the process is adiabatic). After reaching a new pressure level, the portion may have a higher density, less than or equal to that of the surrounding environment. The air parcel has three possibilities:

- Return to your original pressure level, but not necessarily the initial pressure level. In this case, the layer the parcel is in is stable.
- Keep ascending. In this case, the layer the parcel is in is unstable.
- Stabilize at the current pressure level. In this case, the layer of the parcel is in neutral equilibrium.

According to Houze (1993), convective or cumuliform clouds occur when the humid air becomes floating (a portion of air in an unstable environment) and accelerates vertically upwards in regions with a horizontal extension between 0.1 and 10 km. In cases of intense buoyancy, wet convection can become deep and produce storm clouds that are classified as cumulonimbus.

Salby (1996) defines cumuliform clouds as an isolated development of air plumes that ascend due to positive buoyancy and are responsible for the vertical transport of heat in the troposphere:

> Cumuliform clouds develop from isolated air plumes that ascend buoyantly. Associated with cellular convection, cumulus clouds grow through positive buoyancy supplied via sensible heat transfer from the surface and latent heat released to the air during condensation, both of which make these clouds dynamic. Updrafts are of order 1 $m.s^{-1}$ in developing cumulus but can be several tens of $m.s^{-1}$ in organized mature cells like cumulus congestus and cumulonimbus. The

> characteristic lifetime of cumulus clouds ranges from a few minutes to hours (SALBY, 1996, p. 277).

According to Wallace and Hoobs (2005, p. 345), deep convection develops within a large-scale environment with horizontally uniform temperature, humidity, and wind. The vertical profiles of temperature and humidity in the environment play a fundamental role in defining the region of the atmosphere in which deep convection develops spontaneously. The vertical wind profile determines the direction and rate of movement of the storm and profoundly influences the structure and evolution of the system.

The conditions for deep convection to occur are:

- Existence of a conditionally unstable adiabatic gradient.
- Very wet boundary layer.
- Convergence at low levels (or lifting) sufficient to release instability.

Thermodynamically unstable environments favor the appearance of storm clouds. The potential for atmospheric instability can be determined by the CAPE index (Convective Available Potential Energy).

CAPE is determined by the Bjerknes parcel method (1938), where it is considered that a portion of air must be lifted from the surface with a dry adiabatic gradient up to the Lifting Condensation Level (LCL). The air portion saturates and starts to rise with a humid adiabatic gradient to the Level of Free Convection (LFC). For the air parcel to travel from the surface to the NCE, there must be minimum energy known as Convection Inhibition Energy (CIN). From the LFC, the air parcel rises freely until it reaches the equilibrium level (EL), at this level, the parcel must stabilize. CAPE represents the energy with which the air parcel ascends freely between the NCE and the NE (HOUZE JUNIOR, 1993; WALLACE; HOBBS, 2005; STENSRUD, 2007).

Through the skew-t diagram, it is possible to visualize the CAPE as the blue area in Figure 2.5 between the LFC and the EL.

Figure 2.5 – Hypothetical Skew-t Profile.

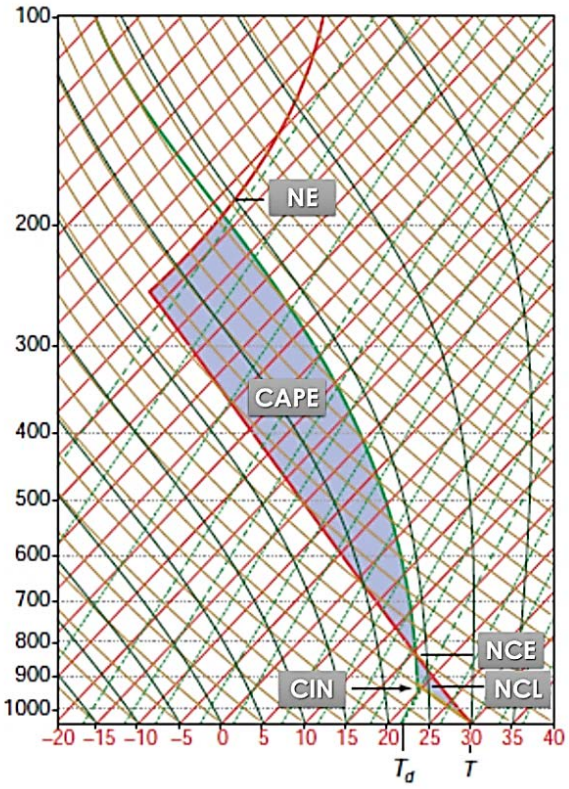

Source: Wallace and Hobbs (2005).

CAPE is calculated using equation 2.1

$$CAPE = g \int_{NCE}^{NE} \frac{\theta(z) - \bar{\theta}(z)}{\bar{\theta}(z)} dz \qquad (2.2)$$

Where g is gravity, θ potential temperature of the plot, $\bar{\theta}$ potential temperature of the environment, and z is the height of the air parcel.

According to Wallace and Hobbs (2005), CAPE values above 2500 J/kg are indicative of severe storms.

2.3 Atmospheric chemistry

In the last 3.5 billion years, the chemical composition of the Earth's atmosphere has undergone several changes. In the primitive world, it is believed that there was a strong predominance of carbon dioxide, methane, sulfur, nitrogen, and argon in the air of planet Earth. The modern terrestrial atmosphere is composed

of nitrogen (78.1%), oxygen (20.9%), and argon (0.9%) which add up to 99.9% of the atmospheric mass. The rest of the atmosphere is made up of water, carbon dioxide, a large number of waste gases, and small liquid and solid particles called aerosols.

The closer to the Earth's surface, the greater the concentration of air molecules, that is, the greater the atmospheric pressure and the density of the air. More than 75% of the entire mass of the Earth's atmosphere is concentrated in the layer closest to the surface, the troposphere, due to the planet's gravitational pull. It is in the troposphere where living beings are and, therefore, it is extremely important to study the chemistry of the air in this layer, mainly because small variations in residual gases (or tracers) can cause air pollution. These variations of polluting chemical species can be caused naturally, such as emissions from erupting volcanoes, and by human actions, such as the combustion of vehicles powered by fossil fuels.

Air pollution can be defined as the presence of excess contaminants or substances in the air that cause negative effects on human health or well-being or produce other harmful environmental effects (VALLERO, 2008). Air pollution is connected to a sequence of events: the production of pollutants and their emission from a source; its transportation, transformation, and removal from the atmosphere; and its effects on humans, materials, and ecosystems. As it is generally economically unviable or technically impossible to zero emissions of air pollutants, we seek to control emissions at a level such that the effects are non-existent or minimized (FLAGAN; SEINFELD, 1988).

Air pollution is not a recent problem. Anthropogenic actions for the survival and evolution of the species have led to soil degradation, deforestation, water, and air pollution even in ancient times. In ancient Rome, for example, more than 2000 years ago, the senate was already working on environmental legislation and introduced a law that “prohibited polluted air”, cited as aerem corrumpere non licit. Several texts from that time, such as poems and letters, portrayed the pollution of Rome as a dark smoke caused by burning wood that warmed homes (BORSOS et al., 2003).

Measurements of ice cores in Greenland found that, around 1200 (AD), regions close to the Mediterranean Sea and in China (during the Song dynasty) showed an increase in the concentration of copper in the air due to the production of coins from that time (HONG et al., 1996).

Between the middle of the 17th century and the beginning of the 19th century, England was heavily dependent on burning coal for its economy as a result of the industrial revolution. This led the city of London to a catastrophic situation about air quality due to the high number of small solid particles suspended in the atmosphere that affected the population's health causing respiratory problems. At that time, London was as polluted as a large current capital like Delhi, India (FLINN, 1984; CHURCH, 1986).

In modern times, post-industrial revolution, the burning of fossil fuels, soil management, burning of biomass, industrial activity, are examples of the sources of anthropogenic pollutant emissions into the atmosphere. The chemical species emitted react in the atmosphere due to sunlight, changes in temperature, and/or molecular collisions.

Gas-phase reactions are divided into photolysis (or photodissociation) and kinetic chemical reactions (JACOBSON, 2002). In the case of photolysis, the reactions are unimolecular, that is, there is only one reagent. In this case, solar radiation, at a given wavelength, collides with a molecule and causes a break, such for example:

$$NO_2 + h\nu \rightarrow NO + O \tag{2.3}$$

In the photodissociation reaction above, a dinitrogen oxide molecule (NO2) was broken down by a photon ($h\nu$) to generate nitric oxide and oxygen. This photochemical reaction generally occurs for wavelengths less than 420 nm.

Commonly, chemical kinetic reactions involve two reactants (bimolecular), but in some rare cases, three reactants can collide simultaneously, a process known as thermolecularly reaction. The bimolecular reaction has a general form as:

$$A + B \rightarrow C + D \tag{2.4}$$

Kinetic chemical reactions occur in thermal dependence and/or collisions. Thermal kinetic reactions are processed more quickly at high temperatures, for example:

$$N_2O_5 \xrightarrow{M} NO_2 + NO_3 \quad (2.5)$$

Where M is the molecule that provides energy for the reaction due to collision. M can be any molecule present in the atmosphere. Generally, M represents nitrogen or oxygen, as they represent the highest percentage of the atmospheric composition. M does not change the concentration.

The kinetic chemical reactions of collision occur in the presence of active reagents that collide with each other, for example:

$$CH_4 + OH \rightarrow CH_3 + H_2O \quad (2.6)$$

Anthropogenic emissions of air pollutants generally occur on the surface of planet Earth. In this lower part of the troposphere (from the surface at 500-3000 meters of altitude), also called the planet boundary layer, pollutants accumulate or escape to the free atmosphere depending on the stability of the layer. When unstable, in the presence of convection, for example, pollutants escape into the free atmosphere and can be transported long distances before being removed from the air (generally, the magnitude of the wind is greater as we ascend the troposphere).

3 BIBLIOGRAPHIC REVIEW

In this chapter, the main works that support this proposal will be presented. The content covered in this chapter, on the prognosis of precipitation and electrical activity in the atmosphere, involves work from the early 20th century to the present day.

3.1 Evaluation of the Eta model precipitation forecasts

The forecast for precipitation in numerical models is made through two parameterizations: cloud microphysics and convection. The Eta model of CPTEC/INPE has two versions of parameterization of cloud microphysics and two versions of convection:

- Cloud Microphysics: Zhao and Carr (1997), Ferrier (1994).
- Convection: Kain-Fritsch (KAIN; FRITSCH, 1990; hereafter KF), Betts-Miller-Janjic (JANJIC, 1994; hereafter BMJ).

In the Eta model of CPTEC/INPE, the BMJ convection scheme can be combined with the microphysics of Zhao and Carr (1997) or Ferrier (1994). However, for the KF scheme, there is only available to combine it with Ferrier (1994). This information is not dated in the literature but is easily found when analyzing the model code.

Gallus Junior (1999) evaluated the performance of the Kain-Fritsch and BMJ convection schemes in a study on the sensitivity of the prognosis in different spatial resolutions in the Eta model. There were no indications of the parameterization of cloud microphysics used in the work. Among the results obtained, the author noted that, by increasing the spatial resolution, BMJ decreased the production of rain, while KF presented an increase in rainfall. In terms of location and timing of the precipitating systems, BMJ obtained reasonable results but underestimated the maximum precipitation peaks. On the other hand, KF showed errors in positioning the rain, but it was efficient to simulate the magnitude of intense precipitation.

Chou and Silva (1999) carried out an objective assessment of the precipitation predictions of the Eta model over South America. The model was configured with the parameterization of BMJ convection and the microphysics of Zhao and Carr (1997). The authors noted that forecasts of 24 to 60 hours ahead of more intense precipitation (mm / day) (above 25.4 mm) are underestimated.

Two years later, Kain et. al. (2001) compared precipitation simulations of the Eta model, operational by the NCEP (National Centers for Environmental Prediction), using the KF and BMJ convection parameters. There were also no specifications regarding the cloud microphysics scheme used in this study. The authors noted that there are advantages and disadvantages between BMJ and KF, where one scheme tends to compensate for the other's deficiency. BMJ, for example, tends to activate shallow convection over a much larger area than KF. This is because KF does not activate shallow (or deep) convection if there is more than 9 $J.kg^{-1}$ of CIN, while BMJ does not have a system of restrictions for activation. For the case studied, the results showed more realistic surveys using the KF scheme. On the other hand, KF tended to overestimate the moisture in the boundary layer, apparently caused by not activating shallow convection. The authors concluded that it would be valid to complement the model's predictions with the two parameterizations

Cataldi et al (2007) evaluated the precipitation predictions of the Eta regional model up to ten days ahead. The parameterization of convection used was that of BMJ and the microphysics of clouds was that of Zhao and Carr (1997). The results showed that, for precipitations above 10 mm, the prognoses tend to underestimate the observed precipitation. Best results were obtained when the rain accumulated for three days or more.

Vasconcellos and Cavalcanti (2010) carried out two case studies to evaluate the performance of the predictions of intense precipitation in the regional Eta model. The schemes to parameterize the rains were KF convection and Ferrier's microphysics (1994). The results showed that the magnitude of the simulated intense rainfall was well represented when compared to observations. However, there were errors in positioning the more intense precipitation bands.

Tanessong et al. (2012) evaluated the prognostications of the Eta model in Central Africa. The author used both available convection parameterization schemes (KF and BMJ) to compare with TRMM (Tropical Rainfall Measuring Mission) precipitation data. The cloud microphysics scheme used was that of Ferrier (1994). The authors concluded that the model represented well the temperature at 2 meters and the pressure at the average sea level. However, the accumulated precipitation (mm/6h) predicted did not obtain satisfactory results (both with KF and BMJ), due to the low dexterity in representing the spatial distribution. Besides, there was an underestimation of the magnitude of the maximum precipitation values.

Moura (2016), in his master's dissertation, carried out updates on the momentum transport of the KF scheme. Four versions of the KF scheme were compared. The cloud microphysics used was that of Ferrier (1994). Precipitation simulations (mm/24h) were compared with precipitation data estimated by the satellite CPC MORPHing Technique (CMORPH). Their results showed underestimations of rainfall above 12.7 mm for all members.

Calada et al. (2017) analyzed the performance of the Eta model in simulations by precipitation set in a case study. The members used were combinations of the parameterization schemes of cloud microphysics and convection available in the Eta model (including variations of the KF scheme). The rain forecasts (mm/24h) were compared with data from rainfall stations and data estimated by a satellite called MERGE (ROSANTE ET AL., 2010). Their results showed an underestimate to simulate intense rainfall for almost all members, both 24 hours in advance of the event and 48 hours in advance. Only one member, using the Kain-Fritsch scheme, showed an overestimation.

For predictions or simulations of very high resolution (~ 1km), numerical models can explicitly solve convection. In this case, the parameterization of convection can be turned off and only the microphysics of clouds will solve the rain of subgrade.

Lianet (2016) evaluated the precipitation predictions of the Eta model at a very high resolution (1km) using only Ferrier's cloud microphysics (1994). Its results showed that the Eta model overestimated the rainfall maximum when compared to satellite estimated precipitation data.

Summarizing the results of the works presented in this section (Table 3.1), it is noted that there is a tendency for the Eta model to underestimate heavy rain forecasts when configured with the BMJ convection parameterization regardless of the microphysics used. For cases in which the Eta model used the KF convection scheme (combined with Ferrier's microphysics), the model presented system positioning errors with a divergence of results concerning rainfall intensity. There have been cases in which KF overestimated, underestimated, or showed dexterity to predict rainfall. However, apparently, for intense rains, the KF scheme tends to present values closer to that observed concerning BMJ.

Table 3.1 – Summarize the results obtained in this section concerning simulations of intense rain.

	Convection parameterization	**Parameterization of Microphysics**	**Results of the Simulations of the Eta Model**
Gallus Junior (1999)	BMJ e KF	Não especificado	*BMJ positioned the rain well but underestimated the maximum peaks. KF represented the intensity of heavy rains well but presented positioning errors.*
Chou e Silva (1999)	BMJ	Zhao e Carr (1997)	*It underestimated the intense rains.*
Cataldi et al (2007)	BMJ	Zhao e Carr (1997)	*Underestimation of rainfall above 10 mm.*
Vasconcellos and Cavalcanti (2010)	KF	Ferrier (1994)	*It represented the intensity of the rain maximum, but with positioning errors.*
Tanessong et al. (2012)	BMJ e KF	Ferrier (1994)	*Underestimations of intense rains and positioning errors.*
Moura (2016)	KF (different versions)	Ferrier (1994)	*All versions had underestimated rainfall above 12.7 mm.*
Lianet (2016)	Not used	Ferrier (1994)	*Overestimated in simulations of intense rain.*
Calado *et al.* (2017)	BMJ e KF (different versions)	Ferrier (1994) e Zhao e Carr (1997)	*Only one KF member generated overestimation. All other members underestimated heavy rains.*

3.2 Storm cloud electrification

According to Wallace and Hoobs (2005, p. 252), all clouds have some level of electrical activity. However, only in deep convection clouds is the separation of electrical charges sufficient to break the dielectric strength of the air, resulting in electrical discharges.

The first step for an electrical discharge to occur in the atmosphere is the separation of charges, polarization or electrification of the cloud. The normal charge distribution of a storm, known as tripolar, can be seen in Figure 3.1. Charge distribution can be reversed, but it is less common (RUST & MACGORMAN, 2002).

Figure 3.1 – Distribution model of electrical charges in a typical and relatively simple storm.

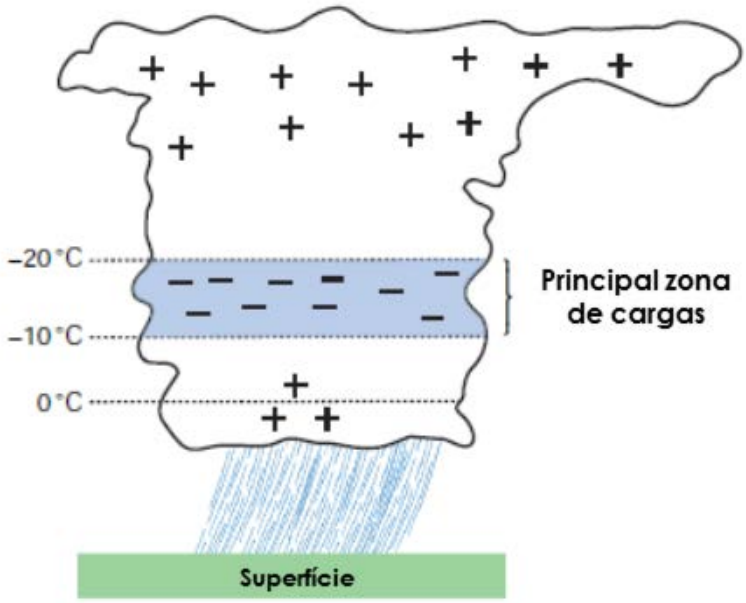

Source: Adapted from Wallace and Hobbs (2005, p. 252).

Due to the complexity, the processes that lead to the electrification of clouds are not yet fully understood. According to Sauders (1993), in the last century three main theories were discussed: convective, inductive, and non-inductive.

3.2.1 Convective theory

In the convective theory, initially developed by Grenet (1947, apud SAUDERS, 2008, p. 337) and defended by Vonnegut (1954), the electrical charge of the

cumuliform cloud occurs by the accumulation of positive ions at the base of the cloud that is transported vertically by currents ascending. Positive ions ascend to the top of the cloud. In this region, the positive ions attract negative ions from the environment that end up penetrating the lateral edges of the cloud through the entrainment. The entrained air is colder and denser than the air in the cloud and therefore produces downward movements, transporting the negative ions to the base of the cloud. The cloud then becomes polarized as shown in Figure 3.2.

Figure 3.2 – Scheming of convective theory. a) Start of vertical movement and formation of the cloud composed of positive ions; b) upward current takes positive ions to the top and attracts negative ions from the environment; c) the downward movements take positive ions to the base and polarize the cloud.

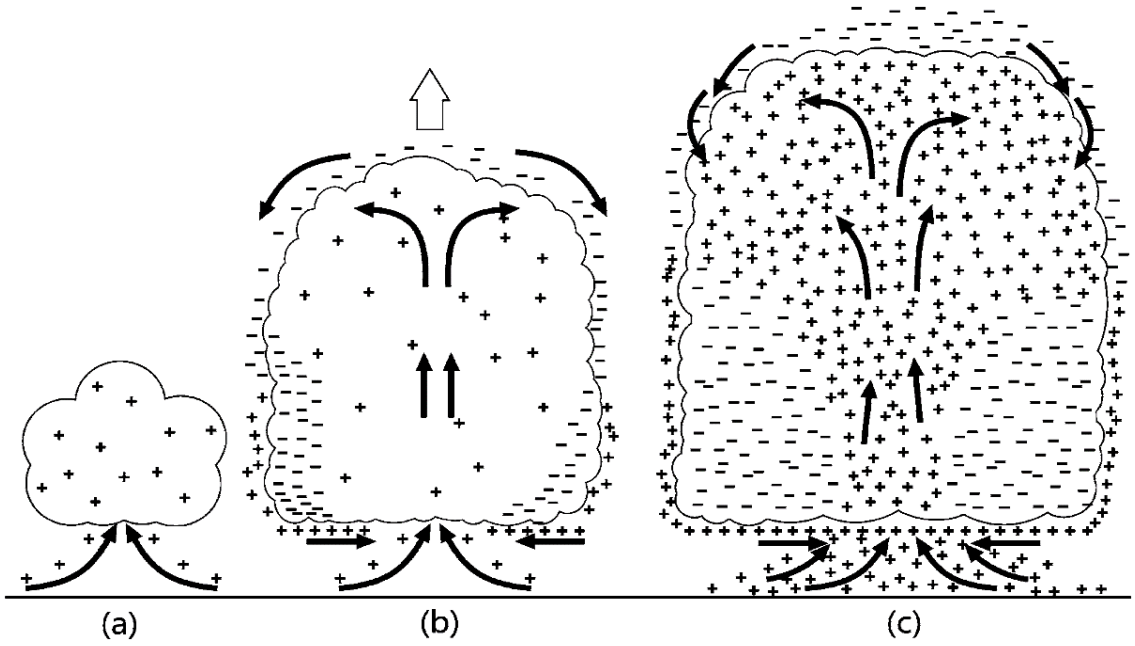

Source: Sauders (2008, p. 337).

Although vertical movements are important for separating charges in convective clouds, the convective theory appears to have a major problem for positive ions below the cloud base. For this to happen, it would be necessary that a cloud electric charge had previously occurred in the region. Therefore, the convective

theory is usually dismissed as an initial mechanism for electrifying clouds (SAUNDERS, 1993).

3.2.2 Inductive theory

The inductive theory was initially proposed by Elster and Geitel (1913, apud SAUNDERS, 1993, p. 645) and suggests that the polarization of the cloud depends on the pre-existence of a vertical electric field. This electric field acts by polarizing the particles of the cloud. When a small particle, which rises upward, hits a large particle, which is falling in the cloud, there is a charge neutralization (Figure 3.3).

Figure 3.3 – Description of inductive theory. a) the particles of the cloud become polarized due to the planetary electric field; b) during the collision of the particles, there is neutralization; c) the particles follow their electrically charged path.

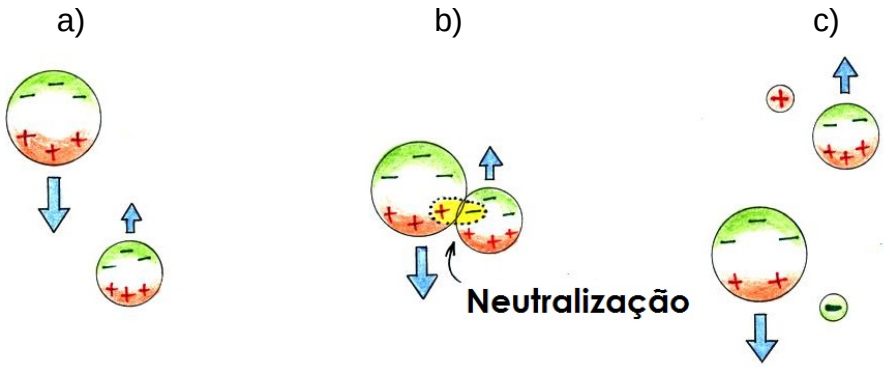

Source: Adapted from the University of Arizona (2015).

According to the review by Sauders (2008), liquid particles tend to coalesce in most cases during a collision. Therefore, charge separation in inductive theory occurs by the collision between ice particles.

Although the inductive theory presents itself as a more likely candidate in the electrification process of the cloud concerning the convective theory (due to the convective theory not being considered as an initial mechanism of electrification of storm clouds), there is still a major problem.

Christian et al. (1980) developed an observational study for the initial period of electrification of storm clouds in New Mexico. The study showed that hail particles had higher charges than could have been generated at the maximum

strength of an electric field measured in a storm. The authors concluded that the inductive theory would be unlikely to explain the first electrical discharges from a storm and that other processes must occur to explain the high values of charges in the hail particles.

3.2.3 Non-inductive theory

The non-inductive theory, or Reynolds-Brook-Gourley theory, was proposed by Reynolds et al. (1957) and suggests that the cloud is polarized by the shock between ice particles without the need for the pre-existence of an electric field. The non-inductive theory is directly related to cloud microphysics and, as it does not require external factors, the concept can be applied in the microphysics parameterization of numerical models of weather and climate. For this reason, the non-inductive theory will be described in more detail in the paragraphs below.

Reynolds et al. (1957) carried out experiments in the laboratory to understand the electrification process of storm clouds. He was a pioneer in this type of study where the electrification of the cloud did not involve external factors. The authors observed that the collision between particles of hail and ice crystal generated separation of charges and electrified the cloud. They also noted that liquid water content and temperature were important factors in cloud polarization. The charge transfer occurs due to the exchange of mass during the shock between the ice particles. For cloud regions with temperatures below -15ºC, hail is negatively charged and the ice crystal is positively charged after the collision. In regions of the cloud with temperatures above -15ºC, the reverse occurs. The result of this separation of charges is a triple polarization of the cloud as can be seen in Figure 3.4.

Due to the theory developed by Reynolds et al. (1957) is related to temperature, it is also known in the literature as thermoelectric theory. Despite this, the liquid water content is also a variable of great importance. During the experiment, the authors noticed that the electric charge of ice crystals became very small when there were few droplets.

Figure 3.4 - Exemplification of the triple polarization of storm clouds according to the Reynolds-Brook-Gorley theory.

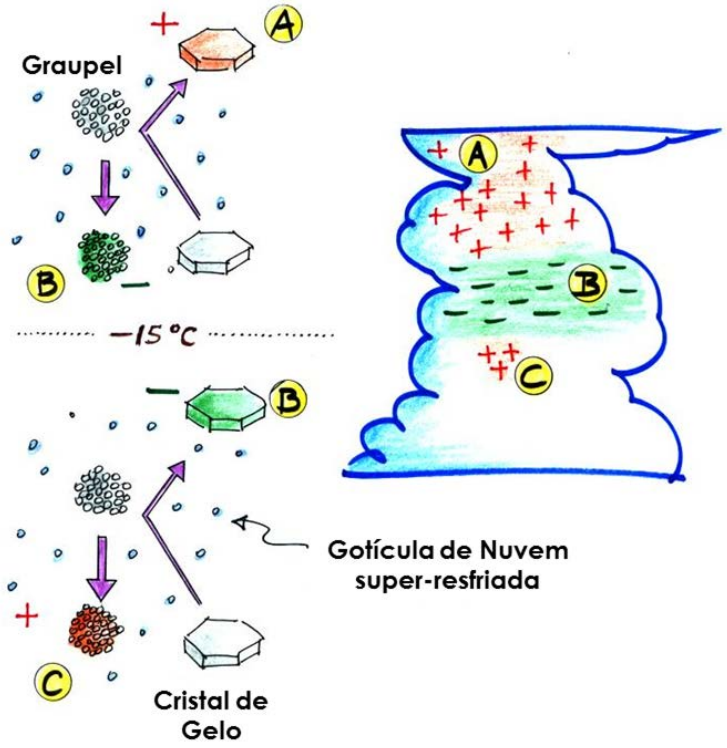

Source: Adapted from the University of Arizona (2015).

Jayaratne et al. (1983) observed that ice crystals, in the absence of droplets, grow by deposition, and can acquire charge. However, in the presence of droplets, the acquired charge is much greater. He also noticed that, in addition to liquid water, the transfer of charges depends on the temperature, speed of fall, and the chemical composition of the droplets.

Two years later, Jayaratne and Saunders (1985) noticed that, in the presence of small droplets (less than 6 micrometers) enough to not be collected by the ice, the crystals grow by deposition and the magnitude of the charge is similar to that found in the experiment with large droplets by Jayaratne et al (1983). Therefore, significant cargo transfers need the presence of liquid water, but not necessarily the ice particle will grow by accretion, as they can grow by deposition.

Baker et al. (1987) observed that significant charge transfers occur when the ice particles grow by deposition. However, the presence of supercooled water

droplets is indispensable. Baker also noted that the "surface state" of the ice particle was important in determining charge transfer. The author suggested that particles that grow faster by deposition are positively charged during the collision.

Sauders et al. (1991) studied the effect of liquid water on the electrification of storm clouds. According to the authors, the presence of liquid water is an essential requirement for the transfer of charges within the cloud. It was concluded that liquid water and temperature are essential variables to determine the signal of the charge during the collision between the ice particles (hail and ice crystals). Figure 3.5 presents the main result of this study, where the authors presented zones of positive and negative charges of hail as a function of temperature and effective liquid water content (fraction of liquid water that is collected by hail).

Figure 3.5 – Positive and negative charge zones of hail as a function of temperature and effective liquid water content (EW).

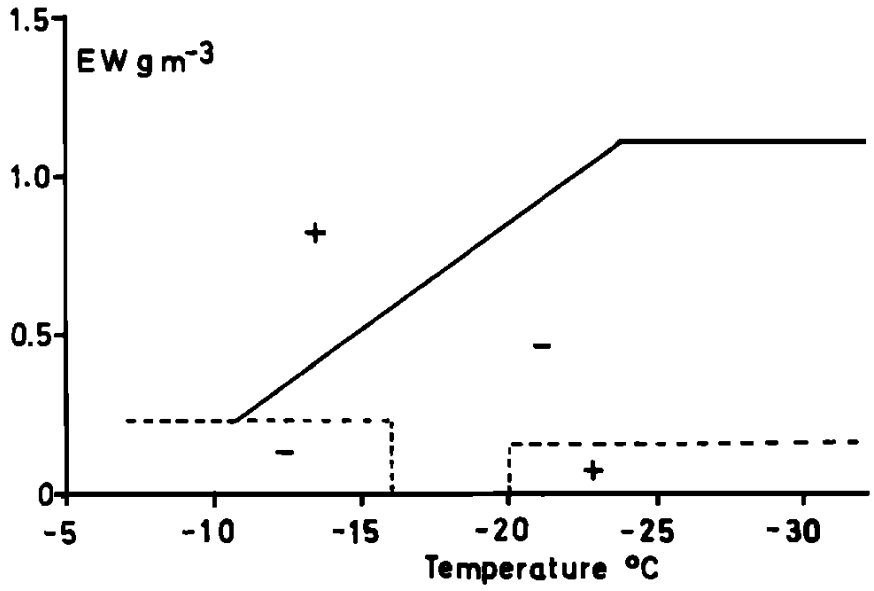

Source: Saunders *et al*. (1991, p. 11014).

Until then, the studies addressed situations that favored the polarization of the cloud, but no study addressed what led to the transfer of charges. Questions

like "what happens in the ice particle to separate charges during the collision?" began to have answers from the 90s, even if not yet fully understood. Baker and Dash (1994) observed that 1) particles that grow faster by deposition are positively charged. 2) Positive charging occurs due to the loss of electrons during the collision between the ice particles. 3) The transfer of charges increases when there is disorder or irregularities on the surface of the ice particle during its formation. He suggested that further studies be done separating the formation of the ice surface during the accretion process and the deposition process and, thus, to understand the irregularities on the ice surface.

In the late 1990s, Avila et al. (1999) studied the effect of the droplet spectrum on charge transfer during collisions of ice particles. During the experiment, the temperature varied between -10ºC and -30ºC, and the droplets were separated into two spectra of different sizes: spectrum A, which had a concentration of smaller particles, and spectrum B, which had a concentration of larger particles. The target particle (hail) grew by the accretion process.

Avila et al. (1999) pointed out that cloud droplets can serve as a source for increasing steam, causing hail and ice crystal to grow by deposition, a mechanism known as the Bergeron process (BERGERON, 1935). For the case of Hail in this experiment, there were two sources of water vapor for growth by deposition: 1) by the environment vapor that is supersaturated concerning ice; 2) by the droplets of water that freeze on the hail surface. However, the freezing process releases latent heat and changes the temperature on the hail surface. This allows the hail surface to remain warmer concerning the environment. According to the author, this can result in sublimation. Therefore, due to the presence of droplets, the final effect is that different regions of the hail surface grow in different proportions.

> […] we see that droplet concentration has important effects in the charge-transfer mechanism. We know that cloud droplets are a source of water vapour leading to graupel and crystal growth by vapour deposition. The vapour can be provided at the surface of the graupel in two ways, from the environment, (which is supersaturated relative to ice because of the presence of the droplets) and from those droplets which freeze over the graupel surface. But, the latent heat released by riming warms the graupel particle, so that it remains warmer than the environment, and induces sublimation of the surface.

> The net effect is that different regions on the surface of a graupel particle grow at different rates […] (Avila et al., 1999, p.1676)

The results showed that the droplet size distribution is important to define the charge signal during transfer. The hail was positively charged at all temperature values (between -10 and -30) for small droplets. However, below -18ºC in the presence of large droplets, Hail was negatively charged. This second result is similar to the study by Reynolds et al. (1957), who noticed that hail is negatively charged below temperatures of -15ºC.

Dash et al. (2001) created a model that describes the transfer of mass and charge of ice particles. The theory used was based on the studies already presented. Finally, a study at the molecular level has stipulated a theory about what happens on the ice surface during the collision. In addition to the studies already cited, it was based on studies on the rapid growth by deposition on solid surfaces by Pines and Huppert (1985, apud Dash et al, p. 20395), Krim and Palasantzas (1995, apud Dash et al, p. 20395) and Kouchi et al. (1994, apud Dash et al, p. 20395). Rapid growth by deposition produces a rough and coarse surface, with internal defects caused by molecular diffusion that does not incorporate the entire structure. In the case of water, the OH- ions are positioned at the edge of the ice surface, while the positive ion (H +, or proton) diffuses faster away from the surface and towards the center of the ice. This behavior causes the ice surface to become negatively charged and the center to be positively charged.

> […] The OH^- ions are bound to sites by their remaining hydrogen bonds, while positive ions diffuse more readily away from the surface into the ice, thereby creating a charged double layer and a negative surface potential […]. (DASH *et al.*, 2001, p. 20395)

Accelerated growth leads to a higher density of charges. During the collision, the ice particles melt locally on the surface. The OH- ions diffuse in the liquid region, while the positive ion remains more in the center of the ice. The hydrometeor that grew faster (and consequently has a higher density of charges) has a greater fusion and loses negative charges in the collision, being positively charged. Despite the progress, the author did not detail the accretion processes and focused only on the deposition process.

Sauders et al. (2006) carried out a laboratory study with a chamber that simulated the growth of the ice crystal by deposition and the growth of hail by accretion. The objective was to detect the signal of the charge transferred during the collisions of the ice particles. The ice crystals grew in a chamber separate from the supercooled water droplets. Only at the moment of collision with hail were the particles mixed. This methodology was used to avoid ice supersaturation during crystal growth (Bergeron process).

> The present data were obtained by mixing ice crystals grown in one cloud chamber, having a limited vapour supply, with supercooled droplets from a second chamber where they experienced no competition for vapour. The two clouds were mixed on their way to a riming target representing a falling graupel pellet and the charge sign during ice crystal rebounds was detected. The mixing time was sufficiently short that the ice crystals had insufficient time to increase their temperature to the appropriate value for their enhanced growth in the higher supersaturation. The continually replenished droplet cloud is above water saturation while the crystal cloud, because of competition for the limited vapour available, is subsaturated with respect to water, but supersaturated with respect to ice. (SAUNDERS *et al.*, 2006, p. 2669)

During the mixing of the hydrometeors, the ice crystal passes into an environment saturated concerning water and supersaturated concerning ice and experiences rapid growth by deposition. This would lead to rapid growth of the ice crystal. The author's idea was based on Baker (1987) who detected a significant transfer of charges when the ice grows rapidly. The author concluded that the droplet is important for growth by deposition of ice, which is important for creating a high magnitude of charge separation during ice collisions, and for determining the particle signal during charge transfer in the collision.

3.3 Electric discharges in the atmosphere

As the polarization of the cloud increases, the magnitude of the electric field also increases. Lightning must appear to diminish or neutralize the electric field of the cloud (MACGORMAN; STRAKA; ZIEGLER, 2001).

Lightning can be defined as an atmospheric electrical discharge that, in general, occurs in storm clouds due to the large accumulation of electrical charges (PINTO JUNIOR, 2005, apud ZEPKA, 2011, p. 23-37). Lightning have different classifications according to their origin and final position (Figure 3.6).

> Os relâmpagos mais freqüentes começam e terminam dentro da nuvem e são chamados intranuvem (IN). O raio é definido como relâmpagos que ocorrem da nuvem para o solo. Eles representam cerca de 70% do número total de relâmpagos e isso se deve ao fato da capacidade isolante do ar diminuir com a altura em função da diminuição da densidade do ar e devido à maior proximidade de centros de carga de polaridades opostas. Relâmpagos mais raros que terminam na atmosfera são as descargas no ar (DA). Os outros tipos de relâmpagos conectam-se ao solo e são os nuvem-solo (NS) e solo-nuvem (SN). Dependendo da carga efetiva que é transferida para o solo, eles ainda podem ser separados em positivos e negativos. O mais comum dos relâmpagos NS é o nuvem-solo negativo (NS-), observado em cerca de 90% dos casos. Os restantes 10% são basicamente nuvem-solo positivos (NS+). (PINTO JR., 2000, apud ZEPKA, 2011, p. 35-36).

Figure 3.6 – Types of lightning in storms.

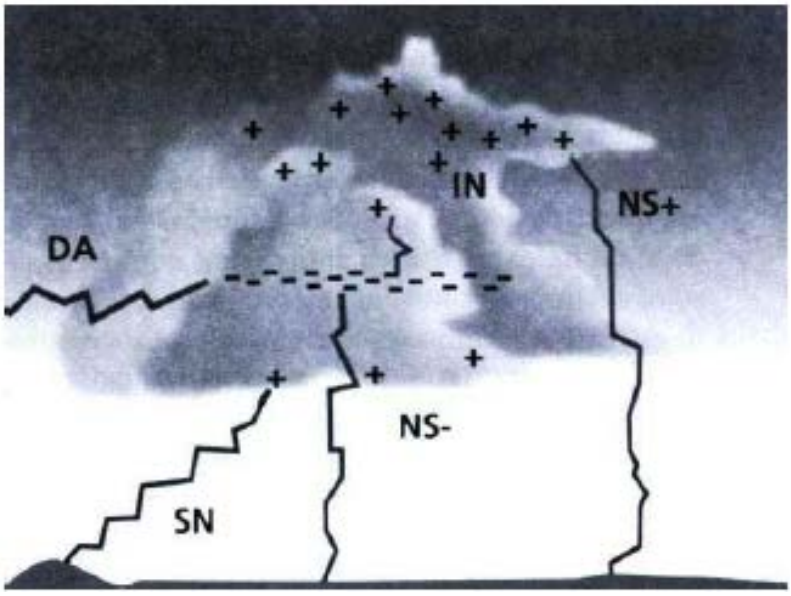

Source: Pinto Junior (2000).

The average global distribution of lightning strikes can be seen in Figure 3.7, which was produced through satellite observations. Note that the lowest electrical activity is concentrated on the oceans, while the opposite occurs on the continent (CRISTIAN ET AL., 2003).

According to the Atmospheric Electricity Group (ELAT) of the National Institute for Space Research (INPE), due to its territorial extension, Brazil is the country with the highest incidence of lightning per year. There are about 78 million

discharges that cause, on average, 100 deaths, and an annual loss of R$ 1 billion (ELAT, 2009).

Figure 3.7 – Average annual distribution of the total lightning strikes observed by satellites.

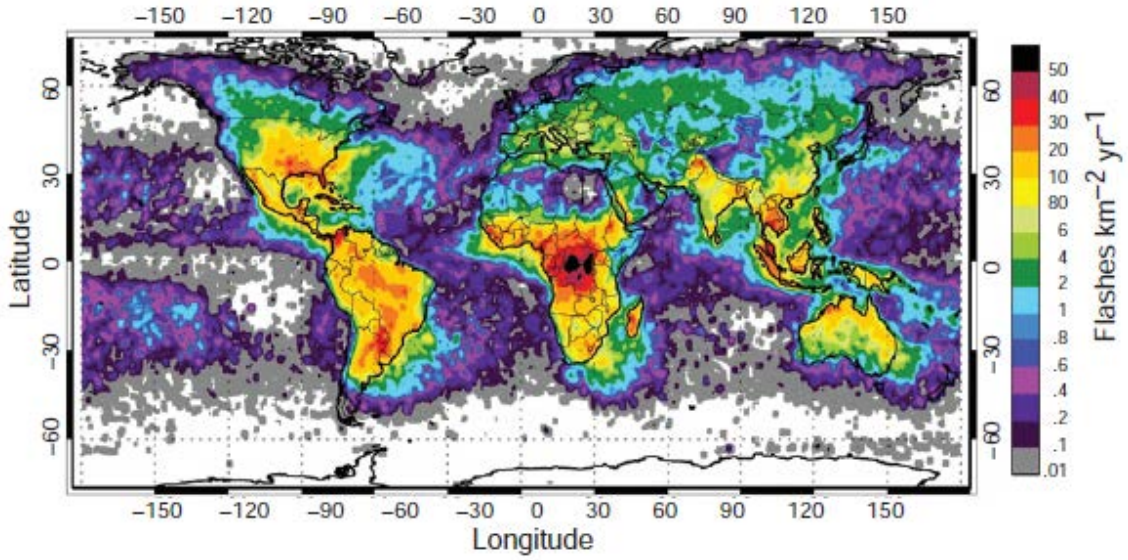

Source: Cristian et al. (2003, p. 5).

3.4 Prognosis of electrical discharges in numerical models

Although complex and not fully understood, lightning strikes can be predicted. Several studies have shown an effort to present methodologies capable of predicting the occurrence of lightning using numerical models of the atmosphere (PRINCE; RIND, 1992; MACGORMAN *et al.*, 2001; MCCAUL JUNIOR, *et al.*, 2009; ZEPKA, 2011).

But what would be the importance of obtaining an accurate prognosis of electrical discharges? The lightning forecast can be used in studies on the climatology of the electrical activity of storms, global electrical circuit, production of NO_x, identify possible areas of fires, assist short-term forecasting (PRINCE and RIND, 1992), and, as will be seen in the next section, the influence of electrical activity on cloud droplets autoconversion (consequently on rain production).

Price and Rind (1992) developed a simple lightning prediction methodology based on an empirical relationship between the occurrence of lightning and the height of the top of the cloud. The authors generated different formulations to diagnose the electrical discharge over the continent and the ocean since the storm dynamics in these regions differ and the frequency of lightning strikes is much lower over the ocean. The authors obtained results that are in agreement with the distribution and frequency of the observed data used.

MacGorman et al. (2001) developed a method to diagnose the occurrence of lightning in numerical models to simulate the location and structure of rays individually. The authors' idea was based on the electric field within the storm clouds generated by the separation of charges. As the polarization increases, the magnitude of the electric field increases. The electrical discharge must arise to neutralize or limit the magnitude of the electric field. The authors' methodology adopted a limit value of the electric field (150 kV.m-1) so that the parameterization was initiated and a lightning bolt was generated. The simulations showed that the structure of the electrical discharge was similar to that of the discharges observed.

McCaul Junior. et al. (2009) developed a lightning forecasting methodology in the Weather Research and Forecast Model (WRF), based on the concepts of cloud microphysics in the non-inductive theory of Reynolds et al. (1957). The method is completely based on the ice fields generated by the WSM6 cloud microphysics of the WRF model. Initially, the authors developed two empirical equations to predict electrical discharges. The first (named F1) was a function of the vertical flow of hail in the column in the mixed-phase region of the cloud at -15ºC. The second (named F2) was based on the vertical integration of ice in the column (according to the authors, when integrating the entire column of ice, it is also considered rays that occur in the cumulonimbus anvil). F1 and F2 were compared with data observed for calibration and detection of minimum values for the occurrence of an electrical discharge.

$$F1 = k_1(wq_g) \quad (3.1)$$

$$F2 = k_2 \int \rho\,(q_g + q_s + q_i)dz \quad (3.2)$$

Where, w is the vertical velocity, q_g is the hail mixing ratio, q_s is the snow mixing ratio, q_i is the ice crystal mixing ratio, k_1 and k_2 are adjustment coefficients

After analyzing the results, McCaul Junior et al. (2009) noted that F1 was better to represent the time series and F2 better represented the area of electric discharges. To merge the temporal representation with the coverage area, the author generated a third methodology (named F3).

> Our observations of lightning threat indicate that ice detrained in storm anvils, which is accounted for by threat F2 and its contribution to the blended threat F3, should not be neglected in the assessment of the total lightning threat (MCCAUL JR.; GOODMAN; LACASSE; CECIL, 2009, p. 727).

More recently, ZEPKA (2011) developed a probabilistic methodology to determine the occurrence of lightning. His work was based on a series of atmospheric indices and meteorological variables produced by the numerical model WRF: CAPE, Survey index (LI), K index (KI), average vertical speed between 850 and 700 hPa, integration of the ice mixing ratio from 700 to 500 hPa. The combination of these indices and variables was performed by two methods (linear and normalized) to determine the probability of electrical discharge occurring. Their results showed that the normalized method was the one that best represented the probabilistic occurrence of electrical discharges, pointing out the most propitious regions for the occurrence of events.

Perhaps the biggest difference between the work of McCaul Junior et al. (2009) and Zepka (2011) is the possibility of quantitatively determining electrical discharges. Probabilistic forecasts are essential to determine areas of possible activity of the meteorological phenomenon. Quantitative predictions of electrical discharges may (or may not) present positioning errors. This occurs because the parameterization of electrical discharges (or any other parameterization) is a function of other meteorological variables calculated directly in the model grid,

which can be predicted with a certain degree of the deficiency by the numerical model during its integration.

However, only in quantitative forecasting is it possible to define the degree of intensity of the phenomenon, useful for issuing danger alerts, for example (besides, when the variable is quantified, it is possible to propagate its effects in the atmospheric model grid, as will be seen in session 4.3)

3.5 Electric discharge and storm rain production

Over the years, many studies have shown the relationship between electrical discharges and increased rain production (MOORE ET AL, 1962; MOORE ET AL, 1964; LATHAM, 1969; SARTOR, 1973; LIST; FREIRE, 1981; ZHOU ET AL, 2002; KOUTROULIS ET AL., 2012).

> It was observed here that lightning strokes from clouds frequently occurred in the absence of intense precipitation echoes nearby, that shortly after the discharge a new echo suddenly appeared within the cloud and intensified rapidly, and that heavy rain fell to the ground 60 to 180 seconds after the stroke (MOORE *et al.*, 1962, p. 207).

Sartor (1954) published a laboratory study relating the collision and coalescence efficiency of droplets in the presence of an electric field. The author concluded that the electrical force can generate coalescence between cloud droplets. Goyer (1960) also carried out a laboratory study and obtained results similar to Sartor's (1954). The author noted that the electric field can influence the growth process of the cloud droplet.

Moore et al. (1962) and Moore et al. (1964), through observations, detected that the electrical discharge is the cause and not the result of the large volume of rain during storms with electrical activity. Moore et al. (1964) concluded that 30 seconds after an electrical discharge the mass of some cloud droplets increases by up to 100 times. The result is the formation of raindrops. Besides, Moore et al. (1964) observed that the increase in the size of the cloud droplet occurred both in regions below and above the 0ºC isotherm. However, Latham (1969) and Sartor (1973) concluded that only droplets below the 0ºC isotherm level grew during electrical activity.

In the 1960s, many studies pointed out that the cloud's electric field promotes collisions between small cloud droplets that would not collide in the absence of the electric field (PRUPPACHER, 1963; LINDBLAD; SEMONIN, 1963; WOODS, 1965; PLUMLEE; SEMONIN, 1965; SEMONIN; PLUMLEE, 1966; LATHAM, 1969).

But why does the electric field mainly influence cloud droplets? The trajectory of hydrometeors within the cloud is a function of gravitational, aerodynamic, and electrical forces. The small cloud droplets undergo a greater change in trajectory due to their low inertia (PLUMLEE; SEMONIN, 1965).

> The rain gush frequently observed after a lightning discharge is an expected consequence of the electrical forces acting on the charged particle terminal velocities in a direction that tends to accumulate them in regions of strong electric fields. (SATOR, 1973, p.31)

Much of the studies that relate the electrical activity of storms to collision efficiency or coalescence of particles is applied to cloud droplets that are not electrically charged, that is, they take into account only the electric field of the cloud. However, some studies include the individual influence of the electrical charge of particles on the collision and coalescence process (WOODS, 1965; SEMONIN; PLUMLEE, 1966; SUMIYOSHITANI, 1994).

Figure 3.8 shows the difference in jobs that treat hydrometeors as neutral and jobs that treat as electrically charged. The electric field acts differently in these cases.

Figure 3.8 – Actuation of the force ($\vec{F}$) of an electric field on a negatively charged particle (left) and a neutral particle (right).

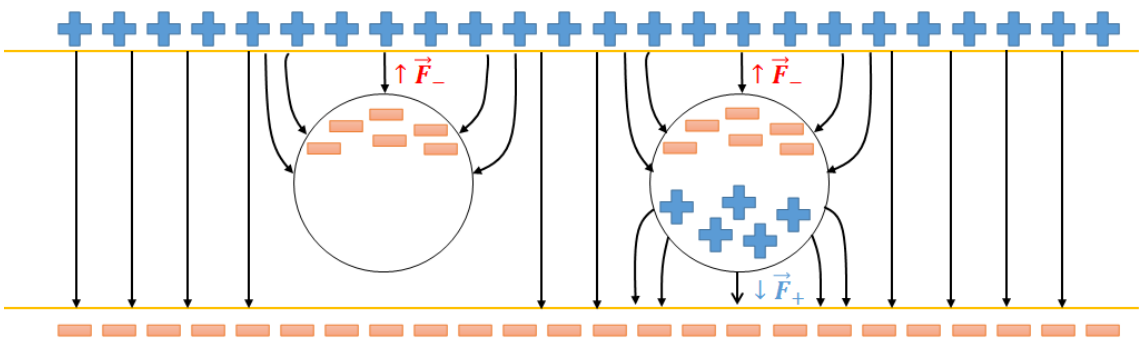

Semonin and Plumlee (1966), for example, carried out a laboratory study on the collision efficiency between charged cloud droplets. They concluded that the particle must have a charge of at least $10^{-16}C$ or the electric field of the cloud must exceed 900 v/cm for the electrical effects to influence the collision efficiency.

Woods (1965), also in a laboratory study, experimented on the effect on the coalescence of electrically charged cloud droplets of the same size. He noted that for cloud droplets with radii less than 40 μm the electrical charge of the particles must be opposite and at least $5 \times 10^{-5} e.s.u$ [1]. For particles with a radius bigger than 40 μm, coalescence occurs spontaneously, even when the droplet is not electrically charged. However, the coalescence rate increases linearly with the electrical charge of these particles

A more complete study was done by Sumiyoshitani (1994), the author considered the interaction between water droplets in an environment with and without an electric field (the electric field could change direction during the experiment). It was also considered that the particles could have a high electrical charge, a low charge, or be neutral. The objective was to understand the changes in the efficiency of collecting cloud droplets in the presence of electrical activity of the cloud. For that, Sumiyoshitani (1994) created a model that generated all the necessary interactions. The author concluded that the electric field has a great influence on the trajectory of the droplets. Neutral or lightly charged particles experience an increase in collection efficiency. On the other hand, in highly charged particles the collection efficiency decreased.

> From the calculated results, the driving of a droplet by the electric field has a large effect on collection efficiency in CDS (charged droplet scrubbers). For slightly charged or neutral particles, the increase of a droplet velocity by the electric field increases the collection efficiency. For well-charged particles, the increase of a droplet velocity by the electric field decreases the collection efficiency (SUMIYOSHITANI, 1994, p. 71).

[1] e.s.u ou statcoulomb (statC) is a unit of measurement for electrical charges which has a value of approximately $3{,}33564 \times 10^{-10} Coulombs\ (C)$.

Unlike Semonin and Plumlee (1966) and Sumiyoshitani (1994), Woods (1965) did not present results regarding the effects of the electric field in his experiments. On the other hand, Semonin and Plumlee (1996) did not include neutral particles and variations in the electric field as Sumiyoshitani (1994). Due to complexity and uncertainties, laboratory and computational studies tend to present methodologies and results with different approaches.

Despite this, the results of the works show an increase in the efficiency of collision, coalescence, or collection when there is an electrical activity for a collision between cloud droplets (mainly the smaller ones), except for particles with charges of the same signal or highly charged.

A study, neither laboratory nor computational, with details on the influence of the electrical activity of storm clouds and the orientation of hydrometeors was done by Metcalf (1994). The author conducted an observational study using a polarimetric radar and noted rapid changes in the cloud's electric field caused by electrical discharges. According to the author, these rapid changes in the electric field have changed the orientation of hydrometeors within the cloud.

Another study using data observed in the field was that of Soula and Chauzy (2001). The authors studied the correlation between Cloud-to-Ground electrical discharges and precipitation during storms. The results showed that positive electrical discharges are associated with a greater volume of rain about negative electrical discharges. Considering the contribution of each lightning strike, the authors were able to estimate the production of rain from each electrical discharge.

Zhou et al. (2002) also estimated precipitation based on data from lightning strikes. Using data from weather radar, the authors sought the correlation between rain and lightning data and subsequently developed an empirical equation to estimate precipitation.

> We have studied the convective systems that developed during two cold front processes passing over the observation area and found that the cloud-to-ground lightning can be an important factor in the precipitation estimation (ZHOU; QUIE; SOULA, 2002, p. 107).

More recently, Koutroulis et al. (2012) presented an article that related the electrical activity of storms to high rainfall values that lead to the occurrence of flooding on the island of Crete. The maximum significant correlation was obtained in a circular area with a 15 km radius around the rain region that was accumulated for 15 min after the electrical discharge. The authors noted an increase in the electrical activity of the cloud during the onset of storms that produced the floods.

3.6 Lightning NOx

Lightning NOx is produced from the division of diatomic molecules of N2 and O2 as a result of the extreme heat around the electrical discharge channel. The temperature can be higher than the surface of the Sun exceeding 25,000ºC. It leads to the formation of NO in a process known as the Zel'dovich Mechanism (Zeldovich et al., 1947) described by:

$$O_2 \leftrightarrows O + O$$
$$O + N_2 \leftrightarrows NO + N$$
$$\underline{N + O_2 \leftrightarrows NO + O}$$
$$N_2 + O_2 \rightleftarrows 2NO$$

The Zel'dovich Mechanism and the photodissociation process lead to fundamental implications for the chemistry of the atmosphere and, consequently, for the Earth climate. Tropospheric ozone is formed as a nonlinear function of NOx concentration (in the presence of carbon monoxide and volatile organic compounds). In clear air outside of the cloud, increasing NOx concentration (but not too much) leads to O3 production (LIU, 1977; SCHUMANN; HUNTRIESER, 2007; BOND ET AL., 2002; EHHALT; ROHRER, 1994). Unlike ozone in the stratosphere that acts by limiting the amount of ultraviolet radiation reaching the surface of planet Earth, tropospheric ozone is an important greenhouse gas that acts on global warming.

Since thunderstorms are becoming more frequent as a response to global warming (DIFFENBAUGH ET AL., 2013; SEELEY; ROMPS, 2015; YE ET AL.,

2016), it reflects in more lightning NOx production. As a consequence, lightning NOx could contribute to large concentrations of tropospheric O3 that act to increase the radiative forcing and may lead to more warming and more thunderstorms. Therefore, lightning NOx should contribute to positive feedback in Earth's climate (WILLIAMS ET AL., 1992; SCHUMANN; HUNTRIESER, 2007).

Using atmospheric electric discharge data from the US National Lightning Detection, Kaynak et al (2008) calculated NOx emissions from lightning over the United States of America based on DeCaria et al (2005), which estimated 500 moles NOx per flash. The results show that lightning NOx accounts for 30% of the total NOx emissions between July and August. In some cases, the lightning NOx emissions caused a significant increase in ozone surface concentration simulated in the Community Multi-scale Air Quality Model (CMAQ).

Gressent et al (2014) investigated the influence of lightning NOx on large-scale O3 plumes in the upper troposphere. The authors used O3 observations measured MOZAIC programme (Measurement of Ozone, water vapor, nitrogen oxides, and carbon monoxide). The large-scale plumes were observed downwind of the thunderstorm. The results show that in 74% of the large-scale plumes there was a positive west to the east zonal gradient of O3. The authors concluded that the positive gradient of O3 is associated with photochemical production from lightning NOx.

Murray (2016), studying the influence of lightning NOx in the air quality, concluded that NOx produced by lightning has a strong influence on O3 concentration. However, the author pointed out that the magnitude and distribution of lightning NOx are poorly understood and this can be minimized by improving the ability of models to reproduce the climatology of lightning obtained by satellites.

Lightning NOx remains one of the least understood sources of NOx and it shows large variability in estimations that causes a lot of uncertainties (Schumann and Huntrieser, 2007). In a literature review on the production of

NOx by lightning, Schumann and Huntrieser (2007) noted estimates of NOx ranging from 33 to 600 mol per lightning strike. The authors suggested that the value of 250 mol/flash can be used as a global average estimate.

Studies suggest that CG lightning produces more NOx than those of the IC type (PRICE ET AL., 1997; KOSHAK, 2014). However, IC lightning accounts for 70% of global electrical discharges and therefore contributes as much as CG lightning in the global NOx balance.

Using data observed in situ of NOx in India in pre-monsoon and monsoon periods, Pawar et al (2012) noted values of mixing ratio between 2 and 9 ppbv of NOx one day before and one day after the occurrence of electrical storms at lower levels the troposphere. Maximum peaks of up to 60 ppbv of NOx were observed during electrical storms.

Evaluating a three-dimensional cloud model that produces NOx as a function of lightning at high levels in the troposphere, Ott et al (2007) found the average value of 2.62 ppbv in the simulations and reported that the average observed data was 2.4 ppbv. Globally, at low levels in the troposphere, the average NOx mixing ratio is approximately 0.25 ppbv. On the other hand, near the cities and over the surface, NOx concentrations are of the order of 100 ppbv (TRIJONIS, 1978).

NO3 and N2O5, NOx related chemical species, measurements on an aircraft as part of the New England Air Quality Study campaign between July and August 2004 showed values between 0.001 and 0.05 ppbv of NO3 and values between 0.025 and 0.17 ppbv of N2O5 in the lower troposphere (BROWN ET AL., 2007). During the global chemical expeditions of GAMETAG (Global Atmospheric Measurement Experiment of Tropospheric Aerosols and Gases), values between 0.2 and 0.8 ppbv of HNO3, also a NOx related chemical specie, were observed in middle latitudes and the lower troposphere (HUEBERT; LAZRUS, 1978).

Tie et al. (2002) developed a parameterization to calculate a lightning activity and thereafter the NOx production by electric discharge. The parameterization

is based on the height of the convective clouds and in global NOx production estimated from satellites. The results are compared to airborne measurements to find the global production of NOx due to lightning activity. The authors reported that during the simulations lightning was responsible to increase the NOx concentrations by more than 500% in the tropical troposphere.

Lamarque et al. (1996) a study to detect the relative contributions of different NOx sources in the troposphere. The authors modified a three-dimensional global chemistry transport model to obtain the individual contribution of each NOx source. The results suggest that lightning is the most dominant source of NOx in the southern hemisphere, while in the northern hemisphere is most influenced by combustion and aircraft.

Bond et al. (2002) pointed out the importance of lightning NOx in the tropics using lightning measurements from the Lightning Imagine Sensor (LIS). Following the suggested values of Price et al. (1997), the authors adopted the production values of 6.7×10^{26} and 6.7×10^{25} NO molecules for each cloud-to-groud (CG) and Intracloud (IC) flashes, respectively. The results showed annual NOx production by lightning is estimated to be approximately 23% of the total within the tropics. Considering only emissions over the ocean, lightning represents almost all NOx emissions

Table 3.1 – Seasonal nitrogen oxide production by sources in the tropics (Tg N).

	Anthropogenic activity	***Biomass burning***	***Soil release***	***Lightning discharges***
DJF	1.95	1.46	1.34	1.34
MAM	1.97	2.25	1.20	1.66
JJA	1.94	1.68	1.61	1.60
SON	1.95	2.89	1.29	1.73
Annual	7.81	8.28	5.44	6.33

Source: Adapted from Bond et al. (2002).

In addition to the type of lightning, the production of NOx by electrical discharge may be a function of other factors, such as the duration of the lightning and its polarity. These factors are even more complex to account for. Due to the

difficulty of indirect measurements of NOx production by electrical discharges, there are uncertainties in the real contribution of lightning to the chemistry of the Earth's atmosphere. To deal with these uncertainties, several studies have adopted average values of NOx emission by electric discharge obtained through campaigns, laboratory studies, and/or numerical studies (WANG ET AL., 1998; OTT ET AL., 2007, OTT ET AL. , 2010).

Another important issue concerns the vertical profile of NOx produced by lightning. Pickering et al (1998) developed a parameterization to build mass distribution profiles of NOx produced by lightning using information from a cloud resolution model. The authors determined a vertical profile of NOx with a small fraction of mass in the average levels and most of it distributed in the high and low levels as a result of the transport of the upward and downward currents of the storms.

However, Murray (2016) pointed out that this C-shaped profile is out of date and that recent studies (OTT ET AL, 2010) show a unimodal distribution with maximum NOx values in the average troposphere levels in cases of storms in the middle and maximum latitudes of NOx in the upper troposphere in cases of storms in the tropics.

4 MATERIALS AND METHODS

The present work has for objective to propose a methodology of prognosis of electric discharges in the regional model Eta through the information of the microphysics of clouds and the convection. Subsequently, the effects of lightning on rain production must be included in the numerical model grid. In 4.1 a brief description of the Eta regional model and parameterization, in 4.2 the cloud microphysics that will be used in this study, in 4.3 the parameterization of electrical discharges proposed will be detailed, in 4.4 details of the assessment methods, and 4.5 the data that will be used throughout the experiments and simulations.

4.1 Eta Model

The Eta model (MESINGER ET AL. 2012) is a finite volume regional atmospheric model. The Eta model uses Arakawa E in the horizontal grid. The vertical coordinate η names. The step topography includes the “cut-cell” treatment. The model can be executed in hydrostatic or non-hydrostatic mode. Further details regarding the dynamics of the model can be obtained in Mesinger et al. (2012).

The model is formed by the set of mass, momentum, and energy conservation equations in the Eta coordinate (Eq. 4.1, 4.2 e 4.3, respectively).

$$\frac{\partial}{\partial \eta}\left(\frac{\partial p}{\partial t}\right) + \nabla \cdot \left(\vec{V}\frac{\partial p}{\partial \eta}\right) + \frac{\partial}{\partial \eta}\left(\eta \frac{\partial p}{\partial \eta}\right) = 0 \qquad (4.1)$$

$$\frac{d\vec{V}}{dt} + f\boldsymbol{k} \times \vec{V} + \nabla\phi + \frac{RT}{p}\nabla p = 0 \qquad (4.2)$$

$$\frac{dT}{dt} - \frac{R}{Cp}\frac{T}{p}\omega = 0 \qquad (4.3)$$

d/dt is the total time derivative, f is the Coriolis parameter, $\boldsymbol{k}$ is the vertical unit vector, ϕ is the geopotential, R is the ideal dry gas constant, c_p is the specific heat at constant pressure, $\vec{V}$ is the wind vector, p is the pressure and T is temperature.

The references to the physics of the Eta model are listed in Table 1.

Table 4.1 – Parameterization schemes of the Eta Model.

PARAMETERIZATION SCHEMES	REFERENCES
Short wave radiation	Lacis and Hansen (1974)
Longwave radiation	Fels and Schwarzkopf (1975)
Terrestrial surface	Ek et al. (2003)
Convection	Janjic (1994)
Cloud microphysics	Ferrier (1994)
Free Atmosphere Turbulence	Mellor and Yamada (1982) level 2.5
Surface Layer Stability Functions	Paulson (1970)

The simulations performed on the Eta model are detailed in Table 4.2.

Table 4.1 – Eta Model Settings during Experiments.

Cases	Cases for the summer of 2017 were selected according to the data available from ELAT (see section 4.5)
Runs	Three continuous runs for each summer month of 2017: 1. From 01/01/2017 0000 UTC to 31/01/2017 2300 UTC; 2. From 01/02/2017 0000 UTC to 28/02/2017 2300 UTC; 3. From 01/03/2017 0000 UTC to 31/03/2017 2300 UTC;
Resolution	10km horizontal and 50 vertical levels
Initial and Boundary Condition	Climate Forecast System Version 2 (CFSRV2) - 0.5ºx0.5 (Saha et al, 2014)

The topography of the domain used during the experiments of this work can be seen in Figure 4.1. The area corresponds to the Southeast region of Brazil.

Figure 4.1 – Topography (m) in the domain of the Eta regional model simulations.

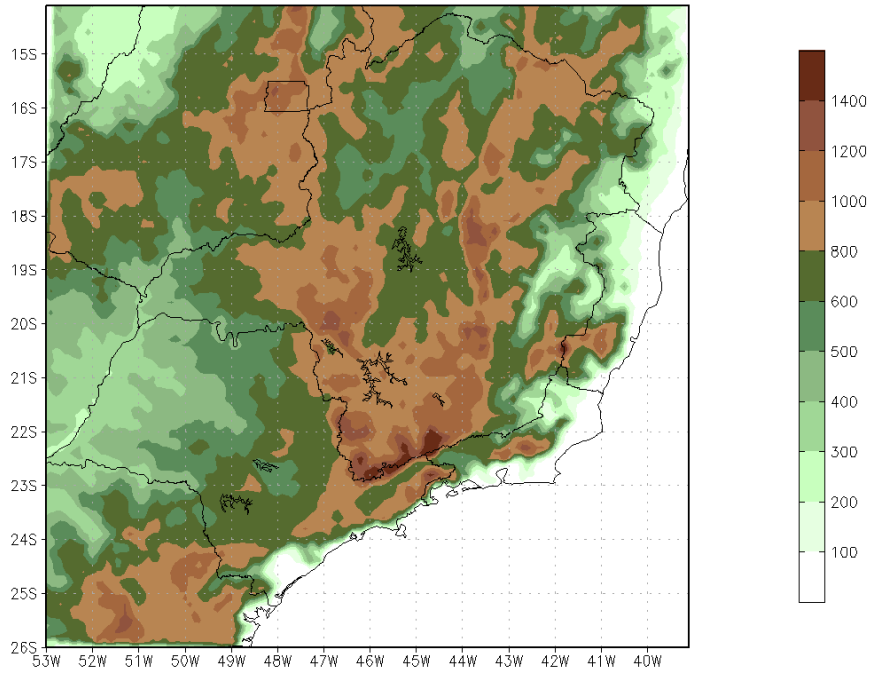

4.2 Ferrier microphysics scheme

The cloud microphysics scheme is the key for the electrical discharges parameterization proposed (which is detailed in section 4.3). Information about hydrometeor species is important for determining possible locations of electrical activity in the cloud.

Although the Eta model of CPTEC/INPE has two versions of cloud microphysics, only Ferrier (1994) parameterization will be used due to the low number of hydrometeor species that are calculated by the cloud microphysics scheme of Zhao and Carr (1997). Therefore, it is necessary to detail the scheme of Ferrier (1994).

Ferrier's microphysical parameterization (hereinafter FR1) is classified as a double-moment Bulk scheme (Double-Moment). FR1 (as well as other microphysical schemes) works with the humidity adjustment in the grid column of the numerical model.

The scheme calculates the mixing ratio of water vapor (q_v), cloud droplet (q_w), raindrop (q_r), ice crystal (q_i), snow (q_s), graupel (q_g), hail (q_h) and liquid water

from precipitating ice species that are growing or thawing into the cloud. Besides, it also simulates the concentration (n) (m^{-3}) of all ice species.

FR1 assumes that the distribution of cloud droplets volume has an exponential form, given by:

$$n(v) = \left(\frac{n_w}{v_0}\right) e^{\left(-\frac{v}{v_0}\right)} \quad (4.4)$$

Where, v is the cloud droplets volume, v_0 is the mean droplet volume and n_w is the droplet number concentration, $n(v)$ is the concentration of a given cloud droplet volume.

The size distributions for raindrops and all ice species is represented by a gamma function, given by:

$$n_x(D) = n_{0x} D_x^{\alpha_x} e^{(-\gamma D_x)} \quad (4.5)$$

Where, n_{0x} is the interception parameter, γ is the slope parameter, α_x is the shape parameter of the distribution, D_x is the diameter of the hydrometeors species.

There are some differences between the original Ferrier scheme and the version that is implemented in the Eta model of CPTEC/INPE (hereinafter FR2). Analyzing the model code, it is noted that the FR2 microphysics scheme has been simplified and is capable of providing the following output variables: mixing ratio of water vapor (q_v), total condensed water (q_{cw}), total ice (q_{ti}), cloud water (q_w), accumulated rain (q_r), and large ice on the surface (q_{li}).

Although FR2 provides only the variable “mixing ratio of total ice”, it is possible to separately obtain precipitable ice (which refers to the sum of graupel, snow, and hail and cloud ice (which refers to ice crystals, which does not precipitate), as both are calculated internally in the algorithm.

Besides, within the FR2 code, the degree of ice accretion is calculated (*Rime Factor*)[1], which makes it possible to differentiate hail from other precipitable particles, as shown in Table 4.3.

Table 4.2 – Degree of ice accretion (Rime Factor) for different hydrometeor species.

Rime Factor	**1.0**	**>1 to ~8**	**~8 to ~40**	**>40**
Hydrometeor Type	Snow without accretion	Snow with accretion	Graupel and Hail	Sleet

Source: Adapted from Barthold e Bodner (2009).

FR2 uses only the exponential function (eq. 4.5) to describe the distribution of all species of hydrometeors. In FR2, cloud droplets that reach 20 μm become available to form raindrops through autoconversion (further details will be presented in 4.3.3). The raindrops are formed with an average diameter varying between 50 μm e 450 μm. The average diameter of precipitable ice particles varies between 50 μm and 1000 μm and depends on the temperature.

Ferrier scheme allows a mixed phase in the cloud in the range of vertical levels with isotherm values between 0ºC and -10ºC. These values differ from the literature, where the mixed phase of the cloud goes from the isotherm level of 0ºC to approximately -40ºC (HOUZE, 1993; STENSRUD, 2007; STRAKA, 2009). This matter will be addressed again in 4.3.

The cloud processes parameterized by FR2 are summarized in Figure 4.1. The precipitable ice particles grow by accretion, aggregation, or deposition. Cloud ice grows only through deposition. The condensation, evaporation, deposition, and sublimation of liquid water are calculated using the Asai algorithm (1965). For the heterogeneous freezing process of liquid particles, the Bigg method (1953) is used.

[1] According to Barthold and Bodner (2009) and Workoff et al. (2013) the degree of accretion (Rime Factor) is defined as the amount of ice growth by the accretion process, where supercooled liquid water collides and freezes on the ice surface.

Figure 4.2 – Summary of processes parameterized by FR2.

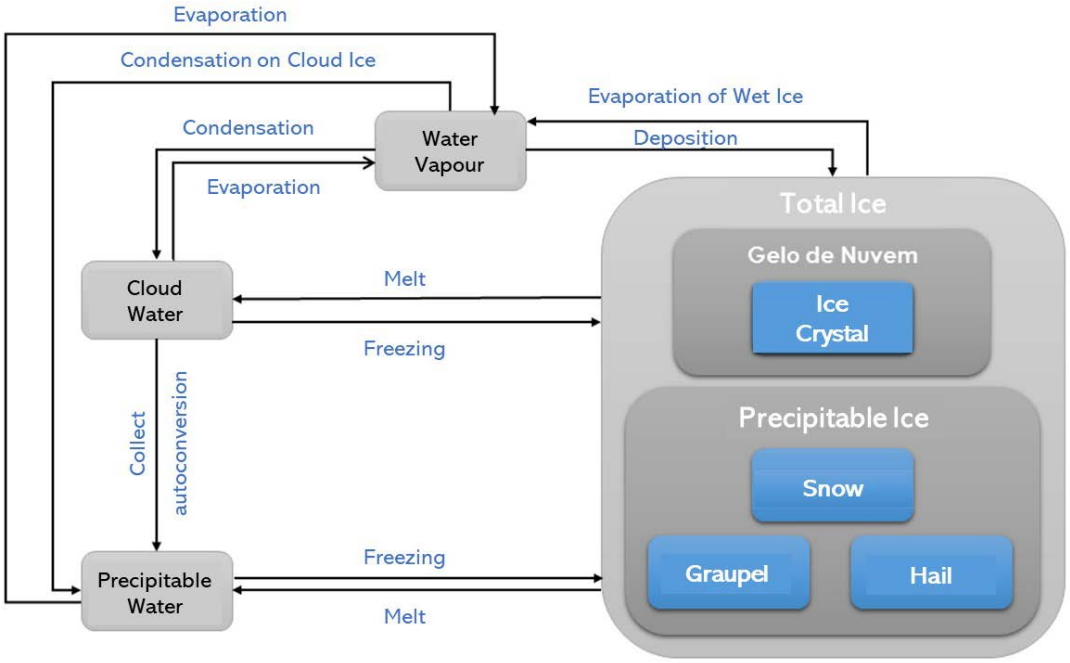

4.3 Parameterization of electric discharges

Most microphysics parameterization schemes can distinguish ice species and physical processes within the cloud, this information can be used to diagnose the occurrence of electrical activity in the grids of numerical models.

As seen in Section 3.2.3, the non-inductive theory of Reynolds et al. (1957) states that the polarization of cumulonimbus clouds occurs due to the collision between particles of ice crystals and hail. The collision between the particles must occur in the presence of super-cooled liquid water and the particles must grow through the process of accretion and deposition.

In the present work, the methodology for the detection of lightning strikes uses information from the Ferrier cloud microphysics scheme and the BMJ convection. Two modifications to the Ferrier cloud microphysics scheme are applied:

1. The calculation of graupel using the precipitable ice diagnoses and the rime factor, which should be between 8 and 40 for graupel particles. The graupel is a type of ice relevant to the electrification process of the cloud according to the non-inductive theory.

2. The increase in the depth of the mixed-phase layer in the cloud to adopt the values known in the literature, which variates between the isotherms of 0ºC and -40ºC (Houze Junior, 1993). The justification for this modification is due to the mixed-phase of the cloud being an important region for the separation of electrical charges (TAKAHASHI 1978; SAUNDERS ET AL. 1991; PEREYRA ET AL. 2000, 2008) and for the growth of ice particles both supercooled liquid water and ice are used in the diagnosis of electrical discharges. The parameterization of lightning needs a cloud layer that contains these conditions.

The parameterization is divided into three parts: 1) Trigger function; 2) Formulation of Electric Discharge; 3) Effects on cloud microphysics and atmospheric chemistry.

4.3.1 Trigger function

For an electrical discharge to occur, there must be a favorable environment for the separation of charges within the cloud. It is important to note that the charge separation in the cloud is not efficient in the initial moments of the storm's life. Assuming that young clouds do not have strong vertical currents to generate graupel particles, electrical discharges will be identified only in storms already developed. The cloud is considered to be electrically charged according to the following criteria:

- Convection parameterization indicates the presence of deep convection.
- Parameterization of the cloud microphysics indicates the presence of ice crystals, graupel, and supercooled water in the mixed-phase layer of the cloud.

Figure 4.3 shows the ingredients in the cloud necessary for the charge separation that may result in an electrical discharge.

4.3.2 Electric discharge formulation

After detecting clouds with storm characteristics and with potential for electrification, the scheme formulates the electrical discharge in the model grid. In addition to ice, liquid water content is also an important factor for the

separation of electrical charges in the cloud, as it determines the sign of the electrical charge transferred during ice collisions and plays a key role in the growth of ice by the Bergeron process (CASTELLANO ET AL. 2004, 2014). Therefore, super-cooled liquid water was also considered to determine cloud electrification.

Based on the study by McCaul Junior et al. (2009) and Lopez (2016), the Latent Cloud Electrification (LCE) variable is defined as the potential energy available for the occurrence of lightning, which is the energy within the cloud that produces the separation of electrical charges. The LCE ($J.m^{-2}$) is calculated by:

$$LCE = \ CAPE_{MP} \int_{Bs_{MP}}^{Top_{MP}} \rho.(q_G + q_i + q_w)\, dz \qquad (4.6)$$

Where, Top_{MP} is the top of the mixed-phase, Bs_{MP} is the base of the mixed-phase, ρ (kg/m^3) is the density of the air, q_G (kg/kg) is the mixing ratio of the graupel, q_i (kg/kg) is the mixing ratio of the ice crystal, q_w (kg/kg) is the mixing ratio of supercooled liquid water. $CAPE_{MP}$ (J/kg) refers to the Available Potential Energy for Convection in the Mixed Phase Layer of the cloud, which is calculated by:

$$CAPE_{MP} = g \int_{BsMP}^{TopMP} \frac{\theta(z) - \bar{\theta}(z)}{\bar{\theta}(z)} dz \qquad (4.7)$$

Where g is gravity, θ is the potential temperature of the air parcel, $\bar{\theta}$ the potential temperature of the environment and z is the height of the air parcel is.

The LCE identifies clouds that contain enough energy for lightning to occur. To obtain the electrical discharges as a function of LCE, the LCE is compared with observations of lightning. A linear regression equation is adjusted to estimate the number of lightning strikes:

$$f_r = a + b.LCE \qquad (4.8)$$

Where, f_r is the lightning rate (number of lightning per timestep and per grid box), which is linearly correlated to LCE through the coefficients a and b. The

scheme accounts for the total lightning and it does not differentiate between intracloud (IC) or cloud-to-ground (CG) types of lightning. a and b are given by:

$$a = \overline{Obs} - b\overline{LCE} \tag{4.9}$$

$$b = \frac{\sum_{i=1}^{n}(LCE_i - \overline{LCE}).(Obs_i - \overline{Obs})}{\sum_{i=1}^{n}(LCE_i - \overline{LCE})^2} \tag{4.10}$$

Where, Obs refers to the observed data of lightning, and the superscript bar refers to the average of the variables in the period. a is a constant that represents the intercept of the line with the vertical axis and b is a constant that represents the slope of the line (slope).

Because some clouds can present ingredients for lightning activity (as ice and supercooled water) and even though do not generate an electric discharge, probably due to the dielectric strength of air (WANG ET AL., 2016), it is imposed a condition in LCE to avoid lightning activity in all situations: the LCE is calculated only if $CAPE_{MP} > 500\ \mathrm{J/kg}$. This condition can be tuned in the future.

Figure 4.3 – Hypothetical Skew-T log p profile with the essential ingridients for the electrification of the storm cloud: ice, super-cooled water, and instability (mixed-phase CAPE). T is the temperature of the environment and T_d is the environment dew point temperature.

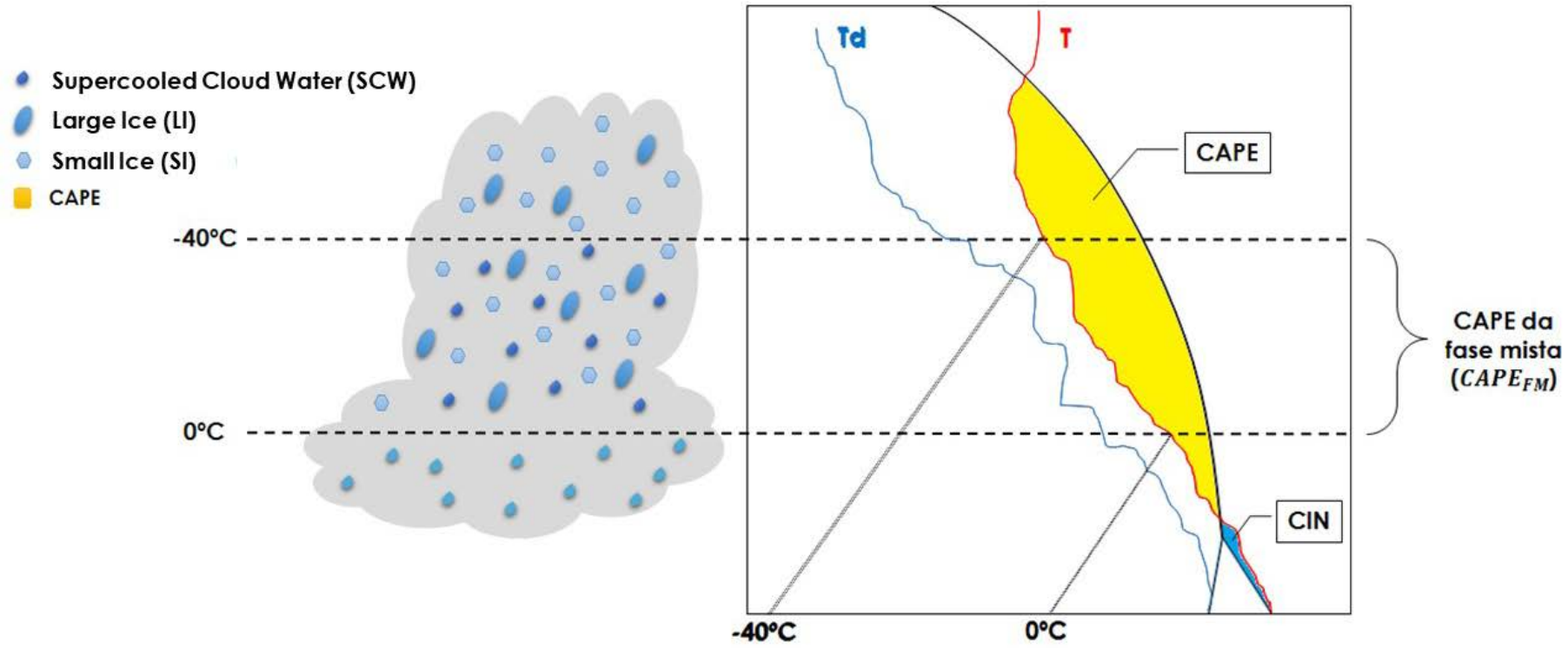

4.3.3 Effects on rain production

Section 3.5 explained the relationship between the electrification of the cloud and an increase in rain production in some cases. As seen, except for electrically charged particles with the same sign and highly charged particles, there is an increase in the collision and coalescence of cloud droplets which increases raindrops.

The natural process of collision and coalescence between cloud droplets begins when the droplet size distribution has a significant concentration with a radius of approximately 20μm. The collision efficiency between droplets with a smaller radius is too small to allow significant population growth. However, during electrical activity, many studies suggest that very small droplets may collide and coalesce (autoconversion) to form raindrops (SEMONIN; PLUMLEE 1966; SATOR 1973; FLETCHER 2013; HORTAL; CARANTI 2012; LUO ET AL. 2016).

The relationship between electrical activity and droplet autoconversion depends on several factors, such as type of lightning, CG or IC, the polarity of the electric discharge, positive or negative, the magnitude of the cloud electric field, duration and intensity of the discharge, droplet concentration, droplet charge, the separation between particles. Due to the complexity of factors involved, the objective in this work was to produce an increase in droplet autoconversion from the relationship between electrical activity and droplet concentration.

In Ferrier parameterization, cloud droplets are available for autoconversion to raindrops when they reach a droplet concentration threshold. To adjust the rate of the autoconversion of cloud droplets to raindrops, it is possible to introduce variations in the value of this threshold. The droplet autoconversion rate (A_T) is given by:

$$A_T = \max\big((q_w - q_{w0}), 0\big) . L \qquad (4.11)$$

Where qw is the cloud water mixing ratio $\left(\frac{kg}{kg}\right)$, qw_0 is the cloud water mixing ratio that should be kept in the cloud $\left(\frac{kg}{kg}\right)$ and L denotes an adjustment

coefficient. Note that q_w must be bigger than q_{w0} for $A_T > 0$. q_{w0} is a function of a droplet concentration threshold:

$$q_{w0} = \left(\frac{\pi}{6}.\rho_l.n_w.{D_w}^3\right)/\rho \quad (4.12)$$

Where n_w is the cloud droplet concentration threshold $\left(\frac{nº\ droplets}{m^3}\right)$, π is equal to 3.1416, ρ_l is the liquid water density $\left(\frac{kg}{m^3}\right)$, D_w is the cloud droplet diameter threshold equal to 20×10^{-6} (m), and ρ is the air density $\left(\frac{kg}{m^3}\right)$. The default value of the autoconversion threshold n_w in the microphysics parameterization of Ferrier is 200x10^6 droplets per m³.

Three experiments are conducted to evaluate the effect of lighting on the autoconversion rate A_T (Table 5.1). The first one is a control experiment (Exp1 in Table 5.1), which has electric discharge diagnoses but no effects on the autoconversion rate A_T. The first experiment uses the default qw_0 equation. In the second experiment (Exp2 in Table 5.1), the n_w threshold value is decreased to 100x10^6 droplets per m³ when:

1. There is electrical activity in the grid in the timestep;
2. In regions of the cloud with temperatures above 0ºC (Latham 1969; Sartor 1973);

In the second experiment the qw_0 is lower than the qw_0 in the first experiment, which means that for $q_w > qw_0$ the autoconversion rate A_T is bigger in the second experiment, then increasing the precipitation in the timestep.

In the first and second experiment, the autoconversion rate A_T is equal to zero in case the droplet concentration does not reach the threshold n_w, in other words, if $q_w \leq qw_0$ then $A_T = 0$. In the third experiment (Exp3 in Table 5.1), qw_0 is equal to 10% of q_w in grid points with lightning activity, which means that 90% of available droplets will be autoconverted to rain. In this situation, the autoconversion rate (A_T) is never equal to zero in the case of electric discharge.

In an observational study, Goyer et al. (1960) applied an electric field to a droplet chamber. The authors noted that the collision efficiency of the droplets increased from approximately 30% to almost 100% after applying the electric field and, consequently, increased the concentration of raindrops. The droplet concentration threshold proposed in this work represents an increase in the production of raindrops under the conditions listed above. This increment aims to correct the underestimation in situations of intense rain in the model.

4.3.4 Effects on NOx production

The lightning scheme calculates the total lightning strikes (CG + IC) in each grid box for each microphysics parameterization time step. Using a simple linear function, it is possible to estimate the amount of NO_x emitted by lightning (LNO_X):

$$LNO_X = N_r . f_r \tag{4.13}$$

Where, f_r is the total of electrical discharges diagnosed by the model and N_r is the NOx emission rate per electrical discharge equal to 250 mol of NOx per electrical discharge following the estimation by Schumann and Huntrieser (2007).

The NO_x generated by the lightning parameterization then undergoes chemical and photochemical reactions. The NO_x chemical reactions can occur in a bimolecular way, where two different molecules participate in the breakdown and formation of chemical bonds; in thermolecular, in which three different molecules participate; or heterogeneous, in which the reaction occurs on the surface of an aerosol particle or a water drop.

All photochemical reactions of the proposed parameterization are estimated using the radiative transfer model of NCAR (National Center for Atmospheric Research), namely Tropospheric Ultraviolet and Visible (TUV) radiation model version 5.3 (MADRONICH; FLOCKE, 1997), as a function of the zenith angle and for many levels of the troposphere.

The lightning effects on atmospheric chemistry start with atmospheric electrical discharges generating NO, calculated from equation 4.13. NO reacts with tropospheric ozone (O_3) to produce NO_2. During the day, NO_2 is photolyzed and returns to NO. Since NO_2 is not photolyzed overnight, it is assumed that all NO is converted to NO_2 and no feedback occurs.

$$NO + O_3 \rightarrow NO_2 + O_2 \tag{4.14}$$

$$NO_2 + hv \rightarrow NO + O \tag{4.15}$$

Where hv represent the photodissociation process.

NO_2 reacts with O_3 to form nitrate radical (NO_3) which in turn reacts with NO_2 to form dinitrogen pentoxide (N_2O_5). During the day, N_2O_5 is destroyed by the photodissociation and collisional decomposition with N_2 or O_2 [M] to return to NO_2 and NO_3.

$$NO_2 + O_3 \rightarrow NO_3 + O_2 \tag{4.16}$$

$$NO_2 + NO_3 \rightarrow N_2O_5 \tag{4.17}$$

$$N_2O_5 + hv \rightarrow NO_2 + NO_3 \tag{4.18}$$

$$N_2O_5 + [M] \rightarrow NO_2 + NO_3 + [M] \tag{4.19}$$

During the day, NO_3 does not reach relevant levels because it efficiently absorbs light in the visible region of the solar spectrum, leading to photolysis for the formation of NO_x. The lifetime of NO_3 during the period of sunlight under typical conditions is approximately 5 seconds.

$$NO_3 + hv \begin{matrix} \rightarrow NO_2 + O \\ \rightarrow NO + O_2 \end{matrix} \tag{4.20}$$

During the day, NO_2 is converted to nitric acid (HNO_3) through a reaction with hydroxyls (OH). HNO_3, in turn, is photolyzed during the day and returns to NO_2.

$$NO_2 + OH \overset{[M]}{\rightarrow} HNO_3 \tag{4.21}$$

$$HNO_3 + hv \rightarrow NO_2 + OH \quad (4.22)$$

Another process of formation of HNO_3 occurs by the heterogeneous reaction between N_2O_5 and water.

$$N_2O_5 + H_2O \rightarrow 2HNO_3 \quad (4.23)$$

Finally, HNO_3 is removed from the atmosphere by diluting it in cloud droplets (rainout) and raindrops below the base of the cloud (washout).

$$HNO_3 + H_2O \rightarrow H^+ + NO_3^- \quad (4.24)$$

The reactions carried out by the proposed scheme are dependent on the concentration of OH and O_3. The concentration of OH and O_3 are obtained using global approximations available in Brasseur and Solomon (2005). These values are only available at certain levels of the atmosphere, so the concentration of O_3 and OH are extrapolated in the vertical column (Figure 4.4) of the model through an adjustment curve according to the vertical pressure levels, given by:

$$OH(p) = 2.47p^2 + 69.60p + 3.74 \times 10^5 \quad (4.25)$$

$$O3(p) = 7.72 \times 10^6(p^2) - 10.25 \times 10^9 p + 3.51 \times 10^{12} \quad (4.26)$$

Where p denotes the vertical pressure levels in hPa.

Figure 4.4 – Vertical profiles of (a) OH and (b) O_3 prescribed in the model.

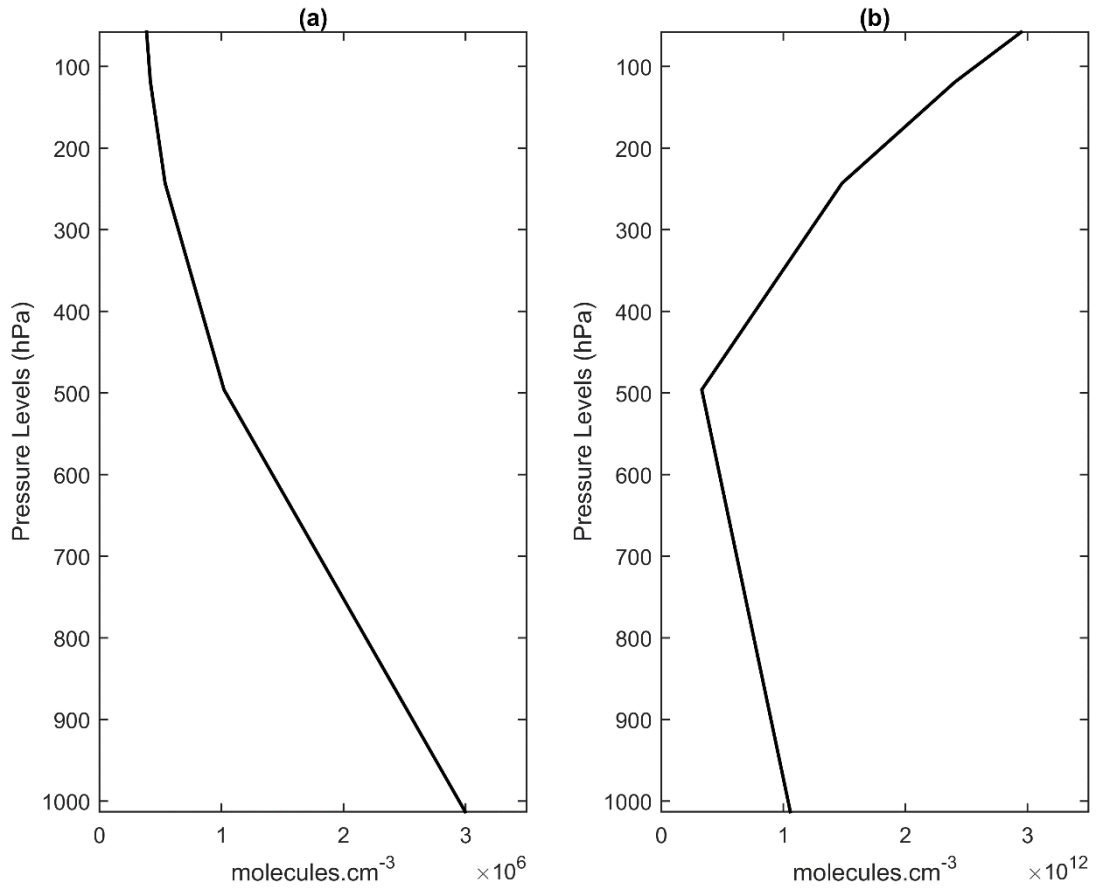

In addition to the washout and rainout of nitric acid, the dry deposition process for NO_x and HNO_3 is also accounted for. The sink dry deposition is the process in which chemical species are transferred from the atmosphere to the planet's surface. The dry deposition flux to the surface (FD) [molecules.cm^{-2}.s^{-1}] is calculated as a function of the density (ρ) and the speed of dry deposition of the species (ddv) [cm.s^{-1}] (BRASSEUR; JACOB, 2017):

$$FD = -ddv.\rho \tag{4.27}$$

The dry deposition rates for NO_x and HNO_3 used in the scheme are 0.5 [cm.s^{-1}] and 4 [cm.s^{-1}], respectively.

The frequency at which chemical reactions occur is calculated using the reaction rate constant (K), given in s^{-1}. All equations below about K were obtained on Brasseur and Solomon (2005).

In the case of bimolecular chemical reactions, K can be calculated by:

$$K(T) = \alpha e^{\left[\frac{-\beta}{T}\right]} \tag{4.28}$$

Where, T is the temperature in Kelvin, α [cm³.s^{-1}] and β [K] are Arrhenius factor and activation temperature, respectively.

In the case of thermolecular reactions, K is calculated by:

$$K_0(T) = K_0^{300}\left(\frac{T}{300}\right)^{-n} \tag{4.29}$$

$$K_\infty(T) = K_\infty^{300}\left(\frac{T}{300}\right)^{-m} \tag{4.30}$$

$$K([M],T) = \left(\frac{K_0(T)[M]}{1+\frac{K_0(T)[M]}{K_\infty(T)}}\right)0.6^{\left\{1+\left[\log_{10}\left(\frac{K_0(T)[M]}{K_\infty(T)}\right)\right]^2\right\}^{-1}} \tag{4.31}$$

Where [M] denotes the density of the air, K_0 and K_∞ are temperature dependent coefficients [cm³.s^{-1}].

The calculation of the reaction rate constant for heterogeneous reactions is proportional to the density of the surface area of the particles and the probability of collision:

$$K = \frac{A\gamma}{4}\sqrt{\frac{8kT}{\pi m}} \tag{4.32}$$

Where A is the surface area density given in $\frac{cm^2}{cm^3}$. A can be calculated if the size distribution of the particles present in the atmosphere is known. k is the Boltzmann constant, γ is the probability of collision, $\pi = 3.14159$, T is the temperature and m denotes the molar mass of the air.

All reactions considered in the model are based on mass conservation and are listed below:

$$\frac{d[NO]}{dt} = LNOX + J_{NO_2}[NO_2] - K_1[O_3][NO] \tag{4.33}$$

$$\frac{d[NO_2]}{dt} = K_1[O_3][NO] + K_6[N_2O_5][M] + J_{HNO_3}[HNO_3] + J_{NO3}[NO_3] + J_{N_2O_5}[N_2O_5] - J_{NO_2}[NO_2] - K_2[OH][NO_2] - K_2[OH][NO_2] - K_3[O_3][NO_2] - K_4[NO_2][NO_3] - FD[NO_2] \tag{4.34}$$

$$\frac{d[HNO_3]}{dt} = K_2[OH][NO_2] + K_5[N_2O_5] - J_{HNO_3}[HNO_3] - K_7[HNO_3] - FD[HNO_3] \tag{4.35}$$

$$[NO_3] = \frac{K_3[O_3][NO_2] + J_{N_2O_5}[N_2O_5] + K_6[N_2O_5]}{J_{HNO_3} + K_4[NO_2]} \tag{4.36}$$

$$[N_2O_5] = \frac{K_4[NO_2][NO_3]}{K_5 + K_6 + J_{N_2O_5}} \tag{4.37}$$

Where, K_1, K_2, K_3, K_4 and K_6 refer to the reaction rate coefficient of reactions calculated by equations 4.17 and 4.20. K_5 is a heterogeneous reaction and it is calculated by equation 4.21, but the calculation of this rate constant is a complex issue that would require a detailed aerosol model. To simplify, it was assumed a conversion lifetime of N_2O_5 to HNO_3 of 2 days, which equals to $5.8 \times 10^{-6}\ s^{-1}$ (BURKHOLDER et al., 2015). K_7 refers to the reaction rate coefficient for wet HNO_3 deposition (rainout and washout) and each J refers to the frequency of photolysis.

The reactions were explicitly discretized, except the equations 4.25 and 4.26, which were implicitly inserted into the parameterization to avoid instability in the simulations because NO_3 and N_2O_5 are short-lived species and the physics time step of the model is too big for the chemical reaction time. The Euler Forward method and the steady-state method (state of equilibrium between the source and the sink of the chemical species without time dependence) were used for explicit and implicit discretization, respectively. Figure 4.5 summarizes the reactions from the lightning NO_x (LNO_X) schematically.

Figure 4.5 – Description of the proposed parameterization scheme.

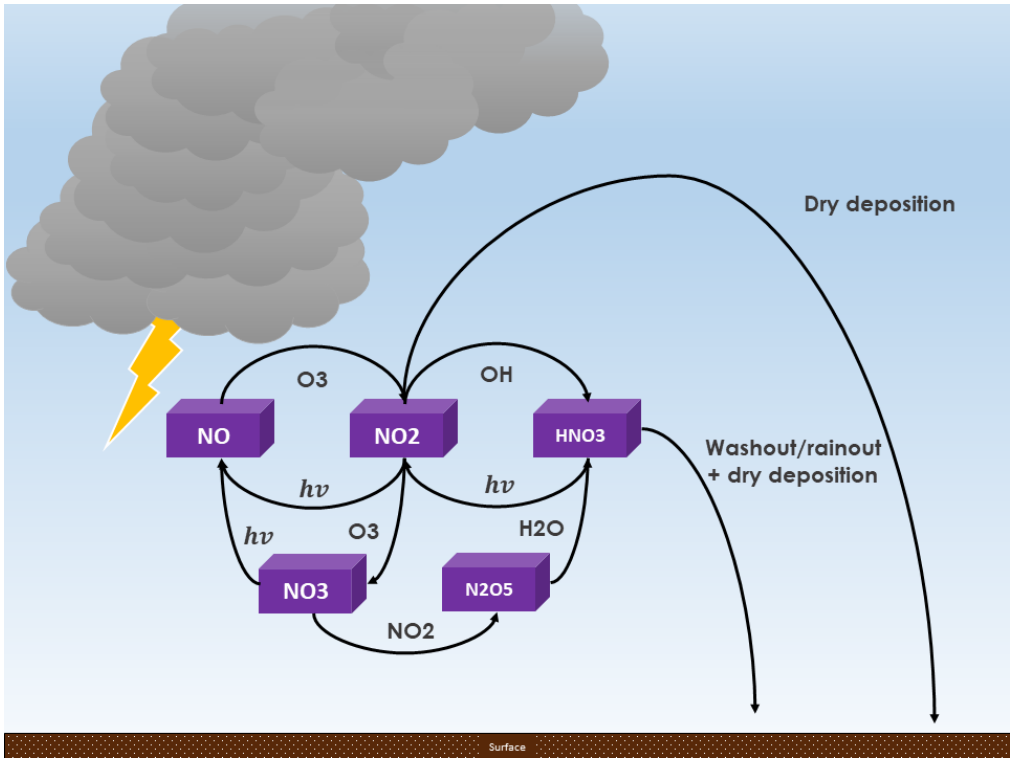

In addition to the natural production of NO_x through lightning, anthropogenic surface emissions dataset derived from the Copernicus Atmosphere Monitoring Service (GRANIER ET AL., 2019) were also included in the scheme.

The vertical distribution profile of NO_x produced by lightning suggested by Ott et al, (2010) is inserted in the parameterization. Since the domain of the model is located within the subtropics, the largest fraction (90%) of NO_x was inserted at upper levels between 400 hPa and 100 hPa. At the top of the model and the surface, the emission of NO_x by lightning is considered null. Of the remaining 10%, 2/3 is prescribed at lower levels between approximately 1000 hPa and 600 hPa and 1/3 at mid-levels between 600 hPa and 400 hPa.

The horizontal dynamic transport of NO_x is done through the Eta model horizontal advection scheme, which conserves the energy and the enstrophy of the grid for a non-divergent two-dimensional flow (JANJIC, 1984). For the vertical advection of NO_x, the Van Leer finite volume scheme of dynamic variables was used (MESINGER ET AL, 2012).

The vertical diffusion of NO_x follows the turbulence by Mellor and Yamada level 2.5 (1982). The convective vertical transport of the NOx is calculated by the vertical mas flux, given by:

$$\frac{\partial[\overline{NO_x}]}{\partial t} = -\frac{1}{\rho}\frac{\partial\overline{\rho w'[NO_x]'}}{\partial z} \tag{4.38}$$

Where the horizontal bar denotes the average in the model grid, the prime refers to the subgrid perturbation. w_c is the cloud vertical speed estimated from the Convective Available Potential Energy (CAPE). It is assumed the convective potential energy is converted to cloud kinetic energy, given by:

$$w_c = \left(\sqrt{2.CAPE}\right) \tag{4.39}$$

Where,

$$CAPE = g\int_{LFC}^{EL}\frac{\theta(z) - \bar{\theta}(z)}{\bar{\theta}(z)}dz \tag{4.40}$$

Where g is gravity, θ is the potential temperature of the air, $\bar{\theta}$ the potential temperature of the environment, z is the height of the air parcel, LFC and EL are level of free convection and equilibrium level, respectively.

4.4 Evaluation of lightning scheme

The performance of lightning and precipitation simulations were assessed using the Equitable Threat Score metric adjusted by the categorical bias (Mesinger 2008), hereafter ETSa, and BIAS are given by:

$$ETSa = \frac{Ha - CH}{2O - Ha - CH} \tag{4.41}$$

$$BIAS = \frac{F}{O} \tag{4.42}$$

Where,

$$CH = \frac{O^2}{N} \tag{4.43}$$

$$Ha = O - \frac{F - H}{ln\frac{O}{O - H}} lambertw\left[\left(\frac{O}{F - H}\right)\left(ln\frac{O}{O - H}\right)\right] \quad (4.44)$$

Where F is the number of events predicted by the model, O is the number of observed events, H the number of hits in the model, CH is the correction for random hits in the model, N is the total number of the sample.

The ETSa index measures the fraction of events that are predicted, corrected by the hits that occur at random, and adjusted by the BIAS. Due to this increased sensitivity, ETSa becomes a better index than the Threat Score. The value 1 indicates a perfect forecast of the phenomenon, while 0 indicates no skill in the forecast.

The BIAS metric was also used, which refers to the relationship between the forecast frequency and the observed frequency. The value of the BIAS index varies to greater, less than, or equal to 1.

- $BIAS$> 1 → The event is predicted more often than is observed;
- $BIAS$ <1 → The event is predicted less frequently than is observed;
- $BIAS$ = 1 → The event is predicted at the same frequency as it is observed.

The thresholds adopted for the daily lightning rate in the calculation of ETSa and BIAS are shown in Table 4.2:

Table 4.2 – Lightning rate contingency table.

LIGHTNING THRESHOLDS (flash.month^{-1})	CATEGORIES
50	**Weak**
200 400 600	**Moderate**
800 1000	**Intense**

The thresholds adopted for the daily precipitation rate in the calculation of ETSa and BIAS can be seen in Table 4.3:

Table 4.3 – Precipitation contingency table.

PRECIPITATION THRESHOLDS (mm.month^{-1})	CATEGORIES
25 50	**Weak**
100 200 300	**Moderate**
400 500	**Intense**

4.5 Data

Observed data from electrical discharges from BrasilDAT, provided by ELAT (http://www.inpe.br/webelat/homepage/), will be used to validate lightning simulations. The observed values are for January, February, and March 2017 and cover southeastern Brazil as shown in Figure 4.1:

Figura 4.1 – BrasilDAT electric discharge detection efficiency map.

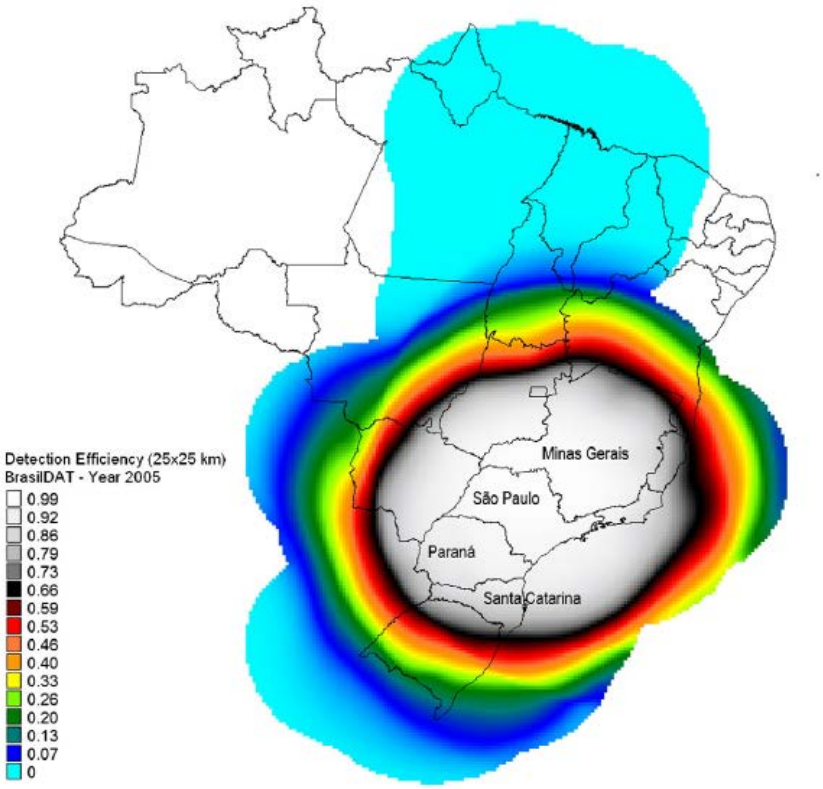

Source: Ballarotti et al. (2006).

The CMORPH (JOYCE ET AL., 2004) satellite estimated precipitation data (CPC Morphing Technique) are used to evaluate the simulated precipitation. The CMORPH data has a resolution of 8 km and it is available between 60ºS and 60ºN. Also, cloud water and cloud ice mix ratio are compared with ERA5 reanalysis data produced by the European Center for Medium-Range Weather Forecasts (HERSBACH ET AL., 2020).

Chemical species data from Copernicus Atmosphere Monitoring Service (CAMS) is used to evaluate NO_x and derived chemical species. The chemical data from CAMS is a global reanalysis dataset (INNESS ET AL., 2019) of the atmospheric composition produced by the European Centre for Medium-Range Weather Forecasts.

5 RESULTS

The results are divided into four sections: calibration of lightning detection in 5.1, evaluation of lightning simulations in 5.2, effects on rain production and distribution in 5.3, and effects on the NO_x production and related chemical species in 5.4.

5.1 Calibration of lightning detection

The calibration of parameters a and b (equation 4.8) were calculated during the case of intense convective activity in southeastern Brazil (Figure 5.1). The case of thunderstorm clouds evidenced a mesoscale convective complex that was born on the night of January 9, 2017, and dissipated during the early morning of January 10, 2017.

The comparison between the LCE variable and the observed data of electric discharges from BrasilDAT is based on the average over the area which contains the intense convective activity (Figure 5.1).

Figure 5.1 – Intense convective activity in Southeastern Brazil on 09/01/2017 2000 UTC. The rightmost highlighted figure is temperature realce infrared satellite image, which shows deep convection.

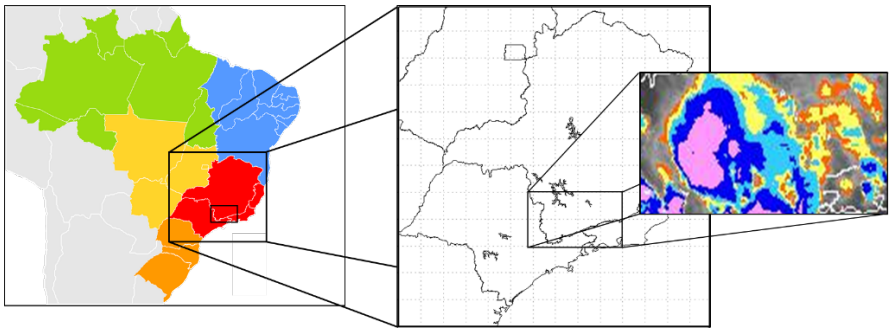

Figure 5.2 shows the calibration of parameters a and b. The Eta model run is initiated on 08/01/2017, 1200 UTC, and the time series of LCE has a time interval of 400 s. The observed data and the LCE in Figure 5.2 are normalized by dividing the time series by the maximum value of the series. The analyzed

period is from 09/01/2017 1400 UTC to 10/01/2017 0000 UTC (period of convective activity over the area analyzed).

Both, LCE and observed data of lightning showed the maximum peak between 1800 UTC and 2100 UTC due to the summer convection at the end of the afternoon. The variable LCE showed to have a high correlation with observed data (Pearson's correlation in the period is 0.97), which suggests that the LCE calculation methodology can be applied to identify grid points of the model with potential energy for lightning activity. The parameters a (flash.km².400s^{-1}) and b (flash.J^{-1}.400s^{-1}) were calculated by equations 4.9 and 4.10 and the values -0.03 and 0.0066 are defined, respectively. Therefore, the lightning diagnosis from equation 4.8 is now given by:

$$f_r = -0.03 + 0.0066\, LCE \qquad 5.1$$

To avoid the case where $LCE = 0$, therefore $f_r = -0.03$, it is assumed that f_r is calculated only if $LCE > 0$.

Figure 5.2 – Calibration of parameters a and b during a case of intense convective activity in the area described in Figure 5.1. a) Time series of observed electrical discharges (flash.km^{-2}.400s^{-1}) and LCE (J.km^{-2}), where both variables are normalized by the maximum value of the series; b) Scatter plot between BrasilDAT data of lightning and the LCE in the period.

a) b)

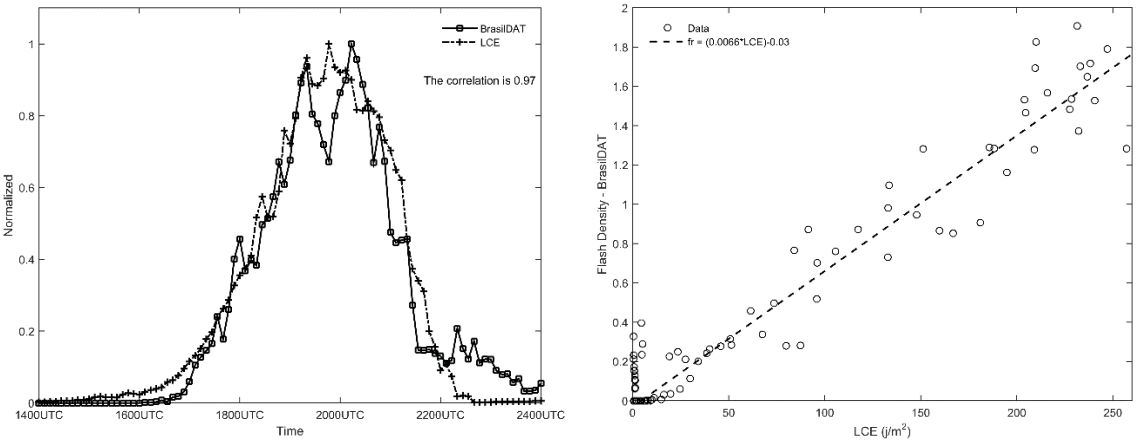

5.2 Lightning simulations

Three experiment runs are conducted and listed in Table 5.1. The objective of the experiments is to evaluate the lightning detection scheme and to assess the effects on cloud droplet autoconversion and the production of rain. Indirect effects on the mixture of water and cloud ice are also analyzed. More details of the experiment run and justification are shown in Section 4.3.2.

Table 5.1 – Experiments run description.

Experiments	Description
Exp1	Lightning detection; No effect on cloud droplet autoconversion. Control experiment.
Exp2	Lightning parameterization; Effects on cloud droplet autoconversion ($n_w = 100 \times 10^6\ droplets/m^3$)
Exp3	Lightning parameterization; Effects on cloud droplet autoconversion ($qw_0 = 0.1\ qw$)

The observed lightning density $(flash.km^{-2}.month^{-1})$ for the quarter from January to March 2017 (Figure 5.3 (a)) is larger in the coastal region of São Paulo and Rio de Janeiro. During summer, cold fronts frequently reach these latitudes near this coast. In the warm sector of the fronts, Low-Level Jets from the northwest carries warm and moist air from the Amazon to the southeast of Brazil. This flow supports the establishment of the South Atlantic Convergence Zone (Kodoma 1992), which can cause summer storms and leads to the production of electrical discharges.

The runs Exp1, Exp2, and Exp3 (Figure 5.3 (b), (c), and (d)) show the simulation of lightning density in the coastal region of São Paulo and Rio de Janeiro. There are underestimations in all runs comparing to lightning observed data, but the distribution of lightning activity over the domain in the simulations seems to agree with observed data performing larger electric discharge density over São Paulo and gradually decreasing along the northeast of the domain. The underestimation of lightning density simulations can be caused by three factors:

1. A rough calibration of the parameters a and b.

2. Underestimation in the quantities of ice and supercooled water in the mixed-phase of the cloud, which can reflect in less lightning activity in the simulations.
3. The imposed condition on the LCE calculation that requires the threshold $CAPE_{MP} > 500\ \mathrm{J/kg}$, described in section 4.3.2, to avoid lightning activity everywhere.

The third factor of the imposed condition on the LCE can be adjusted in future studies. Despite the underestimation in the lightning simulations, the effect of lightning activity in autoconversion of cloud droplets acted to increase the occurrence of electric discharge.

The summarization of all occurrences of lightning over the Southeast of Brazil during the entire period between January and March of 2017, shows that the observed data accumulated about 5.89×10^6 flashes, the Exp1 diagnoses 4.91×10^6 flashes, Exp2 generated 4.95×10^6 flashes and Exp3 simulates 5.30×10^6 flashes. The maximum lightning density over the domain between January and March of 2017 are 44.98 flashes.km^{-2}.month^{-1} for observed data, 21.27 flashes.km^{-2}.month^{-1} for Exp1, 27.91 flashes.km^{-2}.month^{-1} for Exp2, and 26.87 flashes.km^{-2}.month^{-1} for Exp3. The mean lightning density over the domain between January and March of 2017 are 1.17 flashes.km^{-2}.month^{-1} for observed data, 0.96 flashes.km^{-2}.month^{-1} for Exp1, 0.97 flashes.km^{-2}.month^{-1} for Exp2, and 1.05 flashes.km^{-2}.month^{-1} for Exp3.

These numbers show that the electrical activity effect on droplet autoconversion present in Exp2 and Exp3 caused an increase in the production of lightning. Besides, the results also imply that increasing the effect of lightning in cloud droplets autoconversion in Exp3 causes larger lightning activity.

Figure 5.3 – Lightning density (flash km^{-2} month^{-1}) for the period between January and March 2017 for (a) Observation, the (b) Exp1, the (c) Exp2, and the (d) Exp3.

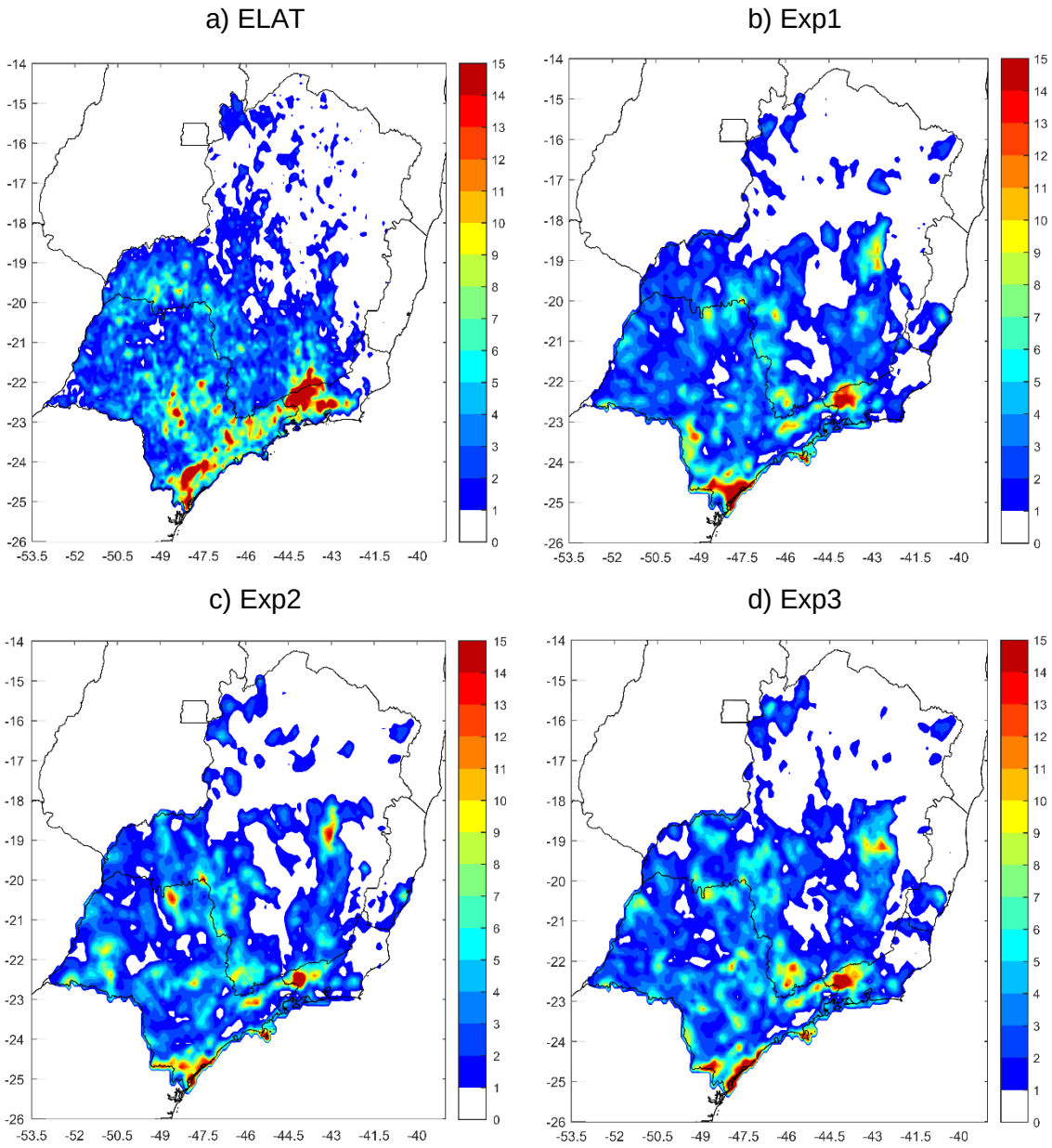

Figure 5.4 shows the ETSa and BIAS metrics for the period between January and March 2017 for electric discharge. All the experiments show similar performance to simulate lightning. For the weak to the moderate thresholds, Exp2 shows the best performance. For intense thresholds, Exp3 shows the lowest performance, which suggests that the excessive increase in the cloud droplet autoconversion may penalize the diagnosis of electrical discharges.

However, the BIAS metrics in Figure 5.4 (b) shows that Exp3 performed the lowest underestimation of lightning activity. The conclusion from these three experiments is that the effect on droplet autoconversion can improve the performance of lightning simulation when not very intense and can increase the occurrence of electrical discharges in the scheme. This conclusion opens the discussion about the increase in lightning activity in response to the process of cloud droplets autoconversion.

Figure 5.4 – (a) ETSa and (b) BIAS scores of the number of lightning per grid box for the period from January to March 2017.

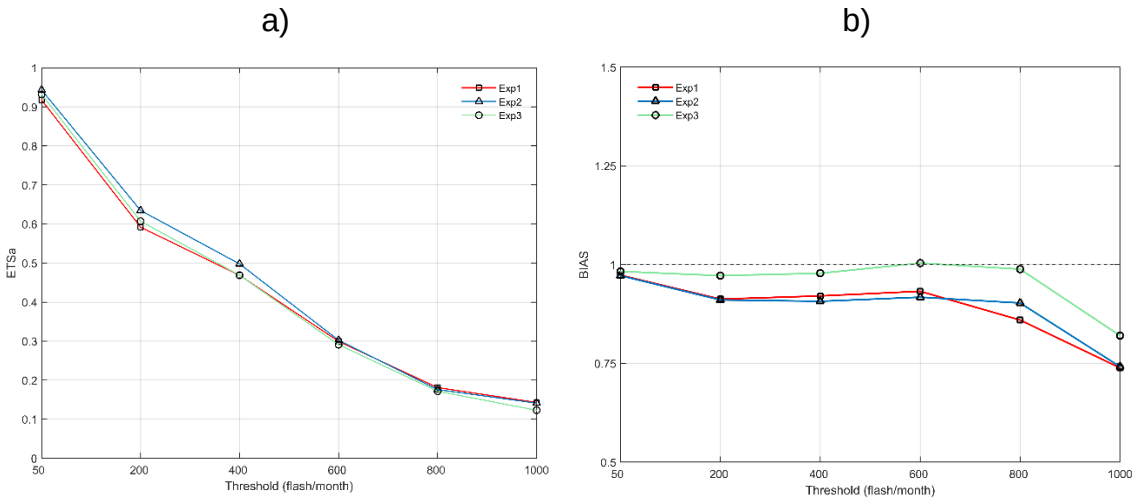

The increase of lightning activity in Exp2 and Exp3 in comparison against to Exp1 (control simulation) can occur if the concentration of cloud ice and/or cloud water also increases in the mixed-phase of the cloud since the lightning scheme is based on these variables.

The simulation of January 2017 is considered to examine the effects of the lightning scheme on cloud water and cloud ice vertical profiles (Figure 5.5 (a) and (b), respectively). The vertical profiles of the autoconversion rate (A_T) and the deposition rate are also included (Figure 5.5 (c) and (d), respectively). The area covers the coordinates 25S-24S and 49W-48W. Figure 5.5 shows the average of the variables over the area at each vertical level.

Figure 5.5 (a) shows a decrease in the cloud water mixing ratio at lower levels, between 820hPa and 630hPa, in Exp2 and Exp3 in comparison with Exp1. The

decrease in the cloud water mixing ratio is expected since the lightning scheme causes the growth of raindrops through the process of cloud droplets autoconversion at levels below the 0ºC isotherm level as described in 4.3.3. Figure 5.5 (c) shows the vertical profile of the cloud droplets autoconversion rate (A_T). The increase in the autoconversion rate for Exp2 and Exp3 in comparison with Exp1 at lower levels confirms that the decrease of cloud water in Exp2 and Exp3 at lower levels is caused by the increase in the autoconversion rate.

In mid-levels and upper levels, there is no relevant concentration of cloud water, but a significant concentration of cloud ice (Figure 5.5 (b)). An increase in cloud ice is found in Exp2 and Exp3 comparing to Exp1 for the mid and upper levels of the troposphere. This increase in the cloud ice mixing ratio in mid and upper levels in Exp2 and Exp3 comparing to Exp1 is the possible cause of the increase in lightning activity. Figure 5.5 (d) shows the rate of water deposition. There is an increase of deposition for Exp2 and Exp3 in comparison to Exp1 in mid-levels and upper levels, which justifies the increase of cloud ice in mid and upper levels of Exp2 and Exp3.

In addition to the increase in cloud ice, another important factor for the electrical activity in the scheme is the thermodynamic instability within the mixed phase of the cloud, obtained as $CAPE_{MP}$. The time series of $CAPE_{MP}$ for the same area and the same period of Figure 5.5 is available in Figure 5.6. The $CAPE_{MP}$ time-series average is 55.8 J/kg for Exp1, 57.7 J/kg for Exp2, and 57.3 J/kg for Exp3. The result implies that the increase in ice cloud mixing ratio and the increase in thermodynamic instability $CAPE_{MP}$ may be the cause of the large electrical activity in Exp2 and Exp3 compared to Exp1.

Figure 5.5 – Simulation of mean vertical profile over an area with thunderstorm activity during January of 2017 for a) Cloud water and (b) Cloud ice and (c) autoconversion rate (A_T) and (d) water deposition rate. The area mean is taken within the coordinates 25S-24S and 49W-48W.

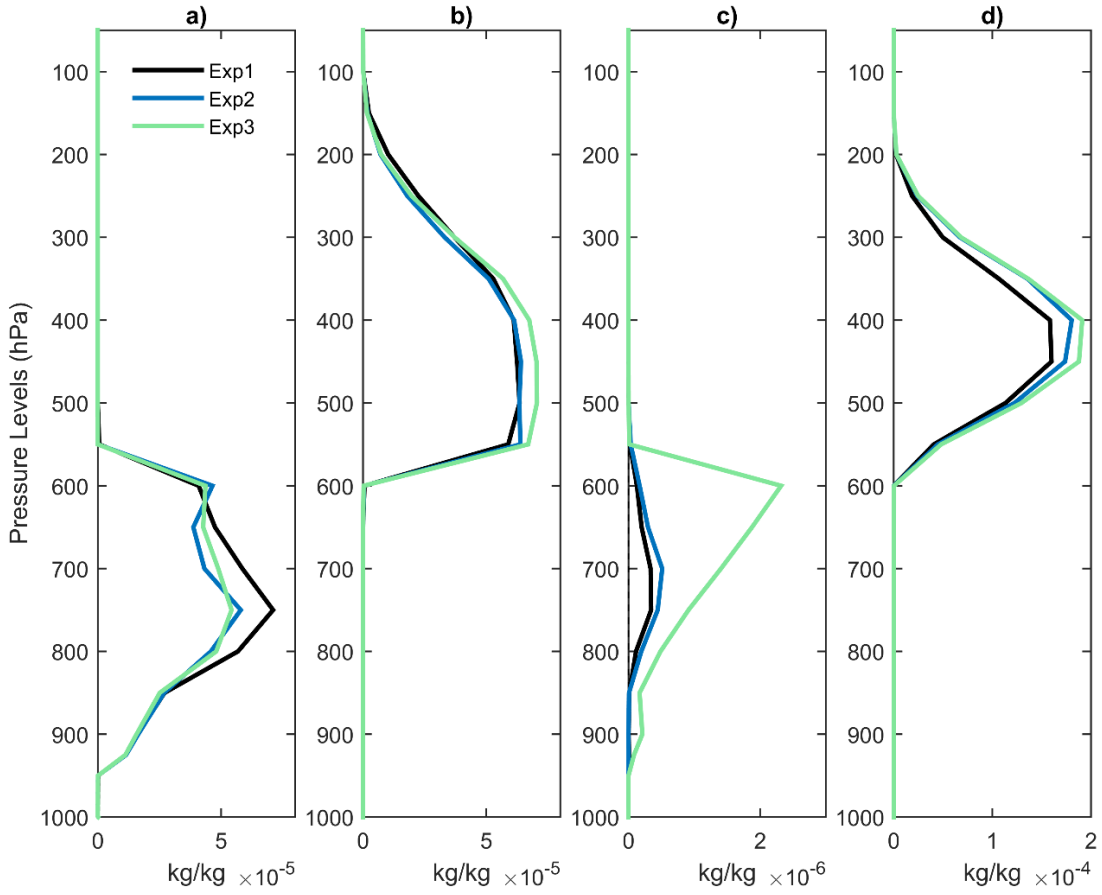

Figure 5.6 – Time series of $CAPE_{MP}$ (J/kg) in January of 2017 over an area with large thunderstorm activity. The $CAPE_{MP}$ is an average over the area in the coordinates 25S-24S and 49W-48W.

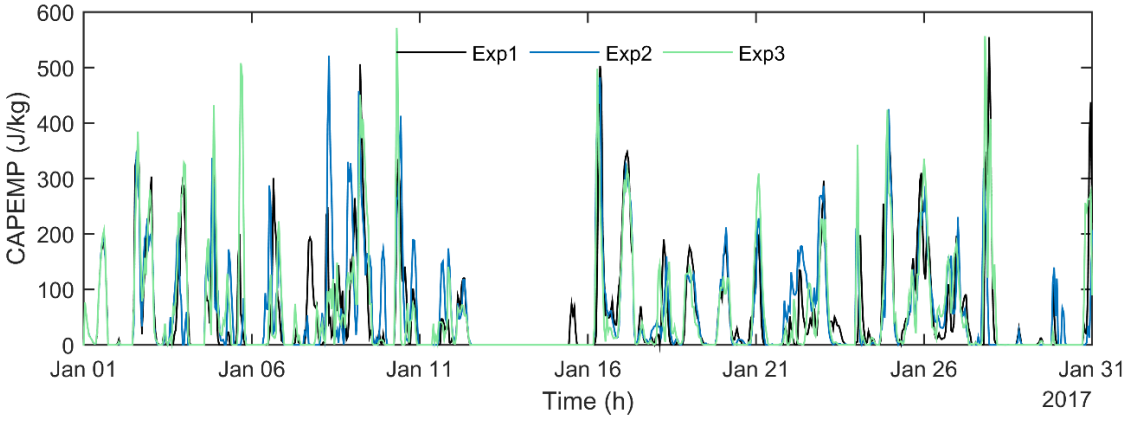

5.3 Lightning effects on rain production

Figure 5.8 shows the accumulated precipitation (mm/month) from January to March 2017. The summer months are the rainiest in most of Brazil. The accumulation of precipitation in this period is strongly influenced by the formation of the South Atlantic Convergence Zone. This system is persistent and causes rain for several consecutive days, mainly in the Center-South region of the country.

The precipitation data estimated by satellite (Figure 5.7 (a), (b), and (c)) show that the rainiest month is January with a large accumulation of precipitation over the state of São Paulo. Between February and March, summer storms decrease as a response to the convection activity that gradually moves toward the Amazon Basin. The simulations reproduced January distribution and intensity of precipitation mainly over São Paulo state. The simulations also performed the February precipitation distribution, however, there is an underestimation compared with CMORPH data. March precipitation simulations showed underestimation over the north of the domain and overestimated near the coast of São Paulo and Rio de Janeiro.

The underestimation of precipitation shown in the simulations in February and over part of the domain in March is an error that has been reported by Chou and Silva (1999) and Calada et al. (2017) when the Eta model is configured with the BMJ convection parameterization scheme (see section 3.1). The insertion of the effect of lightning in the production of rain in Exp2 and Exp3 aims to minimize these underestimations, especially in areas of intense precipitation. The precipitation pattern is very similar between the experiments and only some differences can be noted in intense cells (Figure 5.7 (d) to (l)).

The effect on rain should be more evident when analyzing a smaller time scale. According to Moore *et al.* (1962), rain gush takes between one to three minutes to occur after lightning. To detect the indirect effect of the lightning scheme in precipitation production, the time series for lightning density (Figure 5.8 (a)) and

precipitation (Figure 5.8 (b)) is plotted for the interval of every 400s, which is the timestep of the cloud microphysics parameterization of the model.

Figure 5.7 – Accumulated precipitation (mm/month) of CMORPH (a to c) and simulations Exp1 (d to f), Exp2 (g to i), and Exp3 (j to l), for summer months of 2017.

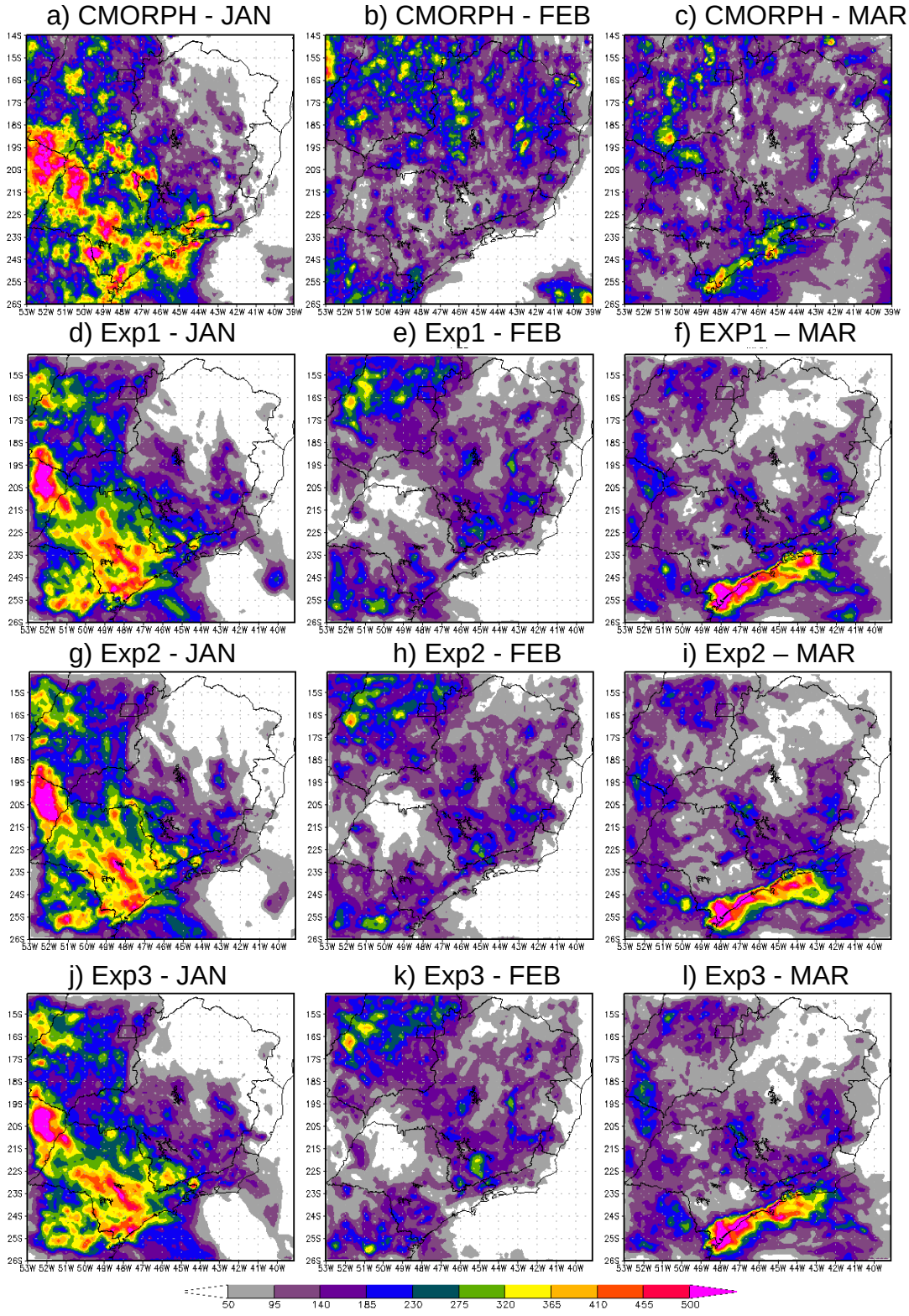

Figure 5.8 shows the 72 hours of simulation between 19/01/2017 0000 UTC and 22/01/2017 0000 UTC. The time series of lightning density (Figure 5.8 (a)) and precipitation rate (Figure 5.8 (b)) are the averages over the area limited by the coordinates 19S-19.5S and 47.5W-48.5W.

Two main peaks of lightning activity and rain, around 20/01/2017 1800 UTC and 21/01/2017 1800 UTC, can be notice during the late afternoon and early evening of each day as a result of summer convective events. In these maximum peaks, it is evident that Exp2 and Exp3 present higher values of lightning density (Figure 5.8 (a)) and precipitation rate (Figure 5.8 (b)) in comparison to Exp1. This result confirms the lightning parameterization effect on rain production.

Although the effect of lightning parameterization on autoconversion rate is stronger in Exp3, the results between Exp2 e Exp3 in Figure 5.8 are similar in this specific case. Not only for the magnitude of the lightning density and precipitation rate, but also for the timing of the peaks which is slightly different from Exp1. The conclusion of the case analyzed in Figure 5.8 is that the effect of lightning on cloud droplet autoconversion was able to increase the two main peaks of electrical activity, and precipitation rate and cause a slight change in the timing of the peak occurrence.

Figure 5.8 – Time series simulation of a) lightning density and b) precipitation rate between 19/01/2017 0000 UTC and 22/01/2017 0000 UTC. The simulations refer to the averages over the area limited by the coordinates 19S-19.5S and 47.5W-48.5W.

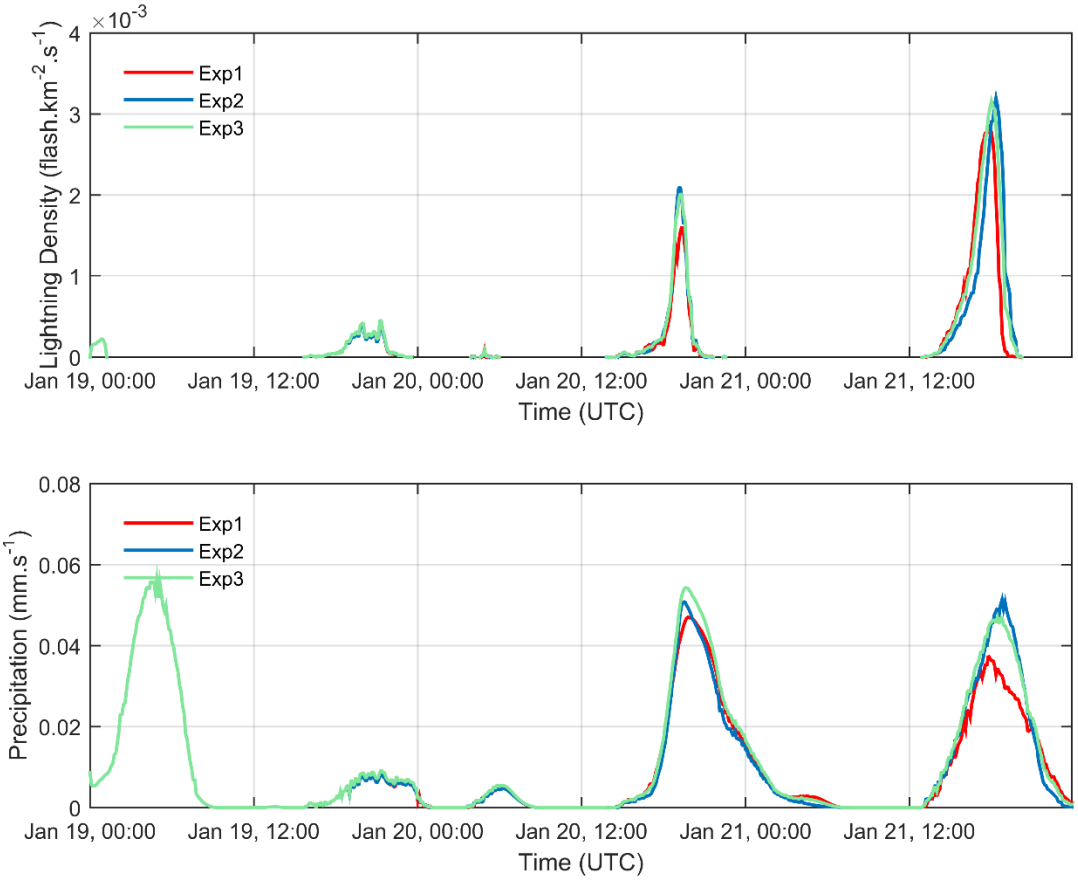

Figure 5.9 shows the occurrence of precipitation events (mm/24h) above the 30 mm/day threshold that may be related to the occurrence of electrical activity and the density of lightning during the summer months of the year 2017. The total number of precipitation events above the threshold (30 mm/day) throughout the period and at all grid points in the domain was 37691 events in Exp1, Exp2 simulated 38087 events, and Exp3 simulated 40838 events (Figure 5.9 (d)). Therefore, there was a higher number of significant rainfall events when the lightning effect on autoconversion rate is included in the Eta model simulations.

Figures 5.9 (a), (b), and (c) show the increase in the frequency of precipitation events above the 30 mm/day threshold on the central and western part of the domain in Exp2 (Figure 5.9 (b)) and Exp3 (Figure 5.9 (c)) that coincides with the

region strongest electrical activity of the period over the continent. This result reinforces that the electrical activity acted to intensify the occurrence of more intense precipitation.

Figure 5.9 – Total occurrences of precipitation (mm/24h) above 30mm threshold that coincides with the occurrence of lightning activity (flash.day^{-1}) in the period from January to March 2017 for (a) Exp1, (b) Exp2, and (c) Exp3; and (d) Time series of total occurrences on the domain for each day.

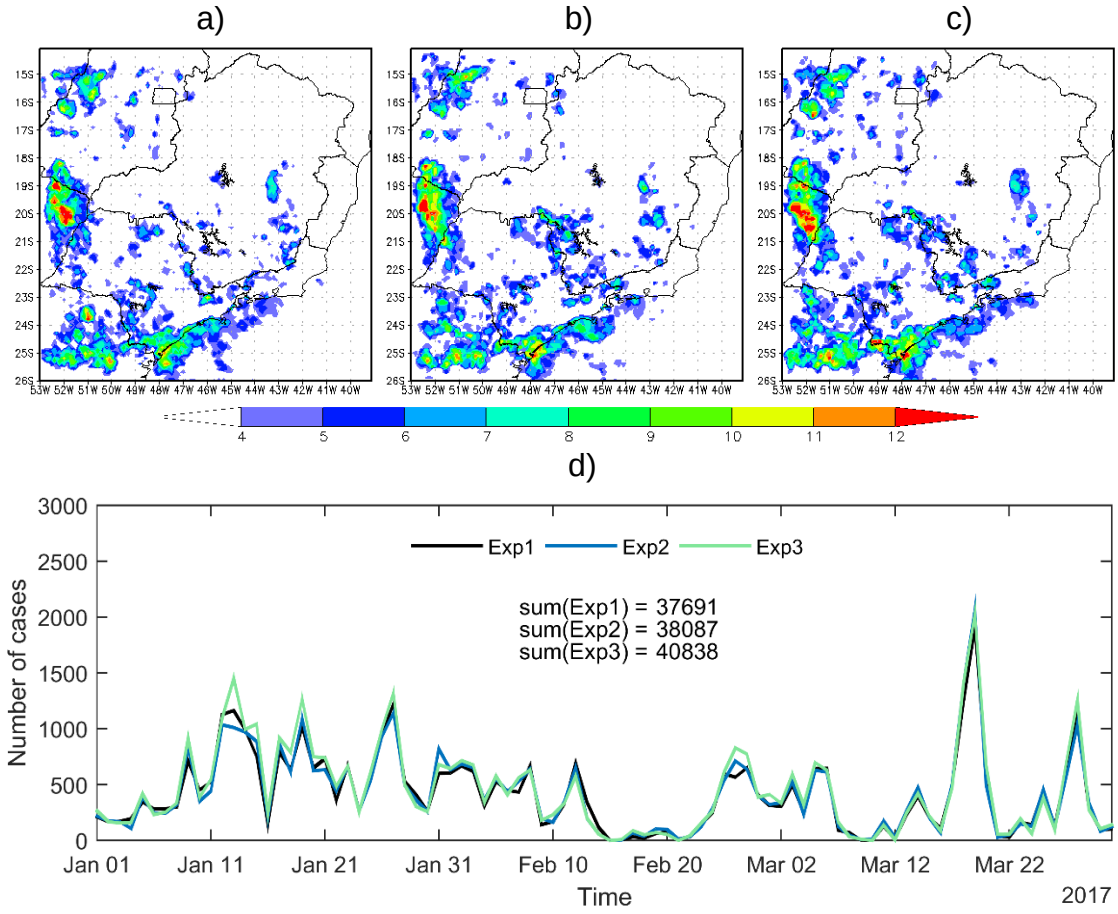

Figure 5.10 shows ETSa and BIAS metrics for the simulations of precipitation and it is calculated comparing to the CMORPH data. The ETSa metrics for precipitation results show that Exp2 and Exp3 improve the forecast for more intense rainfall thresholds (Figure 5.10 (a)). Exp2 reached the highest value of ETSa for heavy rainfall thresholds, which indicates that the intensification of the lightning effect on the cloud droplet autoconversion in Exp3 caused a lower performance gain.

All simulations underestimate precipitation (Figure 5.10 (b)), as BIAS is below 1 for all thresholds. However, the lightning effect on cloud droplets autoconversion in the Exp2 and Exp3 minimized the underestimation for moderate and intense precipitation thresholds. The BIAS difference between Exp2 and Exp3 is small, which suggests that the intensification of the effect on droplet autoconversion does not show significant gains for rain production.

Figure 5.10 – (a) ETSa and (b) BIAS score of precipitation simulations (mm/month) for the period from January to March 2017 in southeastern Brazil.

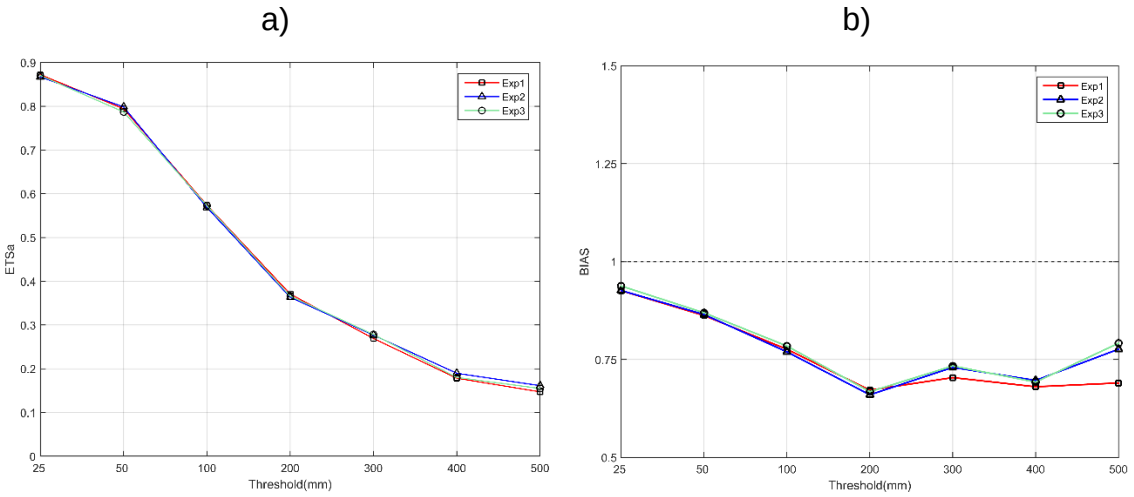

5.3.1 Indirect effects

Indirect effects of the lightning scheme on temperature, humidity, equivalent potential temperature, and omega are also analyzed (Figure 5.11). The vertical profiles in Figure 5.11 represent the average of the period between 09/01/2017 1800 UTC and 10/01/2017 0000 UTC over the area limited by the coordinates 22.5S-21S and 45W-46W. During the analyzed period there was electrical activity and intense rain, which impacts the autoconversion rate of the simulations.

The Eta simulations generated a vertical profile with lower temperatures (Figure 5.11 (a)) than Era5. Between the Eta simulations, the differences are not relevant for the temperature. The vertical profile of specific humidity (Figure 5.11 (b)) showed that Exp2 and Exp3 simulated a drier lower and middle

troposphere compared to Exp1. This result indicates that, in the case under analysis, the effect of lightning on the autoconversion of cloud droplets caused these layers to dry out. All simulations showed a more humid vertical profile compared to Era5 and the decrease in the specific humidity in Exp2 and Exp3 brought the simulations closer to reanalysis in the case analyzed.

The dryness in the lower and middle troposphere in Exp2 and Exp3 impacted the simulation of Equivalent Potential Energy (Figure 5.11 (c)) compared to Exp1. In general, the Equivalent Potential Energy is lower for Exp2 and Exp3. Exp3 generated results of equivalent potential energy closer to the Era5 reanalysis than Exp1 and Exp2.

The results of the vertical movement (Figure 5.11 (d)) show large variations between the simulations from middle to upper troposphere. Between the vertical levels 700hPa and 200hPa, Exp1 simulated the most intense vertical movement, which suggests that the effect on droplet autoconversion acted by minimizing vertical movement. The weakening of vertical movement in the Exp2 and Exp3 simulations brought the Eta model simulations closer to the vertical movement profile of the Era5 reanalysis.

It is concluded that in the case analyzed, Exp2 and Exp3 showed improvements in the simulations of specific humidity, equivalent potential energy, and vertical movement concerning Exp1 when compared with the Era5 reanalysis. In the future, new studies may be done to confirm the indirect effects of the lightning parameterization scheme.

Figure 5.11 – Average vertical profile between 09/01/2017 1800 UTC and 10/01/2017 0000 UTC for a) temperature (ºC), b) specific humidity (kg/kg), c) equivalent potential temperature (ºC) and d) vertical motion (hPa/s), over an area with electric activity and intense precipitation. The area is limited by the coordinates 22.5S-21S and 45W-46W.

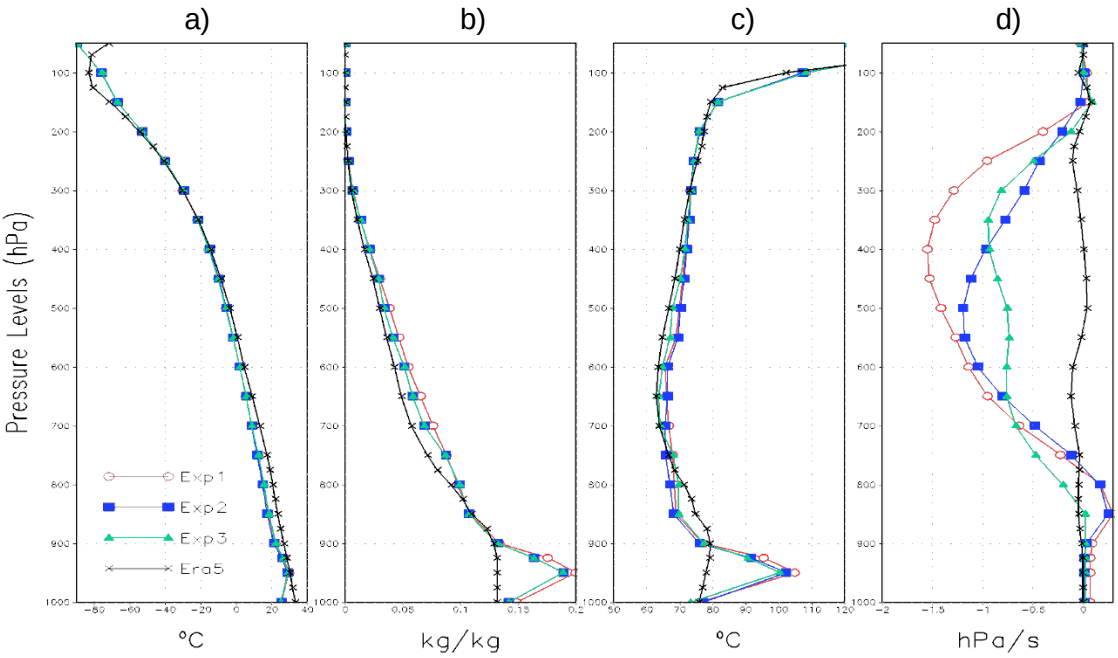

5.4 Lightning effects on NOx production

In addition to the effects on cloud microphysics, lightning causes changes in the chemistry of the atmosphere as discussed in section 3.6. The idea of including the lightning NO_x production in the scheme aims to provide a parameterization that opens up possibilities for climate change studies and highlights the potential use of the lighting scheme.

In this section, the results of the lightning NO_x are divided into the scheme frequency of chemical and photochemical NO_x related reactions (5.2.1), the production and transport of chemical species (5.2.2), and the conservation of mass in the scheme (5.2.3).

5.4.1 Frequency of NOx related reactions

The average values of the reaction rate constant (K) over the domain for each reaction calculated by the model can be seen in Table 5.2. The processes that

"consume" the chemical species more quickly in the scheme are the rainout and washout (K_7), which removes HNO_3 from the atmosphere through the raindrops. Despite being a strong sink of HNO_3, this process is concentrated only in the regions of clouds that precipitate.

This process is minimized by the feedback of HNO_3 to the atmosphere through the evaporation of the raindrops during the trajectory towards the surface. The HNO_3 feedback due to evaporation of precipitating hydrometeors is not included in the parameterization, but it may be an option to update the scheme in the future as it is an important vertical distribution process for HNO_3.

On the other side, the slowest chemical reaction in the scheme is represented by the reaction rate constant K_3, which refer to the production of NO_3 in the day time by the reaction of NO_2 with O_3. Because of the production of NO_3 is very slow and it is very fast destroyed by the photodissociation process during the day (see Figure 5.12 (c)), NO_3 may not have large concentrations in the troposphere. Despite the low concentration, NO_3 is important when reacts with NO_2 to establish an equilibrium with N_2O_5.

Table 5.2 – Average reaction rate coefficient (K) over the domain of the model for January 2017.

Reaction Rate Coefficient	***Related Reaction***	***Rate***
K_1	$NO + O_3 \rightarrow NO_2 + O_2$	$2 \times 10^{-14}\ [cm^3.s^{-1}]$
K_2	$NO_2 + OH \xrightarrow{[M]} HNO_3$	$10^{-11}\ [cm^3.s^{-1}]$
K_3	$NO_2 + O_3 \rightarrow NO_3 + O_2$	$3 \times 10^{-17}\ [cm^3.s^{-1}]$
K_4	$NO_2 + NO_3 \xrightarrow{[M]} N_2O_5$	$10^{-12}\ [cm^3.s^{-1}]$
K_5	$N_2O_5 + H_2O \rightarrow 2HNO_3$	$5.8 \times 10^{-6}\ [s^{-1}]$
K_6	$N_2O_5 \xrightarrow{[M]} NO_2 + NO_3$	$5.8 \times 10^{-2}\ [s^{-1}]$
K_7	$HNO_3 + H_2O \rightarrow H^+ + NO_3^-$	*0.2 (rainout)* $[s^{-1}]$ *0.02 (washout)* $[s^{-1}]$

The vertical profile of the photochemical process frequency (J) is shown in Figure 5.12. Taking the inverse values in Figure 5.12, it is noted that the lifetime of HNO_3 is of the order of months (Figure 5.12 (a)), NO_x is of the order of minutes (Figure 5.12 (b)), NO_3 is of the order of seconds (Figure 5.12 (c)) and

N_2O_5 is of the order of days (Figure 5.12 (d)), within the troposphere. These simulated periods of species lifetime are reasonable when compared with literature (Lippmann et al., 1980; Wallington et al., 1987; Brown et al., 1999; Brasseur and Solomon, 2005).

The results in Figure 5.12 are important not only to understand the photochemical lifetime but also for the time available for the chemical species is transported by the wind. The photochemical lifetime allows HNO_3 to be transported longer than the other species simulated before the photodissociation break HNO_3 to form NO_2.

During the daytime, the scheme NO_2 and NO_3 photodissociation frequency (Figure 5.12 (b) and (c), respectively) are responsible for the fast production of NO essentially at upper levels. The scheme does not consider the NO photodissociation process since NO reacts with ultraviolet radiation in the middle atmosphere (Minschwaner and Siskind, 1993) and the Eta model top is currently at 25 hPa.

Figure 5.12 – Vertical profile of photodissociation frequency calculated by TUV model for (a) HNO_3, (b) NO_2, (c) NO_3 and (d) N_2O_5, at zenith angles of 0º and 45º.

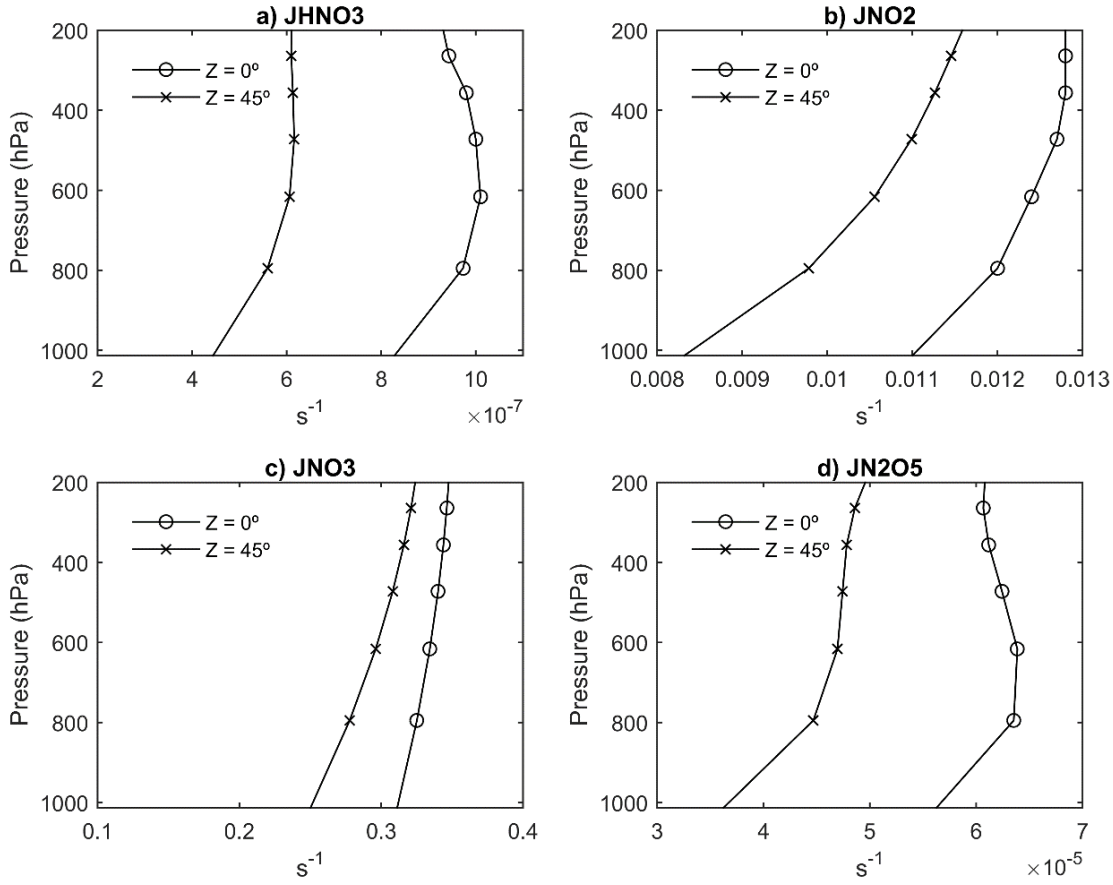

5.4.2 Production and distribution of NOx related species

The NOx related chemical species simulated by Eta model are compared with CAMS reanalysis data in Figure 5.14, which shows the time series of the total column volume mixing ratio of NOx related species over the domain between 01/01/2017 0000 UTC and 31/01/2017 2300 UTC. The Eta model was initiated on 01/01/2017 0000 UTC running continuously. The reanalysis data from CAMS does not assimilate NO_x data produced directly by lightning, however, it assimilates data of NO_x tropospheric column from various satellites. The reanalysis data has a horizontal resolution of 80 km while the Eta was run for 10 km. For the comparison in Figure 5.14, Eta simulations were downgraded and interpolated to the CAMS grid.

All the chemical species simulated by the lighting scheme presented the same order of magnitude comparing to reanalysis data and despite the low Pearson Correlation between the data, the simulations performed reasonably the maximum and minimum peaks.

The NO_x simulation (Figure 5.14 (a)) presented overestimation in the first fifteen days confronting CAMS reanalysis. If the first fifteen days are removed from the series, the correlation increase to 0.47, which is a moderate correlation. To avoid a long period to reach an equilibrium state, the initial value of NO_x in the scheme is 4×10^{-11} kg/kg in the domain, in which the total column of NO_x is approximately 2×10^{-9} kg/kg in the domain. The initial value of the scheme does not appear to be the cause for the overestimation of the first fifteen days of the model integration.

The reason for the overestimation and low correlation of the NO_x simulation in the first fifteen days may be the contribution of the strong convection activity (Figure 5.13) that produces lightning in the first half of January and increased the production of LNO_X in the scheme. Since the CAMS does not assimilate LNO_X, it could be a limitation in the comparison between Eta simulation and the reanalysis data.

Figure 5.13. T-Realce infrared images of the GOES-13 satellite showing the convection activity on different days in the first half of January 2017. The domain of the Eta model is dashed.

a) 02/01/2017 2100 UTC

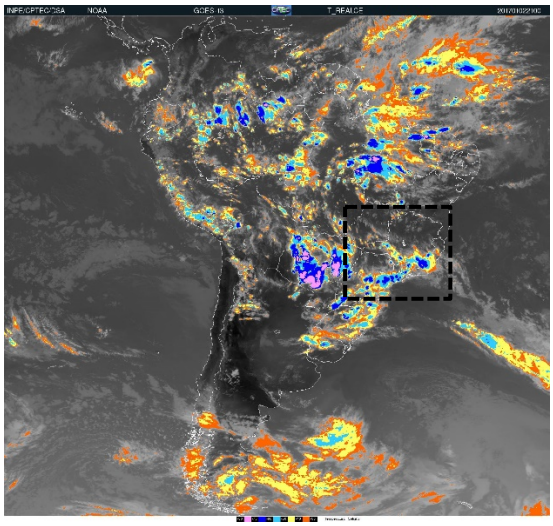

b) 09/01/2017 2100 UTC

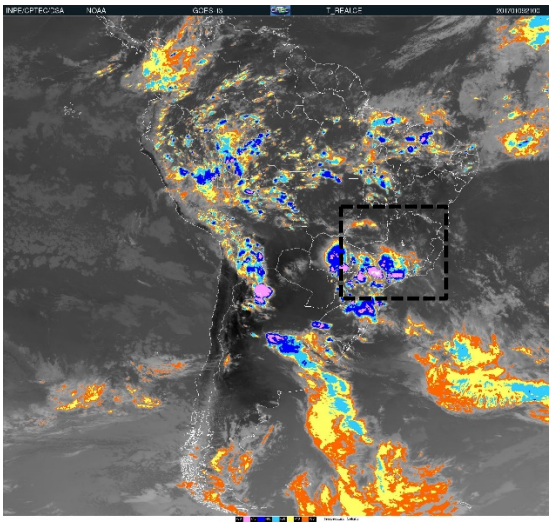

c) 11/01/2017 2100 UTC

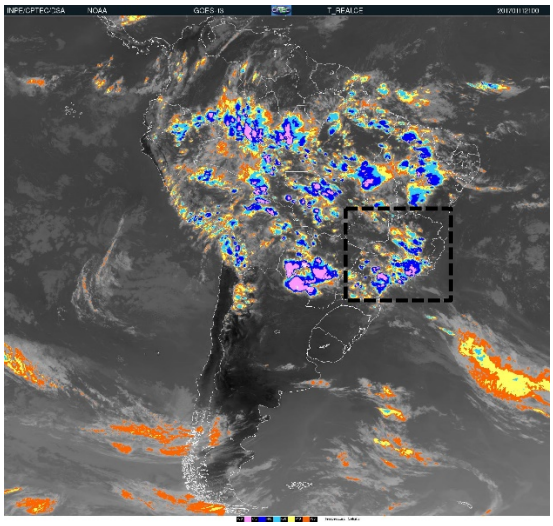

d) 14/01/2017 2100 UTC

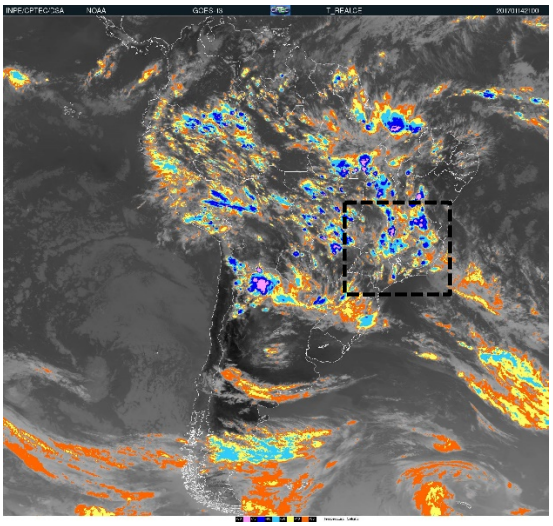

The simulation of HNO_3 (Figure 5.14 (b)) showed overestimation and a negative correlation for the period analyzed against CAMS. Removing the first fifteen days of simulation, the correlation increases to 0.29. Comparing the HNO_3 simulation with other models is difficult since its strongest sink is rain, a complex variable to be predicted in any numerical model. The results of the rain forecast can show significant variations between models that can penalize the comparison of HNO_3. Besides that, the approach of washout and rainout for

HNO_3 was simplified in the lightning parameterization scheme. In the future, improvements may be included.

The simulation of N_2O_5 (Figure 5.14 (c)) showed the best correlation and overestimation in the first fifteen days of the series against CAMS data. If the first fifteen days are removed from the series the correlation increase to 0.68. The reanalysis shows a well-defined daily cycle of N_2O_5 that is reasonably reproduced by the scheme.

The lightning scheme also generated larger maximum peaks of NO_3 (Figure 5.14 (d)) comparing to the reanalysis data. The correlation between the CAMS and NO_3 simulation is weak and it may be caused by the maximum NO_3 peaks simulated by the scheme during night time, when NO_3 reaches large concentrations. Although the correlation is weak, the simulation of NO_3 reproduces the daily cycle of CAMS.

The concentration of NO_3 in the lightning scheme is calculated by Equation 4.36. During day time, NO_3 is rapidly destroyed by the photodissociation process and does not reach a large concentration. During the night, NO_3 should be abundant due to the reaction between NO_2 and O_3 and Equation 4.36 can be rewritten as:

$$[NO_3] = \frac{K_3[O_3]}{K_4} \tag{5.1}$$

The simulation of NO_3 at night is a function of O_3 which is obtained using global approximations extrapolated to Eta model levels and not calculated by the scheme. In the future, the calculation of the O_3 concentration in the troposphere could be included in the lightning scheme.

Figure 5.14 – Time series of NOx related chemical species. The series was built with the average over the domain and the total vertical column for each chemical species. CORR is the Pearson correlation coefficient, RMSE denotes the Root-Mean-Square Error, STD is the Standard Deviation. The Eta model runs the simulation continuously between 01/01/2017 0000 UTC and 31/01/2017 2300 UTC.

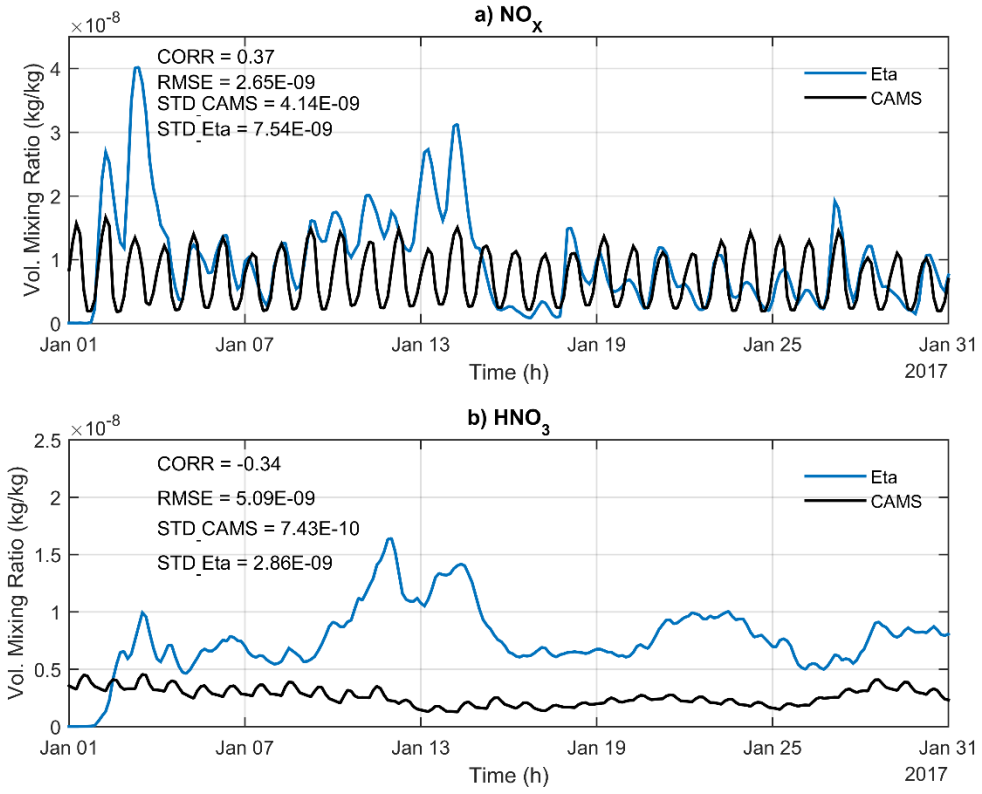

continue

Figure 5.14 – Conclusion.

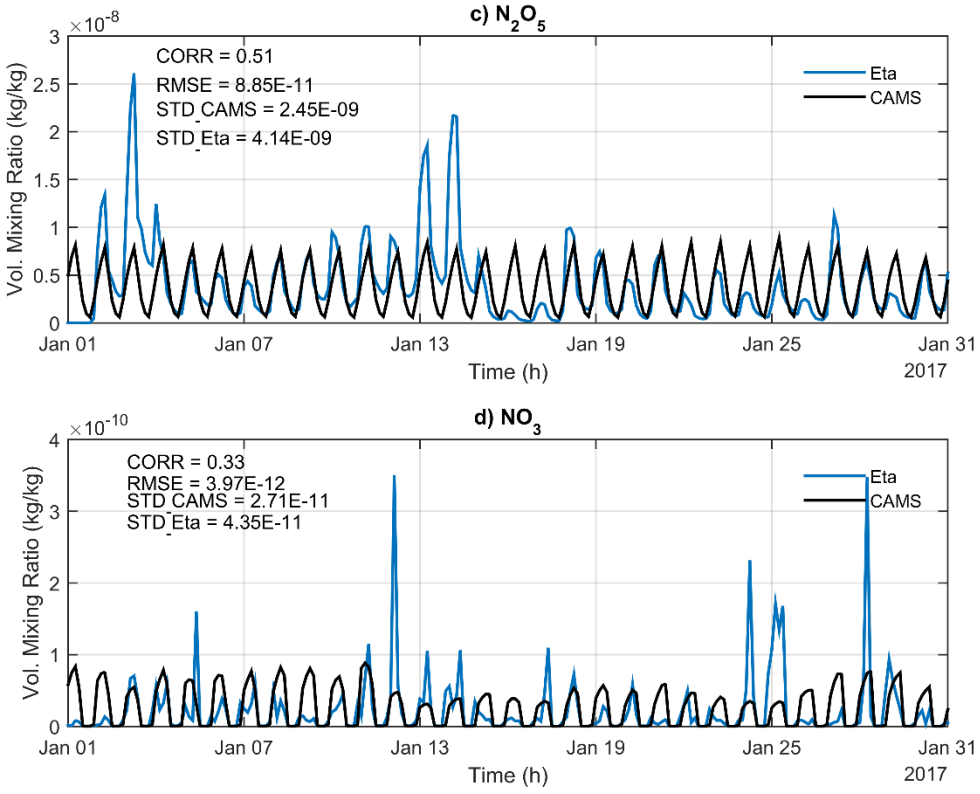

5.4.3 Vertical profile

The average vertical profile of NO_x and HNO_3 for January 2017 over the domain can be seen in Figure 5.15. For the comparison in Figure 5.15, Eta simulations were downgraded and interpolated to the CAMS grid. The results of the average NO_x vertical profile (Figure 5.15 (a)) are encouraging since the Eta model simulation is capable of reproducing the vertical NO_x profile of the CAMS reanalysis data except at upper levels where the lightning parameterization produces overestimation. The probable cause of this overestimation in the scheme is the injection of LNO_X in upper levels.

The results of the average HNO_3 vertical profile (Figure 5.15 (b)) showed a mixing ratio around an order of magnitude higher at lower and upper levels compared to CAMS. The reverse occurred at middle levels. This result suggests that the HNO_3 sink needs to be adjusted. At middle levels, where the rainout

process takes place, there must be an attenuantion of this process to increase HNO_3. At lower levels, where the washout and dry deposition process take place, there must be an intensification of these processes to decrease HNO_3. The overestimation at upper levels must be a consequence of NOx concentration.

Figure 5.15 – Average vertical profile of the simulated chemical species in the period from 01/01/2020 0000 UTC to 31/01/2020 2300 UTC on the domain of the Eta model. The x-axis is on the log scale.

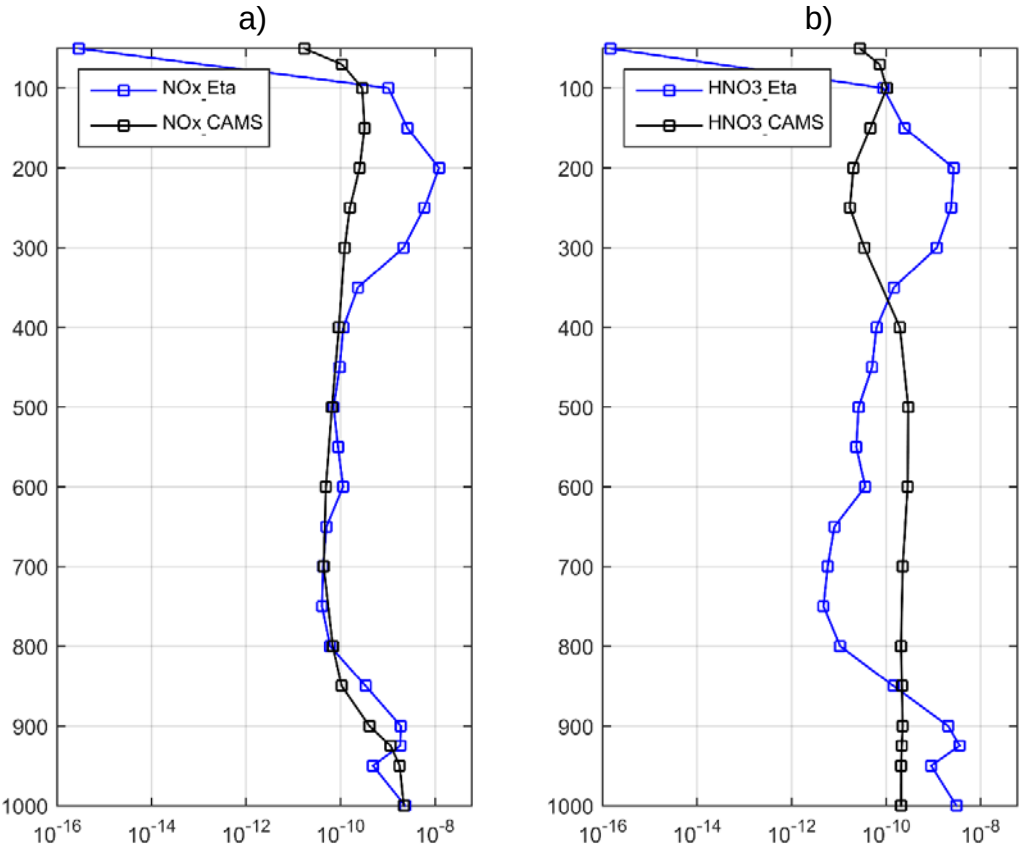

The average mixing ratio of the NOx related chemical species of the papers described in Table 5.3 were taken from different situations of measurements, as latitude and types of sources. Nevertheless, it is still possible to use these values as reference of the magnitude of chemical species in the troposphere and to compare with the lightning scheme simulations. The papers in Table 5.3 are described in section 3.6.

Table 5.3 – Summary of concentrations of chemical species simulated by the proposed scheme and observed/estimated in the literature. ϕ is the average and σ is the standard deviation.

Chemical species	**Simulations (ppbv)**		**Observations / Estimates (ppbv)**		
	Low Levels (925 hPa)	*Upper Levels (250 hPa)*	*Low Levels*	*Upper Levels*	Reference
NOx	$\phi = 1.77$ $\sigma = \pm 1.14$	$\phi = 5.93$ $\sigma = \pm 5.83$	**2.00 - 9.00**	**2.40*** $\sigma = \pm 1.7$* **2.62**** $\sigma = \pm 2.1$**	*Pawar et al (2012)* *Ott et al. (2007)*
HNO3	$\phi = 2.03$ $\sigma = \pm 1.08$	$\phi = 2.37$ $\sigma = \pm 2.67$	**0.20 - 0.86**	**0.03 - 0.30**	*Huebert e Lazrus (1978)*
NO3	$\phi = 0.01$ $\sigma = \pm 0.03$	$\phi = 0.000008$ $\sigma = \pm 0.000001$	**0.001 - 0.050**	**0.00003**	*Brown et al. (2007); Brasseur and Solomon (2005)*
N2O5	$\phi = 0.25$ $\sigma = \pm 0.12$	$\phi = 3.12$ $\sigma = \pm 3.77$	**0.025 - 0.170**	**0.150**	*Brown et al. (2007); Brasseur and Solomon (2005)*

* Observation described in *Ott et al. (2007).*

** Simulation described in *Ott et al. (2007).*

5.4.4 NOx transport

Because the production of NOx by lightning occurs mostly at upper levels, Figure 5.16 shows a simulation of electrical activity and NOx production at 250 hPa. In the early afternoon (Figure 5.16 (a)) 1600 UTC, 14:00h in local time (UTC-2), the lightning activity is small and gradually increases reaching the maximum activity at 2400 UTC (Figure 5.16 (i)), 22:00h in local time, as a response to the summer convection. Consequently, NOx emission also increases throughout the afternoon and evening.

The NOx is advected horizontally toward the northwest of the domain. Around 2100 UTC (Figure 5.16 (f)), a strong electrical activity at 25ºS and between 52W and 48W intensified NOx production, and the strong winds from the upper levels of the troposphere spread NOx efficiently and transported outward of the domain. Locally and during electrical activity, the NOx mixing ratio reached maximum values around 50 ppbv. Vertically, the NOx production in the 25ºS longitudinal section can be seen in Figure 5.17.

Figure 5.16 – Simulation of NOx production at 250 hPa during intense electrical activity. The mixing ratio of NOx in shading and the number of lightning per hour in the model grid in contour lines. Eta model started on 01/01/2017 00 00UTC.

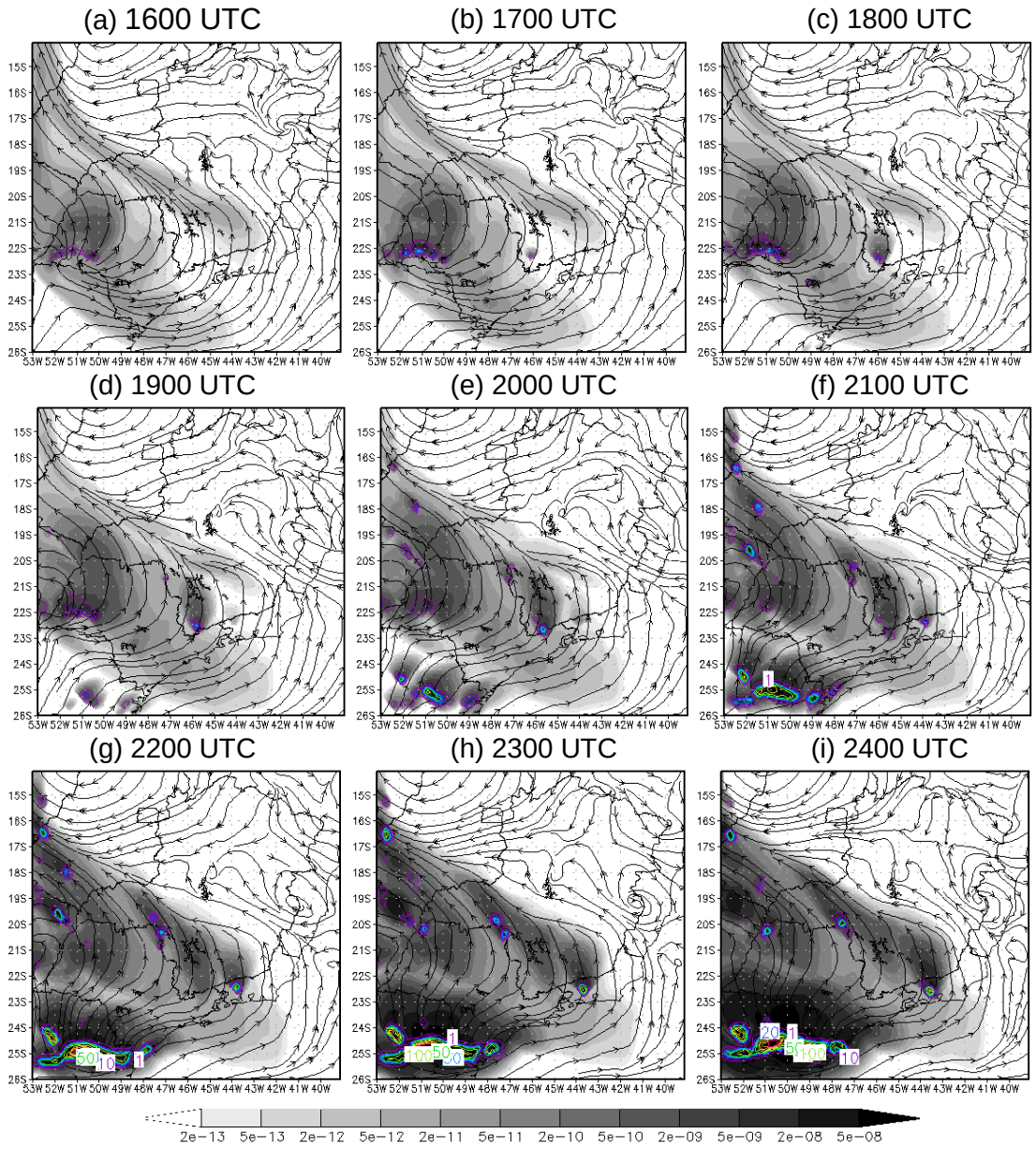

Both vertical diffusion and convection acted on vertical transport in Figure 5.17. The production of NOx by lightning in the region starts at 1900 UTC (Figure 5.17 (d)), which is visible as a shaded vertical stripe. In the previous period, there was no occurrence of electrical discharges (Figure 5.17 (a), (b), and (c)), and the presence of NOx in the low and middle levels is due to anthropogenic

emissions on the surface, being transported vertically and horizontally by the scheme.

Figure 5.17 – Vertical distribution of the longitudinal section of NOx production at latitude 25S during intense electrical activity. Eta model started on 01/01/2017 00 00UTC.

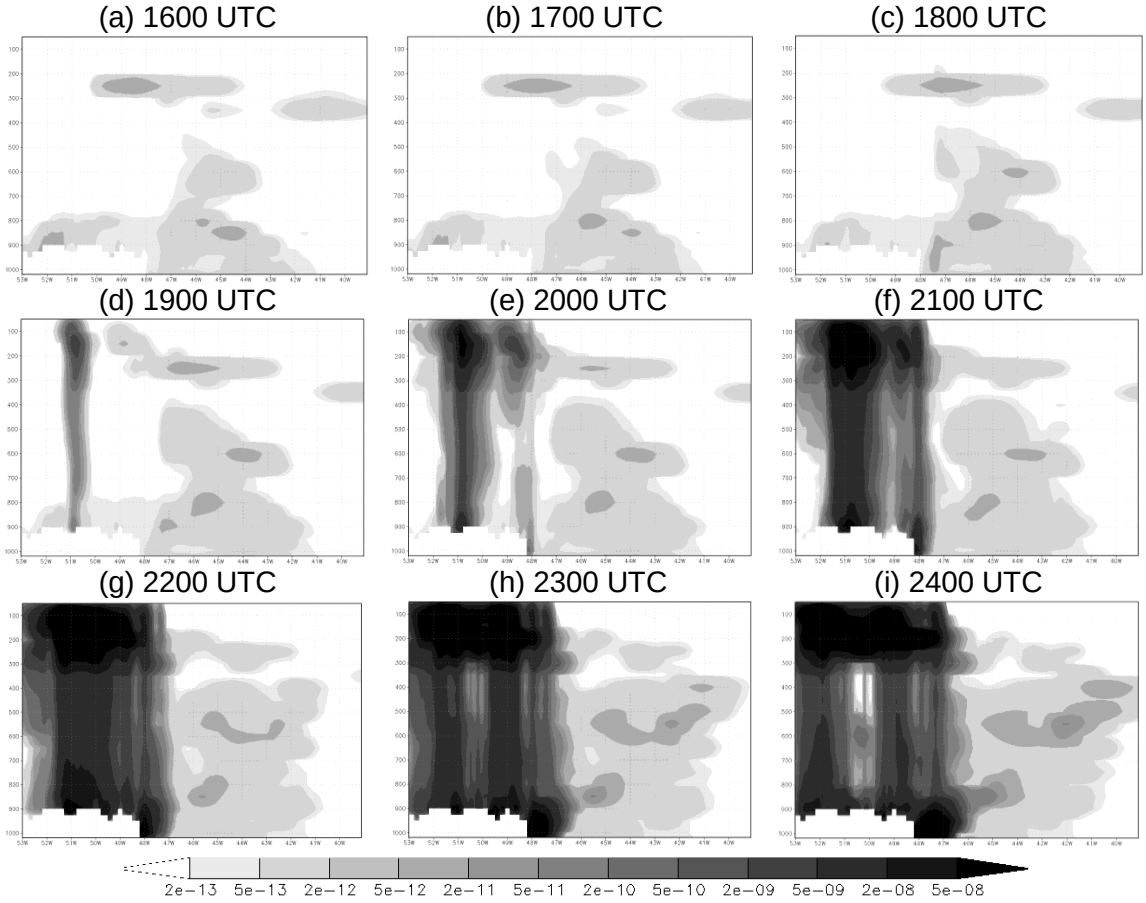

5.4.5 Mass conservation

To evaluate the mass conservation of the parameterization, two experiments were carried out. The first experiment (Figure 5.18 (a)) aimed to detect whether the mass is preserved during the chemical reactions of the scheme. This experiment is important to detect if a spurious mass is created or lost during the reactions. In the first experiment all sources, sinks, and transport were turned off. An initial condition of $1 \times 10^8 cm^{-3}$ of NO_x concentration was given. The experiment showed a decrease in NO_x concentration in the time series as the

concentration of the other species, initially equal to zero, increases. The sum of all species maintained a concentration of $1 \times 10^8 cm^{-3}$, confirming that the mass was conserved in the analyzed period.

The second experiment (Figure 5.18 (b)) aimed to assess whether the mass of NO_x is conserved during the contribution of convection in vertical transport. In this experiment, all sources, sinks, and horizontal and vertical advection were excluded. The chemical reactions were also turned off and an initial condition of $1 \times 10^8 cm^{-3}$ of NOx concentration was given. The results show the vertical trend of NO_x in an area with convective activity, where integration into the vertical trend of the NO_x trend was equal to zero, confirming the conservation of the mass during the contribution of convection.

Figure 5.18 – Mass conservation experiments of the scheme. The Eta model was initiated on 02/01/2017 0000 UTC. (a) Conservation of vertical average of the chemical species of the parameterization and (b) the vertical profile of the NO_x tendency.

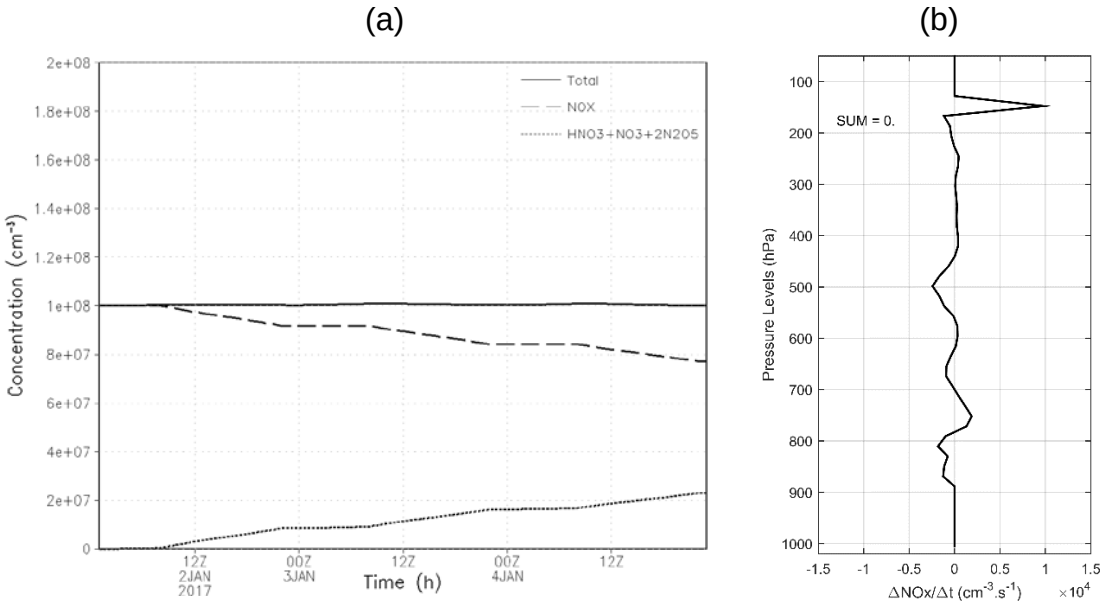

6 CONCLUSION AND FINAL COMMENTS

A parameterization of atmospheric electrical discharge based on cloud microphysics and convection parameters is proposed in this work. The methodology diagnoses the number of total lightning (CG + IC) in the model grid and inserts the effects of electrical activity on the droplet autoconversion rate and the NO_x production.

Three experiments were carried out to evaluate the lightning simulation and rain production during January, February, and March of 2017. The experiments were divided into Exp1, which is a control experiment with no effects on cloud droplet autoconversion, Exp2, which is an experiment with a moderate effect on cloud droplet autoconversion, and Exp3, which is an experiment with an intense effect on cloud droplet autoconversion.

The lightning scheme was able to reproduce the observations of atmospheric electric discharges. All the experiments showed underestimation against observed lightning data. It was found that the effect of lightning on cloud droplet autoconversion caused an increase in the electrical activity of the scheme and there was an improvement in the performance of the lightning simulation. It was also found that the increase in electrical activity was a consequence of the increase in cloud ice content in medium and high levels.

The results of the lightning simulations were encouraging and the scheme can be applied in other regions of the world, as long as it is adjusted. The diagnosis of lightning in the Eta model opens the possibility of climatological studies of lightning, short and medium term forecasts for electric power companies that can use the information to prevent damage to the electricity grid, and short term forecasts for agribusiness for prevention and monitoring of fires caused by lightning strikes and death of farm animals.

Precipitation simulations showed that all experiments underestimated the precipitation estimated by CMORPH satellite. Underestimations were lower in experiments with the effect of lightning on droplet autoconversion. It was found

that Exp2 and Exp3 presented more cases of precipitation above the 30 mm/day threshold that were related to the occurrence of lightning during the analyzed period in comparison to Exp1. The results showed that the increase in the effect of lightning on the droplet autoconversion in Exp3 did not show significant improvement concerning underestimation. There was a small loss of performance of Exp3 in relation to Exp2 in the analysis of ETSa. It is suggested to use the Exp2 configuration in Eta model until further studies are carried out.

The Exp2 configuration was used in the simulation of NOx produced by lightning. To assess the effects of the lightning scheme on the production of NOx and related chemical species, the Eta model was run continuously for January 2017 because it is the month with the highest electrical activity and, therefore, because it has the highest NOx production by lightning.

The simulations of NOx and related chemical species were compared with CAMS reanalysis data. The results showed that the scheme was able to reproduce the averages of the chemical species on the domain when compared to the CAMS reanalysis data. The first fifteen days of simulation showed some peak peaks with overestimation compared to CAMS. These overestimations may be related to a large electrical activity simulated by the scheme in the first half of January 2017. The concentrations of the species showed values close to the values described in the literature. The horizontal and vertical transport of NOx proved to be efficient and the mass of the species was conserved.

The results are encouraging, but new analyses and applications must be carried out to improve the scheme. For future work, it is suggested to include the mass exchange processes of convective transport (entrainment and detrainment), as well as the subsidence induced in the environment. The coupling of the proposed scheme with a chemistry model would also be important for the calculation of O3 and OH. Finally, an evaluation to be carried out is the processes of removing nitric acid through washout and rainout to see if the sink rates applied are effective. Besides, it would be possible to include acid rain forecasts in the model. The inclusion of this parameterization in the global version of Eta model could be very welcoming in the future and climate change

studies with a lightning parameterization could be a breakthrough in the field not only due to possible climatological studies of lightning on the globe, but also the effects on the microphysics of clouds and the production of NOx.

BIBLIOGRAPHIC REFERENCES

ASAI, T. A numerical study of the air-mass transformation over the Japan Sea in winter. **Journal of Meteorological Society Japan**, v. 43, p. 1–15, 1965.

AVILA, E. E. et al. The effect of the cloud-droplet spectrum on electral-charge transfer during individual ice-ice collisions. **Quarterly Journal of the Royal Meteorological Society**, v.125, p. 1669-1679, 1999.

BAKER, B. et al. The influence of diffusional growth rates on the charge transfer accompanying rebounding collisions between ice crystal and soft halstones. **Quarterly Journal of the Royal Meteorological Society**, v. 113, p. 1193-1215, 1987.

BAKER, M. B.; DASH, J. G. Mechanism of charge transfer between colliding ice particles in thunderstorms. **Journal of Geophysical Research**, v. 99, n.D5, p. 10621-10626, 1994

BALLAROTTI, M. G.; SABA, M. M.; PINTO JUNIOR, O. A new performance of evaluation of the brazilian lightning location system (Rindat) based on high speed camera observations of natural negative ground flashes. In: INTERNATIONAL LIGHTNING DETECTION CONFERENCE, 19., 2006, Tucson. **Proceedings...** 2006. Available from: http://citeseerx.ist.psu.edu/viewdoc/download?doi=10.1.1.531.9125&rep=rep1&type=pdf. Access in: Jan. 2021.

BARTHOLD, F.; BODNER, M. **NAM rime factor and ice accumulation rate**, 2009. Available from: www.wpc.ncep.noaa.gov/hmt/seminar_files/rimefactor.ppt. Access in: Feb. 2017.

BERGERON, T. On the physics of clouds and precipitation. **Proces Verbaux de l'Association de Météorologie**, p. 156-178, 1935.

BETTS, A. K.; MILLER, M. J. A new convective adjustment scheme: part II: single column tests using GATE wave, BOMEX and arctic air-mass data sets. **The Quarterly Journal of the Royal Meteorological Society**, v. 112, p. 693-709, 1986.

BIGG, E. K. The supercooling of water. **Proceedings of the Physical Society Section B**, v. 66, n. 8, p.688, 1953.

BJERKNES, J. B. Saturated-adiabatic ascent of air through dry-adiabatically descending environment. **Quarterly Journal of the Royal Meteorological Society**, v. 64, p. 325-330, 1938.

BLACK, T. L. The new NMC mesoscale Eta model: description and forecast. **Weather and Forecasting**, v. 9, n. 2, p. 265-278, 1994.

BRASSEUR, G.; JACOB, D. **Modeling of atmospheric chemistr**y. Cambridge: Cambridge University Press, 2017.

BRASSEUR, G.; SOLOMON, S. **Aeronomy of the middle atmosphere:** chemistry and physics of the stratosphere and mesosphere. Dordrecht: Springer, 2005.

BRASSEUR, G. et al. An interactive chemical dynamical radiative two-dimensional model of the middle atmosphere. **Journal of Geophysical Research**, p. 5639–5655, 1990.

CALADA, R. et al. Avaliação do desempenho das simulações por conjunto do modelo Eta-5km para o caso de chuva intensa na bacia do Rio Paraíba do Sul em janeiro de 2000. **Revista Brasileira de Meteorologia**, v. 33, n. 1, p. 83-96, 2017.

CATALDI, M. et al. Análise das previsões de precipitação obtidas com a utilização do modelo Eta como insumo para modelos de previsão semanal de vazão natural. **Revista Brasileira de Recursos Hídricos**, v. 12, n. 3, p. 5-12, 2007.

CHEN, F.; JANJIC, Z.; MITCHELL, K. Impact of atmospheric surface-layer parameterizations in the new land-surface scheme of the NCEP mesoscale Eta model. **Boundary-Layer Meteorology**, v. 85, p. 391-421, 1997.

CHOU, S. C. Modelo regional Eta. **Climanálise Especial**, 1996. Available from: http://climanalise.cptec.inpe.br/~rclimanl/boletim/cliesp10a/27.html. Access in: Feb. 2021.

CHOU, S. C.; SILVA, M. G. Objective evaluation of ETA model precipitation forecasts over South America. **Revista Climanálise**, v. 1, p.1-17, 1999.

CHRISTIAN, H. E. Global frequency and distribution of lightning as observed from space by the optical transient detector. **Journal of Geophysical Research**, v. 108, 2003. DOI:10.1029/2002JD002347.

CHRISTIAN, H. et al. Airborne and ground-based studies of thunderstorms in the vicinity of Langmuir Laboratory. **Quarterly Journal of the Royal Meteorological Society**, v.106, p.159-174, 1980.

CHURCH, R. **The history of the british coal industry**. Oxford: Clarendon Press, 1986.

DASH, J. G.; MASON, B. L.; WETTLAUFER, J. S. Theory of charge and mass transfer in ice-ice collisions. **Journal of Geophysical Research**, v. 106, n. D17, p. 20395-20402, 2001.

DIFFENBAUGH, N. S.; SCHERER, M.; TRAPP, R. J. Robust increases in severe thunderstorm environments in response to greenhouse forcing. **Proceedings of the National Academy of Science**, v. 110, p.16361–16366, 2013.

DOSWELL, C. A. Severe convective storms: an overview. In: DOSWELL, C.A. (Ed.). **Severe convective storms.** Boston: American Meteorological Society, 2001. p. 1-26.

EK, M. et al. Implementation of Noah land surface model advances in the national centers for environmental prediction operational mesoscale Eta model.

Journal of Geophysical Research: Atmospheres, v. 108, n. D22, p. 1984-2012, 2003.

ELSTER, I.; GEITEL, H. Zur Influenztheorie der niederschlagselektrizitat. **Physikalische Zeitschrift**, v. 14, p. 1287-1292, 1913.

FELS, S. B.; SCHWARZKOPF, M. D. The simplified exchange approximation: a new method for radiative transfer calculations. **Journal of Atmospheic Sciences**, v. 32, p. 1475-1488, 1975.

FERRIER, B. S. A double-moment multiple-phase four-class bulk ice scheme: part I: description. **Journal of the Atmospheric Science**, v. 51, n. 2, p. 249-280, 1994.

FERRIER, B. S. et al. Implementation of a new grid-scale cloud and precipitation scheme in the NCEP Eta Model. In: CONFERENCE ON NUMERICAL WEATHER PREDICTION, 15., 2002. **Proceedings…** American Meterological Society, 2002. p.280-283.

FLETCHER, N. H. Effect of electric charge on collisions between cloud droplets. **Journal of Applied Meteorology and Climatology**, v. 52, p. 517-520, 2013.

FLINN, M. W. **The history of the british coal industry**. Oxford: Clarendon Press, 1984.

GALLUS JUNIOR, W. A. Eta simulations of three extreme precipitation events: sensitivity to resolution and convective parameterization. **Weather and Forecasting**, v. 14, p. 405-426, 1999.

GRENET, G. Essai d'explication de la charge electrique des nuages d'orages. **Annales Géophysicae**, v. 3, p. 306-307, 1947.

GRESSENT, A. et al. Lightning NOx influence on large-scale NOy and O3 plumes observed over the northern mid-latitudes. **Tellus B: Chemical and Physical Meteorology**, v. 66, n.1, 2014.

GRIMM, M. A. **Processo de Bergeron**. Curitiba: Universidade Federal do Paraná, 1999. Notas de Aula. Available from: http://fisica.ufpr.br/grimm/aposmeteo/cap6/cap6-3-1.html. Access in: Feb. 2021.

GRUPO DE ELETRICIDADE ATMOSFÉRICA - ELAT. **Brasil terá mais raios nas próximas décadas**. 2009. Available from: http://www.inpe.br/webelat/homepage/menu/noticias/release.php?id=2. Access in: Nov. 2017.

GRUPO DE ELETRICIDADE ATMOSFÉRICA - ELAT. **Grupo de Eletricidade Atmosférica (ELAT/INPE)**. Available from: http://www.inpe.br/webelat/homepage/. Access in: Oct. 2017.

HERSBACH, H. et al. The ERA5 global reanalysis. **Quarterly Journal of the Royal Meteorological Society**, v. 146, p. 1999– 2049, 2020.

HONG, S. et al. History of ancient copper smelting pollution during Roman and Medieval times recorded in Greenland ice. **Science**, v. 272, p. 246-249, 1996.

HOUZE, R. A. **Cloud dynamics**. San Diego: Academic Press, 1993.

HUEBERT, B.; LAZRUS, A. Global tropospheric measurements of nitric-acid vapor and particulate nitrate. **Geophysical Research Letters**, p. 577-580, 1978.

BURKHOLDER, J. B. et al. **Chemical kinetics and photochemical data for use in atmospheric studies**. Pasadena: Jet Propulsion Laboratory, 2015.

JACOBSON, M. Z. **Atmospheric pollution:** history, science, and regulation. New York: Cambridge University Press, 2002.

JAEGLÉ, L. et al. Sources of HOx and production of ozone in the upper troposphere over the United States. **Geophysical Research Letters**, v. 25, p. 1705-1708, 1998.

JANJIC, Z. I. The step-mountain Eta coordinate model: further developments of the convection, viscous sublayer, and turbulence closure schemes. **Monthly Weather Review**, v. 122, n. 5, p. 927-945, 1994.

JAYARATNE, E. R.; SAUDERS, C. P. Thunderstorm electrification: the effect of cloud droplets. **Journal of Geophysical Research**, v. 90, n. D7, p. 13063-13066, 1985.

JAYARATNE, E. R.; SAUNDERS, P. R.; HALLETT, J. Laboratory studies of the charging of soft-hail during ice crystal interactions. **Quarterly Journal of the Royal Meteorological Society**, v. 109, p. 609-630, 1983.

JOYCE, R. J. et al. CMORPH: a method that produces global precipitation estimates from passive microwave and infrared data at high spatial and temporal resolution. **Journal of Hydrometeorology**, v. 5, p. 487-503, 2004.

KAIN, J. S.; FRITSCH, J. M. A One-dimensional entraining/detraining plume model and its application in convective parameterization. **Journal of Atmospheric Science**, v. 47, n. 23, p. 2784-2802, 1990.

KAIN, J. S.; FRITSCH, J. M. Convective parameterization for mesoscale models: the Kain-Fritsch scheme, in meteorological monographs. **American Meteorological Society**, v. 24, n. 46, 1993.

KAIN, J. S. et al. Utilizing the Eta model with two different convective parameterizations to predict convective initiation and evolution at the SPC. In: CONFERENCE ON MESOSCALE PROCESSES, 2001. **Proceedings…** 2001. p. 91–95.

KOUCHI, J. et al. Conditions for condensation and preservation of amorphous ice and crystallinity of astrophysical ices. **Astronomy and Astrophysics**, v. 290, p. 1009-1018, 1994.

KOUTROULIS, A. G. et al. Lightning activity, rainfall and flash flooding – occasional or interrelated events? a case study in the island of Crete. **Natural Hazards Earth Systems Science**, v. 12, p. 881-891, 2012.

KRIM, J.; PALASANTZAS, G. Experimental observations of self-affine scaling and kinetic roughening at sub-micron lengh scales. **Modern Physics**, v. 9, p. 599-632, 1995.

LACIS, A. A.; HANSEN, J. E. A parameterization of the absorption of solar radiation in the earth's atmosphere. **Journal of Atmospheric Science**, v. 31, p. 118-133, 1994.

LAMARQUE, J. F. et al. Historical (1850-2000) gridded anthropogenic and biomass burning emissions of reactive gases and aerosols: methodology and application. **Atmospheric Chemical Physics**, v. 10, n. 15, p. 7017-7039, 2010.

LIANET, H. P. **Esquema de microfísica de nuvens no modelo Eta:** diagnóstico e testes de sensibilidade. 2016. 121p. Dissertação (Mestrado em Meteorologia) - Instituto Nacional de Pesquisas Espaciais, São José dos Campos, 2016. Avalilable from: http://urlib.net/8JMKD3MGP3W34P/3L9HU3E . Access in: Feb. 2021.

LIPPMANN, H. H.; JESSER, B.; SCHURATH, U. The rate constant of NO + O3 → NO2 + O2 in the temperature range of 283–443 K. Int. **Journal Chemical Kinetics**, v. 12, p. 547-554, 1980.

LIST, R.; FREIRE, E. Comparision of the theorical collision efficiency of uncharged cloud droplets in horizontal and vertical eletric fields. **American Meteorological Society**, v. 38, p. 2257-2263, 1981.

MACGORMAN, D. R.; STRAKA, J. M.; ZIEGLER, C. L. A lightning parameterization for numerical cloud models. **Journal of Applied Meteorology**, v. 40, p. 459-478, 2001.

MADRONICH, S.; FLOCKE, S. Theoretical estimation of biologically effective UV radiation at the Earth's surface. In: ZEREFOS, C.S.; BAIS, A.F. (Ed.). **Solar ultraviolet radiation.** Berlin: Springer, 1997.

MASON, B. L.; DASH, J. G. Charge and mass transfer in ice-ice collisions: experimental observations of a mechanism in thunderstorm electrification. **Journal of Geophysical Research**, v. 105, n. D8, p. 10185-10192, 2000.

MCCAUL JUNIOR, E. W. et al. Forecasting lightning threat using cloud-resolving model simulations. **Weather and Forecasting**, v. 24, p. 709-729, 2009.

MELLOR, G. L.; YAMADA, T. Development of a turbulence closure model for geophysical fluid problems. **Review of Geophysical Space Physics**, v. 20, n. 4, p. 851-875, 1982.

MESINGER, F. A blocking technique for representation of mountains in. **Revista Meteorologica Aeronautica**, v. 44, n. 1/4, p.195-202, 1984.

METCALF, J. I. Radar observations of charging orientations of hydrometeors in thunderstorms. **Journal of Applied Meteorology**, v. 34, p. 757-772, 1995.

MINSCHWANER, K.; SISKIND, D. E. A new calculation of nitric oxide photolysis in the stratosphere, mesosphere, and lower thermosphere. **Journal of Geophysical Research**, v. 98, n. D11, p. 20401, 1993.

MOORE, C. B. et al. Radar observations of rain gushes following overhead lightning strokes. **Journal of Geophysical Research**, v. 67, n. 1, p. 207-220, 1962.

MOORE, C. B. et al. Gushes of rain and hail after lightning. **Journal of the Atmospheric Sciences**, v. 21, p. 646-665, 1964.

MOURA, J. D. **Efeitos do transporte de momentum convectivo na distribuição de chuva**. Dissertação (Mestrado em Meteorologia) - Instituto Nacional de Pesquisas Espaciais, São José dos Campos, 2016.

MURRAY, L.T. Lightning NO x and impacts on air quality. **Current Pollution**, p. 115–133, 2016.

OTT, L.E. et al. Production of lightning NOx and its vertical distribution calculated from three-dimensional cloud-scale chemical transport model simulations. **Journal of Geophysical Research Atmosphere**, v. 115, 2010.

Ott, L. E. et al. Effects of lightning NOx production during the 21 July European Lightning Nitrogen Oxides Project storm studied with a three-dimensional cloud-scale chemical transport model, **Journal of Geophysical Research**, v. 112, p. D05307, 2007.

PAULSON, C. A. The mathematical representation of wind speed and temperature profiles in the unstable atmospheric surface layer. **Journal of Applied Meteorology**, v.9, p. 857-861, 1970.

PEREYRA, R. G.; AVILA, E. E. Charge transfer mensurements during single ice crystal collisions with a target growing by riming. **Journal of Geophysical Research**, v. 107, n.D23, 2002.

PINES, E.; HUPPERT, D. Kinetcs of proton transfer in ice via the pH- jump method: evaluation of the proton diffusion rate in polycrystaline doped ice. **Chemical and Physical Letters**, v. 116, p. 295-301, 1985.

PINTO JUNIOR, O. **A arte da guerra contra os raio**. São Paulo: Oficina de Textos, 2005.

PINTO JUNIOR, O.; PINTO, I. R. **Tempestades e relâmpagos no Brasil**. São José dos Campos: Instituto Nacional de Pesquisas Espaciais, 2000.

PLUMLEE, H. R.; SEMONIN, R. G. Cloud droplet collision effiency in electric fields. **Telus**, v. 17, n. 3, p. 356-364, 1965.

PRINCE, C.; RIND, D. A simple lightning parameterization for calculating global lightning distributions. **Journal of Geophysical Research**, v. 97, p. 9919–9933, 1992.

PRUPPACHER, H. R.; KLETT, J. D. **Microphysics of clouds and precipitation**. 2.ed. Nova York: Kluwer Academic, 2010.

REYNOLDS, S. E.; BROOK, M.; GOURLEY, M. F. Thunderstorm charge separation. **Journal of Meteorology**, v. 14, p. 426-436, 1957.

ROZANTE, J. R. et al. Combining TRMM and surface observations of precipitation: technique and validation over South America. **Weather and Forecasting**, v. 25, p. 885-894, 2010.

RUST, W. D.; MACGORMAN, R. D. Possibly inverted-polarity electrical structures in thunderstorms during STEPS. **Geophysical Research Letters**, v. 29, n. 12, 2002.

SAHA, S. The NCEP climate forecast system version 2. **Journal of Climate**, v. 27, p. 2185–2208, 2014.

SALBY, M. L. **Fundamentals of atmospheric physics**. San Diego: Elsevier, 1996.

SARTOR, D. A laboratory investigation of collision efficiencies, coalescence and electrical charging of simulated cloud droplets. **Journal of Meteorology**, v. 11, p. 91-103, 1954.

SARTOR, J. D. The electrification of thunderstorms and the formation of precipitation. **Naturwissenschaften**, v. 60, p. 19-31, 1973.

SAUNDERS, C. Charge separation mechanisms in clouds. **Space Science Reviews**, v. 137, p. 335-353, 2008.

SAUNDERS, C. P. A review of thunderstorm electrification. **Journal of Applied Meteorology**, v. 32, p. 642-655, 1993.

SAUNDERS, C. P.; PECK, S. L. Laboratory studies of the influence of the rime accretion rate on charge transfer during crystal/graupel collisions. **Journal of Geophysical Research**, v. 103, n. D12, p. 13949-13956, 1998.

SAUNDERS, C. P.; KEITH, W. D.; MITZEVA, R. P. The effect of liquid water on thunderstorm charging. **Journal of Geophysical Research**, v. 96, n. D6, p. 11007-11017, 1991.

SAUNDERS, C. P. et al. Laboratory studies of the effect of cloud conditions on graupel conditions on graupel/crystal charge transfer in thunderstorm electrification. **Quarterly Journal of Meteorological Soceity**, v. 132, p. 2653-2673, 2006.

SCHUMANN, U.; HUNTRIESER, H. The global lightning-induced nitrogen oxides source. **Chemical and Physics**, v. 7, p.3823–3907, 2007.

SEELEY, J. T.; ROMPS, D. M. The effect of global warming on severe thunderstorms in the United States. **Journal of Climate**, v. 28, p. 2443–2458, 2015.

SEIFERT, A. et al. **Cloud microphysics in the COSMO model:** new parameterizations of ice nucleation and melting of snow. 2009. Available from: www.cosmo-model.org/content/consortium/generalMeetings/general2009/wg3/Cloud_Microphys_Seifert.ppt. Access in: Dec. 2020.

SEMONIN, R. G.; PLUMLEE, H. R. Collision efficiency of charged cloud droplets in electric fields. **Journal of Geophysics Research**, v. 71, p. 4271-4278, 1966.

STENSRUD, D. J. **Parameterization schemes:** keys to undestanding numerical weather prediction models. Nova York: Cambridge. 2007.

STEVEN S.; BROWN, R. K.; TALUKDAR, A.R. Rate constants for the reaction OH+NO2+M→HNO3+M under atmospheric conditions. **Chemical Physics Letters**, v. 299, n. 3/ 4, p. 277-284, 1999.

STRAKA, J. **Cloud and precipitation microphysics:** principles and parameterizations. Nova York: Cambridge University Press, 2009.

SUMIYOSHITANI, S. Effects of an applied electric field on collection efficiency by a charged droplet for dust particles in charged droplet scrubbers. **Aerosol Science and Technology**, v. 20, p; 71-82, 1994.

TIE, X. et al. Effects of lightning on reactive nitrogen and nitrogen reservoir species in the troposphere. **Journal of Geophysical Research,** v. 106, n. D3, p. 3167-3178, 2001.

TRIJONIS, J. **Empirical relationships between atmospheric nitrogen dioxide and its precursors**. [S.l.]: Environmental Sciences Research Laboratory, 1978.

UNIVERSIDADE DO ARIZONA. **Hydrology and atmospheric sciences**. 2015. Available from: http://www.atmo.arizona.edu/students/courselinks/spring15/atmo589/ATMO489_online/lecture_11/lect11_cloud_electrification.html. Access in: 24 oct. 2017.

VASCONCELLOS, F. C.; CAVALCANTI, I. F. Uma avaliação das previsões do modelo regional Eta em alta resolução para dois casos de chuva intensa ocorridos na região da Serra do Mar. **Revista Brasileira de Meteorologia**, v. 25, n. 4, p. 501-512, 2010.

VONNEGUT, B. Possible mechanism for the formation of thunderstorm electricity. In: CONFERENCE ON ATMOSPHERIC ELETRICITY, 1954, Boston. **Proceedings...** Boston, 1954. p. 169-181.

WALLACE, J. M.; HOBBS, P. V. **Atmospheric science an introduction survey.** 2.ed. Canada: Elsevier, 2006.

WALLINGTON, T. J. et al. A study of the reaction NO3 + NO2 + M ? N2O5 + M(M = N2, O2). **International Journal of Chemical Kinetics**, v. 19, n. 3, p. 243–249, 1987.

WANG, Y.; ZHUPANSKA, O. Estimation of the electric fields and dielectric breakdown in non-conductive wind turbine blades subjected to a lightning stepped leader. **Wind Energy**, v. 20, p. 927-942, 2016.

WILLIAMS, E. J.; HUTCHINSON, G. L.; FEHSENFELD, F. C. NOx and N2O emissions from soil. **Global Biogeochemical Cycles**, v. 6, n. 4, p. 351– 388, 1992.

WORKOFF, T. E. et al. A case study of the research-to-operations (R20) process at HMT-WPC. 2013. Available from: www.wpc.ncep.noaa.gov/hmt/Workoff_2013_NOAA_Testbed.ppt. Access in: Nov. 2019.

YE, H. et al. More frequent showers and thunderstorm days under a warming climate: evidence observed over Northern Eurasia from 1966 to 2000. **Climate Dynamics**, v. 49, p. 1933–1944, 2017.

ZELDOVICH, Y. B.; SADOVNIKOV, P. Y.; FRANK-KAMENETSKII, D. A. **Oxidation of nitrogen in combustion**. Moscow: Institute of Chemical Physics, 1947.

ZEPKA, G. S. **Previsão de descargas elétricas usando o modelo de mesoescala WRF**. Tese (Doutorado em Geofísica Espacial) – Instituto Nacional de Pesquisas Espaciais, São José dos Campos, 2011.

ZEPKA, G. S.; PINTO JUNIOR, O.; SARAIVA, A. C. Lightning forecasting in southeastern Brazil using the WRF model. **Atmospheric Research**, v.135/136, p. 344-362, 2014.

ZHANG, R.; TIE, X.; BOND, D. W. Impacts of anthropogenic and natural NOx sources over the U.S. on tropospheric chemistry. **Proceedings of the National Academy of Sciences**, p. 1505-1509, 2003.

ZHAO, Q.; CARR, F. H. A prognostic cloud scheme for operational NWP Models. **Monthly Weather Review**, v. 125, p. 1931-1953, 1997.

ZHOU, Q. **The incorporation and initialization of cloud water/ice in an operational forecast model**. Tese (Doutorado) - Universidade de Oklahoma, Norman, 1993.

ZHOU, Y.; QUIE, X.; SOULA, S. A study of the relationship between cloud-to-ground lightning and precipitation in the convective weather system in China. **Annales Geophysicae**, v. 20, p. 107-113, 2002.